CHAPTER 1

INTRODUCTION

This thesis considers the design and adaptation of finite-tap equalizers for combating linear intersymbol interference (ISI) in the presence of additive white Gaussian noise, under the constraint that decisions are made on a symbol-by-symbol basis by quantizing the equalizer output. We also consider quadrature-amplitude modulation (QAM), decision-feedback equalizers (DFE), and multiuser systems, but the linear ISI pulse-amplitude modulation (PAM) channel with a linear equalizer of Fig. 1-1 captures the essential features of the problem under consideration. The channel input symbols x_k are drawn independently and uniformly from an L-ary PAM alphabet $\{\pm 1, \pm 3, \ldots \pm(L-1)\}$. The channel is modeled by an impulse response h_i with memory M and additive white Gaussian noise, yielding a received signal of

$$r_k = \sum_{i=0}^{M} h_i x_{k-i} + n_k . \tag{1-1}$$

The received signal is passed through a finite-tap linear equalizer $\boldsymbol{c}$, the output of which is quantized to produce a delayed input estimate $\hat{x}_{k-D}$, where D accounts for the delay of both the channel and the equalizer. This thesis considers two classic and well-defined questions:

- How should we design $\boldsymbol{c}$?
- How should we adapt $\boldsymbol{c}$?

The conventional answer to the first question is to choose $\boldsymbol{c}$ to minimize the mean-squared error (MSE):

$$\mathrm{MSE} = \mathrm{E}[(y_k - x_{k-D})^2], \tag{1-2}$$

leading to the so-called minimum-MSE (MMSE) equalizer. A common algorithm used to realize the MMSE equalizer is the least-mean square (LMS) algorithm, which is a stochastic gradient algorithm with low complexity. However, a much less understood but nevertheless the most relevant equalizer is that which minimizes the symbol-error rate (SER) or bit-error rate (BER). There has been some work over the last two decades in minimum-BER equalization and multiuser detection [1]–[6], which will be reviewed in section 1.2.3. Some analytical results on minimum-BER equalizer and multiuser detector structures

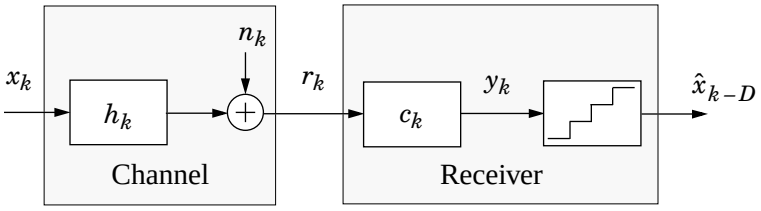

Fig. 1-1. Block diagram of channel, equalizer, and memoryless decision device.

were derived in [1][2][4], and several adaptive minimum-BER algorithms were proposed in [3][5][6]. However, none of the proposed adaptive algorithms guarantees convergence to the global minimum, and the adaptive algorithms proposed in [3][5] are significantly more complex than the LMS algorithm.

In the remainder of this chapter, we review some relevant background materials for this thesis. In section 1.1, we review both ISI channels and multiuser interference channels. In section 1.2, we review general equalizers and multiuser detectors, their conventional design criteria, and some prior work on designing equalizers and multiuser detectors based on the error-probability criterion. In section 1.3, we outline this thesis.

1.1 INTERFERENCE CHANNELS

Interferences in communication channels are undesirable effects contributed by sources other than noise. In this section, we discuss two types of channel interferences: (1) intersymbol interference where adjacent data pulses distort the desired data pulse in a linear fashion and (2) interference in multiuser systems where users other than the intended contribute unwanted signals through an imperfect channel.

1.1.1 Intersymbol Interference

ISI characterized by (1-1) is the most commonly encountered channel impairment next to noise. ISI typically results from time dispersion which happens when the channel frequency response deviates from the ideal of constant amplitude and linear phase. In bandwidth-efficient digital communication systems, the effect of each symbol transmitted over a time-dispersive channel extends beyond the time interval used to represent that symbol. The distortion caused by the resulting overlap of received symbols is called ISI [7]. ISI can

significantly close the eye of a channel, reduce noise margin and cause severe data detection errors.

1.1.2 Multiuser Interference

Multiuser interference arises whenever a receiver observes signals from multiple transmitters [32]. In cellular radio-based networks using the time-division multiple-access (TDMA) technology, frequency re-use leads to interference from other users in nearby cells sharing the same carrier frequency, even if there is no interference among users within the same cell. In networks using the code-division multiple-access (CDMA) technology, users are assigned distinct signature waveforms with low mutual cross-correlations. When the sum of the signals modulated by multiple users is received, it is possible to recover the information transmitted from a desired user by correlating the received signal with a replica of the signature waveform assigned to the desired user. However, the performance of this demodulation strategy is not satisfactory when the assigned signatures do not have low cross-correlations for all possible relative delays. Moreover, even though the cross-correlations between users may be low, a particularly severe multiuser interference, referred to as near-far interference, results when powerful nearby interferers overwhelm distant users of interest. Similar to ISI, multiuser interference reduces noise margin and often causes data recovery impossible without some compensation means.

1.2 EQUALIZATION AND DETECTION

In the presence of linear ISI and additive white Gaussian noise, Forney [22][23] showed that the optimum detector for linear PAM signals is a whitened-matched filter followed by a Viterbi detector. This combined form achieves the maximum-likelihood sequence-detector (MLSD) performance and in some cases, the matched filter bound.

When the channel input symbols are drawn uniformly and independently from an alphabet set, MLSD is known to achieve the best error-probability performance of all existing equalizers and detectors.

Although MLSD offers significant performance gains over symbol-by-symbol detectors, its complexity (with the Viterbi detector) grows exponentially with the channel memory. For channels with long ISI spans, a full-state MLSD generally serves as a mere benchmark and is rarely used because of its large processing complexity for computing state metrics and large memory for storing survivor path histories. Many variants of MLSD such as channel memory truncation [24], reduced state sequence detection [26], and fixed-delay tree search with decision-feedback [25] have been proposed to reach good tradeoffs between complexity and performance.

Because of the often high complexity associated with MLSD, suboptimal receivers such as symbol-by-symbol equalizers are widely used despite their inferior performance [7]. Among all equalizers and detectors used for combating ISI, linear equalizers are the simplest to analyze and implement. A linear equalizer combats linear ISI by de-convolving a linearly distorted channel with a transversal filter to yield an approximate inverse of the channel, and a simple memoryless slicer is used to quantize the equalizer output to reconstruct the original noiseless transmitted symbols. Unlike MLSD, equalization enhances noise. By its design philosophy, a linear equalizer generally enhances noise significantly on channels with severe amplitude distortion and consequently, yields poor data recovery performance.

First proposed by Austin [27], the DFE is a significant improvement of the linear equalizer. A DFE is a nonlinear filter that uses past decisions to cancel the interference from prior symbols [29]–[31]. The DFE structure is beneficial for channels with severe

amplitude distortion. Instead of fully inverting a channel, only the forward section of a DFE inverts the precursor ISI, while the feedback section of a DFE, being a nonlinear filter, subtracts the post-cursor ISI. Assuming the past decisions are correct, noise enhancement is contributed only by the forward section of the equalizer and thus noise enhancement is reduced.

An obvious drawback of a DFE is error propagation resulting from its decision-feedback mechanism. A wrong decision may cause a burst of errors in the subsequent data detection. Fortunately, the error propagation is usually not catastrophic, and this drawback is often negligible compared to the advantage of reduced noise enhancement.

1.2.1 Conventional Design Criteria

For symbol-by-symbol equalization, zero forcing (ZF) is a well-known filter design criterion. Lucky [7]–[10] first proposed a ZF algorithm to automatically adjust the coefficients of a linear equalizer. A ZF equalizer is simple to understand and analyze. To combat linear ISI, a ZF linear equalizer simply eliminates ISI by forcing the overall pulse, which is the convolution of the channel and the equalizer, to become a unit-impulse response. Similarly, the forward section of a ZF-DFE converts the overall response to be strictly causal, while its feedback section completely subtracts the causal ISI.

An infinite-tap ZF equalizer can completely eliminate ISI if no null exists in the channel frequency response. By neglecting noise and concentrating solely on removing ISI, ZF equalizers tend to enhance noise exceedingly when channels have deep nulls. Although it has a simple adaptive algorithm, a ZF equalizer is rarely used in practice and remains largely a textbook result and teaching tool [7].

Following the pioneering work by Lucky, Gersho [11] and Proakis [12] proposed adaptive algorithms to implement MMSE equalizers. Unlike a ZF equalizer, an MMSE equalizer maximizes the signal-to-distortion ratios by penalizing both residual ISI and noise enhancement [7]–[18]. Instead of removing ISI completely, an MMSE equalizer allows some residual ISI to minimize the overall distortion.

Compared with a ZF equalizer, an MMSE equalizer is much more robust in the presence of deep channel nulls and modest noise. The popularity of the MMSE equalizer is due in part to the simple LMS algorithm proposed by Widrow and Hoff [16]. The LMS algorithm, which is a stochastic algorithm, adjusts equalizer coefficients with a small incremental vector in the steepest descent direction on the MSE error surface. Since the MSE error surface is convex, the convergence of the LMS algorithm to the global minimum can be guaranteed when the step size is sufficiently small.

1.2.2 Low-Complexity Adaptive Equalizer Algorithms

To reduce the complexity of the LMS algorithm, several simplified variants of the LMS algorithm have been proposed. The approximate-minimum-BER (AMBER) algorithm we propose in chapter 3 is remarkably similar in form to these LMS-based algorithms even though it originates from a minimum-error-probability criterion.

The sign LMS algorithm modifies the LMS algorithm by quantizing the error to ±1 according to its sign [20]. By doing so, the cost function of the sign LMS algorithm is the mean-absolute error, $E[|y_k - x_{k-D}|]$, instead of the mean-squared error as for the LMS algorithm. The trade-offs for the reduced complexity are a slower convergence rate and a larger steady-state MSE.

The dual-sign LMS algorithm proposed in [19] employs two different step sizes on the sign LMS algorithm. The algorithm penalizes larger errors with a larger update step size and therefore improves the convergence speed of the sign LMS algorithm with a small complexity increase.

The proportional-sign algorithm proposed in [21] modifies the LMS algorithm in order to be more robust to impulsive interference and to reduce complexity. The algorithm uses the LMS algorithm when the equalizer output errors are small and switches to the sign LMS algorithm when the equalizer output errors are large.

1.2.3 The Minimum-Error-Probability Criterion

Minimizing MSE should be regarded as an intermediate goal, whereas the ultimate goal of an equalizer or a multiuser detector is to minimize the error probability. In this section we review prior work that proposes stochastic adaptive algorithms for minimizing error probability or analyzes the structures of the minimum-error-probability equalizers or multiuser detectors [1]–[6].

Shamash and Yao [1] were the first to consider minimum-BER equalization. They examined the minimum-BER DFE structure for binary signaling. Using a calculus of variation procedure, they derived the minimum-BER DFE coefficients and showed that the forward section consists of a matched filter in tandem with a tap-delayed-line filter and the feedback section is a tap-delayed-line filter operating to completely cancel postcursor ISI. While the feedback section is similar to the MMSE DFE, the forward section is a solution to a set of complicated nonlinear equations. Their work focused on a theoretical derivation of the minimum-BER DFE structure and did not consider a numerical algorithm to compute the forward filter coefficients; nor did it compare the performance of the minimum-BER DFE to that of the MMSE DFE. Finally, an adaptive algorithm was not proposed.

For arbitrarily small and arbitrarily large SNR scenarios, Galko and Pasupathy [2] derived the minimum-BER linear equalizer for binary signaling. For the arbitrarily large SNR case, the minimum-BER linear equalizer was formed by maximizing the minimum eye opening. On the other hand, for the arbitrarily small SNR case, they showed that the minimum-BER linear equalizer is the average matched filter and proposed an efficient off-line algorithm to calculate the equalizer coefficients. Minimum-BER linear equalizers for arbitrary SNR and adaptive equalization algorithms were not considered.

Chen *et al.* [3] observed that the decision boundary formed by the minimum-BER equalizer can be quite different from the decision boundary formed by the MMSE equalizer and that significant BER reduction compared with the MMSE equalizer is possible. They proposed a stochastic DFE algorithm based on the BER gradient in an attempt to converge to the minimum-BER DFE. However, their algorithm requires significantly higher complexity than the LMS algorithm to estimate the channel and the noise variance and to compute the gradient of the BER. In addition, the converged DFE coefficients would not be the exact minimum-BER DFE coefficients since noisy, instead of noiseless, channel outputs were used to evaluate the gradient of the BER. Moreover, their algorithm does not guarantee global convergence to the minimum-BER solution.

Lupas and Verdú [4] proposed the maximum asymptotic multiuser efficiency (MAME) linear multiuser detector which, as noise power approaches zero, minimizes BER in a CDMA system. They also proposed the decorrelating detector, which offers a substantial improvement in asymptotic efficiency compared with the conventional matched-filter detector. In fact, the near-far resistance of the decorrelating detector equals that of the optimum multiuser detector. Nevertheless, they showed that asymptotic efficiency of the MAME linear detector is higher than that of the decorrelating detector. However, adaptive

implementation of the MAME detector was not proposed. Moreover, the MAME linear detector does not minimize BER when the noise power is nonzero.

Similar to the approach taken by Chen *et al.* [3], Mandayam and Aazhang [5] proposed a BER-gradient algorithm attempting to converge to the minimum-BER multiuser detector in a direct-sequence CDMA (DS-CDMA) system. They jointly estimated the data of all users in the maximum-likelihood sense and used these estimates to extract an estimate of the noiseless sum of all transmitted signature waveforms. This estimate was then used to compute unbiased BER gradients. The complexity of the algorithm is exceedingly high, especially when the number of users is large. In addition, the algorithm can converge to a non-global local minimum.

Based on a stochastic approximation method for finding the extrema of a regression function, Psaromiligkos *et al.* [6] proposed a simple linear DS-CDMA detector algorithm that does not involve the BER gradient. They derived a stochastic quantity whose expectation is BER and applied a stochastic recursion to minimize it. However, the algorithm can also converge to a nonglobal local BER minimum detector.

Although some important issues on minimum-error-probability equalizers and multiuser detectors were addressed by the above-mentioned prior works, a unified theory for minimum-error-probability equalization and multiuser detection is still not in place. In addition, the performance gap between the MMSE and minimum-error-probability equalizers and multiuser detectors has not been thoroughly investigated. Also, none of the above-mentioned prior works considered non-binary modulation. Most importantly, a simple, robust, and globally convergent stochastic algorithm had not yet been proposed to be comparable to its MMSE counterpart, the LMS algorithm.

1.3 THESIS OUTLINE

This thesis aims to design and adapt finite-tap equalizers and linear multiuser detectors to minimize error probability in the presence of intersymbol interference, multiuser interference, and Gaussian noise.

In chapter 2, we present system models and concepts which are essential in understanding the minimum-error-probability equalizers and multiuser detectors. We first derive a fixed-point relationship to characterize the minimum-error-probability linear equalizers. We then propose a numerical algorithm, called the *exact minimum-symbol-error-rate* (EMSER) algorithm, to determine the linear equalizer coefficients of Fig. 1-1 that minimize error probability. We study the convergence properties of the EMSER algorithm and propose a sufficiency condition test for verifying its convergence to the global error-probability minimum. We also extend the EMSER algorithm to QAM and DFE.

In chapter 3, we use a function approximation to alter the EMSER algorithm such that a very simple stochastic algorithm becomes available. We form a stochastic algorithm by incorporating an error indicator function whose expectation is related to the error probability. The proposed algorithm has low complexity and is intuitively sound, but nevertheless has some serious shortcomings. To overcome these shortcomings, an adaptation threshold is added to the stochastic algorithm to yield a modified algorithm, called the *approximate minimum-bit-error-rate* (AMBER) algorithm. Compared with the original stochastic algorithm, the AMBER algorithm has a faster convergence speed and is able to operate in a decision-directed mode. We compare the steady-state error probability of the AMBER equalizer with that of the MMSE equalizer. In addition, we device a crude characterize procedure to predict the ISI channels for which the AMBER and EMSER equalizers can outperform MMSE equalizers.

In chapter 4, we study the convergence properties of the AMBER algorithm and propose a variant to improve its convergence speed. We first take the expectation of the AMBER algorithm to derive its ensemble average. By obtaining its ensemble average, we analyze the global convergence properties of the AMBER algorithm. We then propose multi-step AMBER algorithms to further increase the convergence speed.

In chapter 5, we extend the results on the EMSER and AMBER equalizers to multiuser applications. Multiuser interference is similar in many respects to the ISI phenomenon in a single-user environment. We study the performance of the AMBER algorithm on multiuser channels without memory.

In chapter 6, we conclude our study and propose some interesting topics for future research.

CHAPTER 2

MINIMUM-SER EQUALIZATION

2.1 INTRODUCTION

As mentioned in chapter 1, an MMSE equalizer is generally different from the minimum-error-probability equalizer. Although most finite-tap linear equalizers are designed to minimize an MSE performance metric, the equalizer that directly minimizes symbol-error-rate (SER) may significantly outperform the MMSE equalizer. In this chapter, we first derive the minimum-SER linear equalizer for PAM. We study the properties of the minimum-SER equalizer by exploring its geometric interpretation and compare its SER performance to the MMSE equalizer. We also devise a numerical algorithm, called the *exact minimum-symbol-error-rate* (EMSER) algorithm, to compute the equalizer coefficients. We study the convergence properties of the EMSER algorithm. Finally we extend the derivation of the minimum-SER linear equalizer for PAM to QAM and DFE.

In section 2.2, we present the system model of the ISI channel and the linear equalizer, and we explain the concepts of signal vectors and signal cones, which are essential tools in deriving and understanding the minimum-SER equalizer and its adaptive algorithm. In section 2.3, we derive a fixed-point relationship to characterize the minimum-SER equalizer, and we compare the minimum-SER equalizer with the MMSE equalizer when the number of equalizer coefficients approaches infinity. In section 2.4, based on the fixed-point relationship, we propose a numerical method to compute the minimum-SER equalizer coefficients. We then study the convergence properties of the numerical method and state a sufficiency condition for testing convergence of the numerical method to the global SER minimum. In section 2.5, we extend the minimum-SER results on PAM to QAM. In section 2.6, we derive the minimum-SER decision-feedback equalizer.

2.2 MODELS FOR CHANNEL AND EQUALIZER

2.2.1 System Definition

Consider the real-valued linear discrete-time channel depicted in Fig. 2-1, where the channel input symbols x_k are drawn independently and uniformly from the L-ary PAM alphabet $\{\pm 1, \pm 3, \ldots, \pm(L-1)\}$, h_k is the FIR channel impulse response nonzero for $k = 0 \ldots M$ only, and n_k is white Gaussian noise with power spectral density σ^2. The channel output r_k is

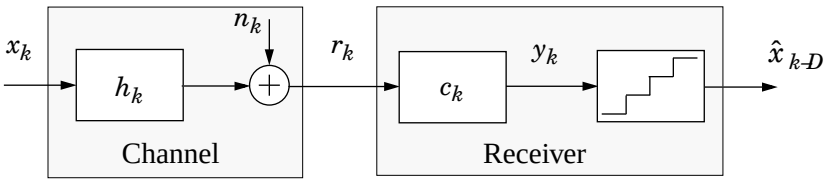

Fig. 2-1. Block diagram of channel, equalizer, and memoryless decision device.

$$r_k = \sum_{i=0}^{M} h_i x_{k-i} + n_k, \tag{2-1}$$

where M is the channel memory. Also shown in Fig. 2-1 is a linear equalizer with N coefficients, described by the vector $\boldsymbol{c} = [c_0 \ldots c_{N-1}]^T$. The equalizer output at time k can be expressed as the inner product:

$$y_k = \boldsymbol{c}^T \boldsymbol{r}_k, \tag{2-2}$$

where the channel output vector $\boldsymbol{r}_k = [r_k \ldots r_{k-N+1}]^T$ is

$$\boldsymbol{r}_k = \mathbf{H}\boldsymbol{x}_k + \boldsymbol{n}_k, \tag{2-3}$$

where $\boldsymbol{x}_k = [x_k \ldots x_{k-M-N+1}]^T$ is a vector of channel inputs, $\boldsymbol{n}_k = [n_k \ldots n_{k-N+1}]^T$ is a vector of noise samples, and $\mathbf{H}$ is the $N \times (M+N)$ Toeplitz channel convolution matrix satisfying $H_{ij} = h_{j-i}$:

$$\mathbf{H} = \begin{bmatrix} h_0 \ldots h_M \ 0 \ldots 0 \\ \ldots \\ 0 \ldots 0 \ h_0 \ldots h_M \end{bmatrix}. \tag{2-4}$$

As shown in Fig. 2-1, the decision $\hat{x}_{k-D}$ about symbol x_{k-D} is determined by quantizing the equalizer output y_k, where D accounts for the delay of both the channel and the equalizer. This memoryless decision device is suboptimal; better error probability performance can be achieved by performing maximum-likelihood sequence detection on the equalizer output.

After presenting the system definition, we are to derive the SER, the averaged probability $\hat{x}_{k-D} \neq x_{k-D}$, of an equalizer $\boldsymbol{c}$ on a PAM system. Let $\boldsymbol{f}^T = \boldsymbol{c}^T\mathbf{H} = [f_0 \ldots f_{M+N-1}]$

denote the overall impulse response, representing the cascade of the channel h_k and the equalizer $\boldsymbol{c}_k$. The noiseless equalizer output is

$$\begin{aligned} \boldsymbol{c}^T \mathbf{H} \boldsymbol{x}_k &= \boldsymbol{f}^T \boldsymbol{x}_k \\ &= f_D x_{k-D} + \sum_{i \neq D} f_i x_{k-i}, \end{aligned} \tag{2-5}$$

where the first term $f_D x_{k-D}$ represents the desired signal level, whereas the second term represents residual ISI. The noisy equalizer output of (2-2) is also expressed as:

$$y_k = f_D x_{k-D} + \sum_{i \neq D} f_i x_{k-i} + \boldsymbol{c}^T \boldsymbol{n}_k. \tag{2-6}$$

Since the residual ISI is symmetric about the desired signal levels, the memoryless quantizer, in the presence of zero-mean Gaussian noise, is optimal with its detection thresholds at the midpoints of successive signal levels, *i.e.* $\{0, \pm 2f_D, \ldots, \pm (L-2)f_D\}$. The SER is evaluated in the following theorem:

Theorem 2.1: With a memoryless quantizer, the SER $P_e(\boldsymbol{c})$ as a function of an equalizer $\boldsymbol{c}$ is

$$P_e(\boldsymbol{c}) = \frac{2L-2}{L} \mathrm{E}\left[Q\left(\frac{\boldsymbol{f}^T \tilde{\boldsymbol{x}}}{\|\boldsymbol{c}\| \sigma} \right) \right], \tag{2-7}$$

where $\tilde{\boldsymbol{x}}$ is a random vector with distribution $P(\tilde{\boldsymbol{x}}) = P(\boldsymbol{x}_k \mid x_{k-D} = 1)$, *i.e.*, $\tilde{\boldsymbol{x}}$ is uniformly distributed over the set of $K = L^{M+N-1}$ L-ary $\boldsymbol{x}_k$ vectors for which $x_{k-D} = 1$.

Proof. The SER for L-ary PAM is computed as follows:

$$\begin{aligned} P_e(\boldsymbol{c}) &= P(\hat{x}_{k-D} \neq x_{k-D}) \\ &= \sum_{l=1}^{L} P(\hat{x}_{k-D} \neq x_{k-D} \mid x_{k-D} = 2l-1-L)\, P(x_{k-D} = 2l-1-L) \end{aligned} \tag{2-8}$$

$$= \frac{1}{L} \sum_{l=1}^{L} P(\hat{x}_{k-D} \neq x_{k-D} \mid x_{k-D} = 2l - 1 - L), \tag{2-9}$$

where we substitute $P(x_{k-D} = 2l - 1 - L)$ with $\frac{1}{L}$ in (2-9) under the assumption that all L symbols are equally likely to be transmitted. Recall that the L-ary PAM alphabet has 2 outer symbols, *i.e.* $\pm(L-1)$, and $L-2$ inner symbols, *i.e.* $\{\pm 1, \ldots, \pm(L-3)\}$. If an inner symbol is transmitted, an error occurs when the equalizer output either exceeds the upper threshold *or* falls below the lower threshold of that particular inner symbol. The events that an equalizer output is above its upper threshold and is below its lower threshold are disjoint and thus the error probability $P[y_k > \text{TOP or } y_k < \text{LOW}]$ equals $P[y_k > \text{TOP}] + P[y_k < \text{LOW}]$. On the other hand, if the outer symbol $(L-1)$ is transmitted, an error occurs only if the equalizer output falls below the lower threshold $(L-2)f_D$; If the outer symbol $-(L-1)$ is transmitted, an error occurs only if the equalizer output exceeds the upper threshold $-(L-2)f_D$. Based on the above observations, (2-9) becomes:

$$\begin{aligned} P_e(\boldsymbol{c}) = \frac{1}{L} \Big\{ & P[y_k > -(L-2)f_D \mid x_{k-D} = -(L-1)] + \\ & P[(y_k > -(L-4)f_D) \mid x_{k-D} = -(L-3)] + P[(y_k < -(L-2)f_D) \mid x_{k-D} = -(L-3)] + \\ & \ldots + P[(y_k < (L-4)f_D) \mid x_{k-D} = L-3] + P[(y_k > (L-2)f_D) \mid x_{k-D} = L-3] + \\ & P[y_k < (L-2)f_D \mid x_{k-D} = L-1] \Big\}. \end{aligned} \tag{2-10}$$

Manipulating the expressions in (2-10) after substituting y_k into (2-10), we get

$$\begin{aligned} P_e(\boldsymbol{c}) = \frac{1}{L} \Big\{ & P[-\boldsymbol{c}^T \boldsymbol{n}_k < f_D + \sum_{i \neq D} f_i x_{k-i}] + \\ & P[-\boldsymbol{c}^T \boldsymbol{n}_k < f_D + \sum_{i \neq D} f_i x_{k-i}] + P[\boldsymbol{c}^T \boldsymbol{n}_k < f_D - \sum_{i \neq D} f_i x_{k-i}] + \ \ldots \ + \end{aligned}$$

$$P[\boldsymbol{c}^T\boldsymbol{n}_k < f_D - \sum_{i\neq D} f_i x_{k-i}] + P[-\boldsymbol{c}^T\boldsymbol{n}_k < f_D + \sum_{i\neq D} f_i x_{k-i}] + P[\boldsymbol{c}^T\boldsymbol{n}_k < f_D - \sum_{i\neq D} f_i x_{k-i}]\Big\}. \quad (2\text{-}11)$$

Note that in (2-11) we have removed the condition on the value of x_{k-D} from all expressions in (2-10) since they do not depend on the condition any more. In addition, the random variables $-\boldsymbol{c}^T\boldsymbol{n}_k$ and $-\sum_{i\neq D} f_i x_{k-i}$ respectively have the same probability distributions as $\boldsymbol{c}^T\boldsymbol{n}_k$ and $\sum_{i\neq D} f_i x_{k-i}$ and we can exchange them to simplify (2-11) as follows:

$$\begin{aligned}
P_e(\boldsymbol{c}) = \frac{1}{L}\Big\{ & P[\boldsymbol{c}^T\boldsymbol{n}_k < f_D + \sum_{i\neq D} f_i x_{k-i}] + \\
& P[\boldsymbol{c}^T\boldsymbol{n}_k < f_D + \sum_{i\neq D} f_i x_{k-i}] + P[\boldsymbol{c}^T\boldsymbol{n}_k < f_D + \sum_{i\neq D} f_i x_{k-i}] + \ \cdots \ + \\
& P[\boldsymbol{c}^T\boldsymbol{n}_k < f_D + \sum_{i\neq D} f_i x_{k-i}] + P[-\boldsymbol{c}^T\boldsymbol{n}_k < f_D + \sum_{i\neq D} f_i x_{k-i}] + \\
& P[\boldsymbol{c}^T\boldsymbol{n}_k < f_D + \sum_{i\neq D} f_i x_{k-i}]\Big\} \\
= \ & \frac{2L-2}{L} P[\boldsymbol{c}^T\boldsymbol{n}_k < f_D + \sum_{i\neq D} f_i x_{k-i}] \\
= \ & \frac{2L-2}{L} \ \frac{1}{K}\sum\nolimits_{i=1}^{K} P[\boldsymbol{c}^T\boldsymbol{n}_k < \boldsymbol{f}^T\boldsymbol{x}^{(i)}] \\
= \ & \frac{2L-2}{L} \ \frac{1}{K}\sum\nolimits_{i=1}^{K} Q\left(\frac{\boldsymbol{f}^T\boldsymbol{x}^{(i)}}{\|\boldsymbol{c}\|\sigma}\right) \\
= \ & \frac{2L-2}{L} \mathrm{E}\left[Q\left(\frac{\boldsymbol{f}^T\tilde{\boldsymbol{x}}}{\|\boldsymbol{c}\|\sigma}\right)\right], \qquad (2\text{-}12)
\end{aligned}$$

where Q is the Gaussian error function, where $\boldsymbol{x}^{(1)}$, $\boldsymbol{x}^{(2)}$, …, $\boldsymbol{x}^{(K)}$ are any ordering of the K distinct $\tilde{\boldsymbol{x}}$ vectors, and where the expectation is over the K equally likely $\tilde{\boldsymbol{x}}$ vectors. *Q.E.D.*

Therefore, minimizing SER of an L-PAM system is equivalent to minimizing the term $\mathrm{E}\left[Q\left(\frac{\boldsymbol{f}^T\tilde{\boldsymbol{x}}}{\|\boldsymbol{c}\|\sigma}\right)\right]$. In the case of a 2-PAM system, the factor $\frac{2L-2}{L}$ in (2-12) reduces to unity.

Even though it is most relevant to minimize the error probability of (2-12), by far the most popular equalization strategy is the MMSE design. With the MMSE strategy, the equalizer $\boldsymbol{c}$ is chosen as the unique vector minimizing $\mathrm{MSE} = \mathrm{E}[(y_k - x_{k-D})^2]$, namely:

$$\boldsymbol{c}_{MMSE} = (\mathbf{H}\mathbf{H}^T + \sigma^2\mathbf{I})^{-1}\boldsymbol{h}_{D+1}, \tag{2-13}$$

where $\boldsymbol{h}_{D+1}$ is the $(D+1)$-st column of $\mathbf{H}$. This equalizer is often realized using a stochastic gradient search known as the least-mean square (LMS) algorithm [7]:

$$\boldsymbol{c}_{k+1} = \boldsymbol{c}_k - \mu(y_k - x_{k-D})\boldsymbol{r}_k, \tag{2-14}$$

where μ is a small positive step size. When training data is unavailable, the equalizer can operate in a decision-directed mode, whereby the decision $\hat{x}_{k-D}$ is used in place of x_{k-D}.

Instead of minimizing MSE, our goal is to minimize SER (2-12). For a binary signaling channel it is obvious that BER is the same as SER. However, for a non-binary PAM channel, the exact relationship between SER and BER is not trivial. With the Gray code mapping of bits, the relationship is well approximated by [13]:

$$\mathrm{BER} \cong \frac{1}{\log_2 L}\,\mathrm{SER}. \tag{2-15}$$

Therefore, if an equalizer minimizes SER, it approximately minimizes BER.

2.2.2 Signal Vectors and Signal Cones

In this section, we introduce the signal vectors and the signal cone, two useful geometric tools that will be used extensively throughout the thesis to derive and understand minimum-SER equalizers.

We now establish the relationship between error probability and signal vectors. Observe that the error probability of (2-12) can also be expressed as

$$P_e(\boldsymbol{c}) = \frac{2L-2}{L}\,\mathrm{E}\left[Q\left(\frac{\boldsymbol{c}^T\mathbf{H}\tilde{\boldsymbol{x}}}{\|\boldsymbol{c}\|\sigma}\right)\right], \tag{2-16}$$

where the expectation is over the K equally likely L-ary $\tilde{\boldsymbol{x}}$ vectors. We define the *signal vectors* by

$$\boldsymbol{s}^{(i)} = \mathbf{H}\boldsymbol{x}^{(i)},\ i = 1 \ldots K. \tag{2-17}$$

From (2-3) we see that these $\boldsymbol{s}^{(i)}$ vectors represent the K possible noiseless channel output vectors given that the desired symbol is $x_{k-D} = 1$. With this definition, (2-16) can be expressed as

$$P_e(\boldsymbol{c}) = \frac{2L-2}{KL}\sum_{i=1}^{K} Q\left(\frac{\boldsymbol{c}^T\boldsymbol{s}^{(i)}}{\|\boldsymbol{c}\|\sigma}\right). \tag{2-18}$$

Observe that the error probability is proportional to the average of the K Q function terms, the argument of each being proportional to the inner product between the equalizer and a signal vector.

In this thesis we will often assume that the channel is *equalizable*:

> **Definition 1.** A channel is said to be *equalizable* by an N-tap equalizer with delay D if and only if there exists an equalizer $\boldsymbol{c}$ having a positive inner product with all $\{\boldsymbol{s}^{(i)}\}$ signal vectors.

A positive inner product with all $\{\boldsymbol{s}^{(i)}\}$ vectors implies that the noiseless equalizer output is always positive when a one was transmitted ($x_{k-D} = 1$); thus, a channel is equalizable if

and only if its noiseless eye diagram can be opened. In terms of the $\{\boldsymbol{s}^{(i)}\}$ vectors, a channel is equalizable if and only if there exists a hyperplane passing through the origin such that all $\{\boldsymbol{s}^{(i)}\}$ vectors are strictly on one side of the hyperplane.

Given a set of signal vectors $\{\boldsymbol{s}^{(i)}\}$ that can be located strictly on one side of a hyperplane passing through the origin, we define the *signal cone* as the span of these vectors with non-negative coefficients:

Definition 2. The *signal cone* of an equalizable channel is the set: $S = \{\Sigma_i \, a_i \boldsymbol{s}^{(i)} : a_i \geq 0\}$.

Observe that if the channel is equalizable, there exists at least one "axis" vector within the signal cone such that all elements of the signal cone form an angle of strictly less than 90˚ with respect to the axis vector. We remark that no such axis vector exists if the channel is not equalizable, because the set $\{\Sigma_i \, a_i \boldsymbol{s}^{(i)} : a_i \geq 0\}$ is a linear subspace of $\mathbb{R}^N$ in this case.

With the signal vectors and the signal cone defined, we are now equipped to characterize the minimum-SER equalizer.

2.3 CHARACTERIZATION OF THE MINIMUM-SER EQUALIZER

2.3.1 Fixed-Point Relationship

Let $\boldsymbol{c}_{EMSER}$ denote an equalizer that achieves exact minimum-SER (EMSER) performance, minimizing (2-16). Observe that because (2-16) depends only on the direction of the equalizer, $\boldsymbol{c}_{EMSER}$ is not unique: if $\boldsymbol{c}$ minimizes SER, then so does $a\boldsymbol{c}$ for any positive constant a. Unlike the coefficient vector $\boldsymbol{c}_{MMSE}$ (2-13) that minimizes MSE, there is no closed-form expression for $\boldsymbol{c}_{EMSER}$. However, by setting to zero the gradient of (2-16) with respect to $\boldsymbol{c}$:

$$\nabla_{\boldsymbol{c}} P_e(\boldsymbol{c}) = \frac{1}{\sqrt{2\pi}\sigma} \mathrm{E}\left[\exp\left(\frac{-(\boldsymbol{c}^T\boldsymbol{s})^2}{2\|\boldsymbol{c}\|^2\sigma^2}\right) \frac{\|\boldsymbol{c}\|^2\boldsymbol{s} - \boldsymbol{c}^T\boldsymbol{s}\boldsymbol{c}}{\|\boldsymbol{c}\|^3} \right] = \mathbf{0}, \tag{2-19}$$

we find that $\boldsymbol{c}_{EMSER}$, which is a global minimum solution to (2-16), must satisfy

$$\| \boldsymbol{c} \|^2 f(\boldsymbol{c}) = \boldsymbol{c}^T f(\boldsymbol{c}) \boldsymbol{c}, \tag{2-20}$$

where we have introduced the function $f : \mathbb{R}^N \to \mathbb{R}^N$, defined by

$$f(\boldsymbol{c}) = \mathrm{E}\left[\exp\left(\frac{-(\boldsymbol{c}^T\boldsymbol{s})^2}{2\|\boldsymbol{c}\|^2\sigma^2}\right) \boldsymbol{s} \right]. \tag{2-21}$$

The expectation in (2-21) is with respect to the random vector $\boldsymbol{s}$ over the K equally likely $\boldsymbol{s}^{(i)}$ vectors of (2-17). Thus, $f(\boldsymbol{c})$ can be expressed as a weighted sum of $\boldsymbol{s}^{(i)}$ vectors:

$$f(\boldsymbol{c}) = \frac{1}{K} \left(e^{-\alpha_1^2/2} \boldsymbol{s}^{(1)} + e^{-\alpha_2^2/2} \boldsymbol{s}^{(2)} + \ldots + e^{-\alpha_K^2/2} \boldsymbol{s}^{(K)} \right), \tag{2-22}$$

where $\alpha_i = \boldsymbol{c}^T\boldsymbol{s}^{(i)} / (\|\boldsymbol{c}\| \sigma)$ is a normalized inner product of $\boldsymbol{s}^{(i)}$ with $\boldsymbol{c}$.

The function $f(\boldsymbol{c})$ plays an important role in our analysis and has a useful geometric interpretation. Observe first that, because the exponential coefficients in (2-22) are all positive, $f(\boldsymbol{c})$ is inside the signal cone. Because $\exp(\cdot)$ is an exponentially decreasing function, (2-22) suggests that $f(\boldsymbol{c})$ is dictated by only those $\boldsymbol{s}^{(i)}$ vectors whose inner products with $\boldsymbol{c}$ are relatively small. Because the $\{\boldsymbol{s}^{(i)}\}$ vectors represent the K possible noiseless channel output vectors given that a one was transmitted (*i.e.* $x_{k-D} = 1$), the inner product $\boldsymbol{s}^{(i)}$ with $\boldsymbol{c}$ is a noiseless equalizer output given that a one is transmitted. It follows that a small inner product is equivalent to a nearly closed eye diagram. Therefore, $f(\boldsymbol{c})$ will be very nearly a linear combination of the few $\boldsymbol{s}^{(i)}$ vectors for which the eye diagram is most

closed. For example, if one particular $\boldsymbol{s}^{(i)}$ vector closes the eye significantly more than any other $\boldsymbol{s}^{(i)}$ vector, then $f(\boldsymbol{c})$ will be approximately proportional to that $\boldsymbol{s}^{(i)}$ vector.

Returning to (2-20) and the problem of finding the EMSER equalizer, we see that one possible solution of (2-20) is $f(\boldsymbol{c}) = \boldsymbol{0}$. We now show that $f(\boldsymbol{c}) = \boldsymbol{0}$ is impossible when the channel is equalizable. Recall that, if the channel is equalizable, then there exists a hyperplane passing through the origin such that all of the $\{\boldsymbol{s}^{(1)}, \ldots, \boldsymbol{s}^{(L)}\}$ vectors are strictly on one side of the hyperplane. Thus, any linear combination of $\boldsymbol{s}^{(i)}$ with strictly positive coefficients cannot be zero. Furthermore, (2-22) indicates that $f(\boldsymbol{c})$ is a linear combination of $\{\boldsymbol{s}^{(i)}\}$ vectors with strictly positive coefficients. Thus, we conclude that $f(\boldsymbol{c}) = \boldsymbol{0}$ is impossible when the channel is equalizable.

Since $f(\boldsymbol{c}) = \boldsymbol{0}$ is impossible when the channel is equalizable, the only remaining solution to (2-20) is the following fixed-point relationship:

$$\boldsymbol{c} = a f(\boldsymbol{c}), \tag{2-23}$$

for some constant a. Choosing $a = 0$ results in $P_e = (L-1)/L$, which is clearly not the minimum error probability of an equalizable channel. The sign of a does not uniquely determine whether $\boldsymbol{c} = a f(\boldsymbol{c})$ is a local minimum or local maximum; however, in order for $\boldsymbol{c} = a f(\boldsymbol{c})$ to be a global minimum, a must be positive:

Lemma 2-1: If $\boldsymbol{c}$ minimizes error probability of an equalizable channel, then

$$\boldsymbol{c} = a f(\boldsymbol{c}) \text{ with } a > 0. \tag{2-24}$$

Proof. By contradiction: Suppose that $\boldsymbol{c} = a f(\boldsymbol{c})$ minimizes error probability with $a < 0$. Then $\boldsymbol{c}$ is outside the signal cone generated by $\{\boldsymbol{s}^{(i)}\}$. Let P denote any hyper-

plane, containing the origin, that separates $\boldsymbol{c}$ from the signal cone. Let $\boldsymbol{c}'$ denote the reflection of $\boldsymbol{c}$ about P such that $\boldsymbol{c}'$ and the signal cone are on the same side of P. It is easy to show that compared with $\boldsymbol{c}$, $\boldsymbol{c}'$ has a larger inner product with all $\boldsymbol{s}^{(i)}$ vectors. From (2-18) it follows that the error probability for $\boldsymbol{c}'$ is smaller than the error probability for $\boldsymbol{c}$, which contradicts the assumption that $\boldsymbol{c}$ minimizes error probability. *Q.E.D.*

Unfortunately, the fixed-point relationship of (2-24) is not sufficient in describing the EMSER equalizer; it simply states a necessary condition that the EMSER equalizer must satisfy. The existence of at least one unit-length vector $\tilde{\boldsymbol{c}} = \frac{\boldsymbol{c}}{\|\boldsymbol{c}\|}$ satisfying (2-23) can be intuitively explained: The hypersphere of all unit-length vectors $\tilde{\boldsymbol{c}}$ is closed, continuous, and bounded. Each point on the hypersphere is mapped to a real value via the differentiable and bounded error probability function of (2-18) and forms another closed, continuous, and bounded surface. Because the resultant surface is everywhere differentiable, closed, and bounded, it has at least one local minimum. In general, there exist more than one local minima, as illustrated in the following example.

Example 2-1: Consider binary signaling $x_k \in \{\pm 1\}$ with a transfer function $H(z) = -0.9 + z^{-1}$ and a two-tap linear equalizer ($N = 2$) and delay $D = 1$. In Fig. 2-2 we present a polar plot of BER (for BPSK, the error probability equals BER) versus θ, where $\frac{\boldsymbol{c}}{\|\boldsymbol{c}\|} = [\cos\theta, \sin\theta]^T$. Superimposed on this plot are the $K = 4$ signal vectors $\{\boldsymbol{s}^{(1)}, \ldots, \boldsymbol{s}^{(4)}\}$, depicted by solid lines. Also superimposed are three unit-length equalizer vectors (depicted by dashed lines): the EMSER equalizer with an angle of $\theta = -7.01^\circ$, the MMSE equalizer with $\theta = -36.21^\circ$, and a local minimum equalizer ($\tilde{\boldsymbol{c}}_{LOCAL}$) with $\theta = 35.63^\circ$. (A fourth equalizer with an angle of $\theta = -5.84^\circ$ is also depicted for future reference: it is the approximate minimum-

BER (AMBER) equalizer defined by Theorem 3.1 of section 3.2.) The shaded region denotes the signal cone. Although both $\tilde{\boldsymbol{c}}_{EMSER}$ and $\tilde{\boldsymbol{c}}_{LOCAL}$ satisfy (2-23) with $a > 0$, the local-minimum equalizer $\tilde{\boldsymbol{c}}_{LOCAL}$ does not minimize BER, and it does not open the eye diagram. These equalizers assume SNR = 20 dB.

While Lemma 2-1 provides a necessary condition for the EMSER equalizer, namely $\boldsymbol{c} = a\boldsymbol{f}(\boldsymbol{c})$ with $a > 0$, the previous example illustrates that this fixed-point condition is not

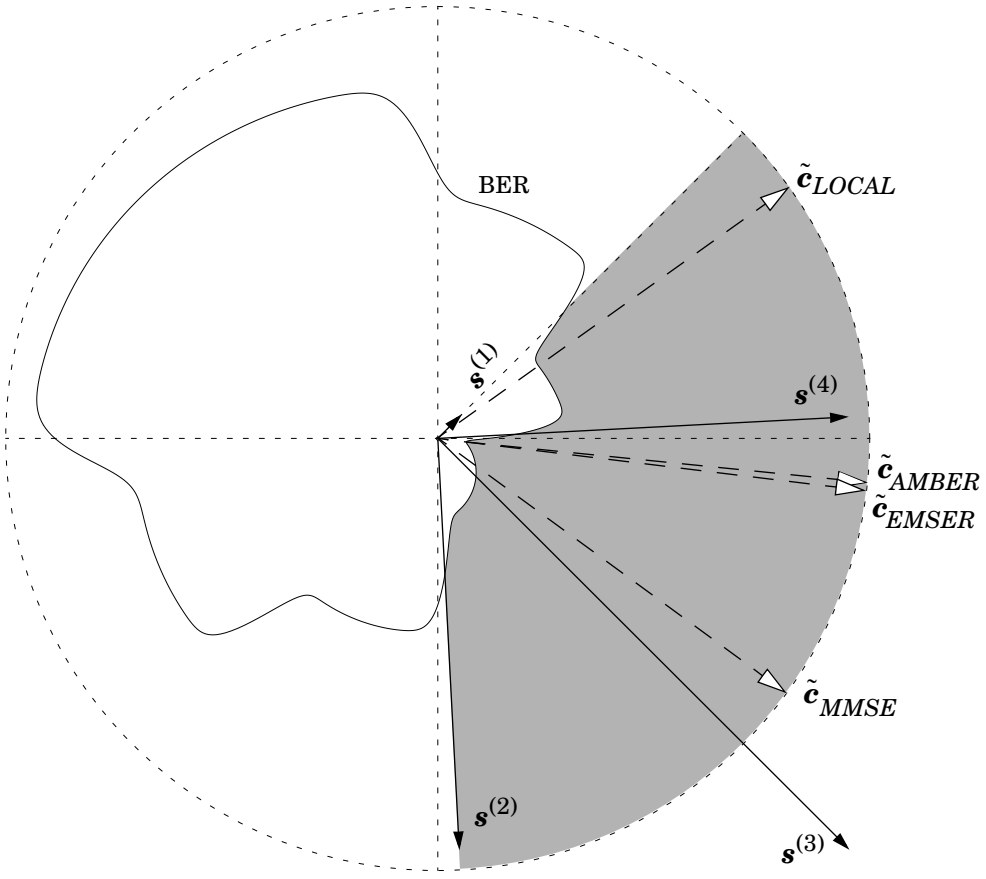

Fig. 2-2. A polar plot of BER versus θ for Example 2-1. Superimposed are the signals vectors (scaled by a factor of 0.5), and four equalizer vectors (dashed lines).

sufficient; both $\boldsymbol{c}_{EMSER}$ and $\boldsymbol{c}_{LOCAL}$ satisfy $\boldsymbol{c} = af(\boldsymbol{c})$ with $a > 0$, but only $\boldsymbol{c}_{EMSER}$ minimizes error probability.

As an aside, an interesting example can be constructed to show that the EMSER equalizer may not open the eye even when opening the eye is possible (*i.e.* when the channel is equalizable). The following example is somewhat counter-intuitive and is a result of the highly irregular shape of the error probability surface.

Example 2-2: Consider the binary signaling channel $H(z) = 1 - z^{-1} + 1.2z^{-2}$ with a two-tap equalizer, $D = 3$, and SNR = 10 dB. Although the channel is equalizable, neither the EMSER equalizer nor the MMSE equalizer opens the eye.

2.3.2 The MMSE Equalizer vs. the EMSER Equalizer

We now compare the MMSE and the EMSER equalizers. With a finite number of taps, the MMSE and the EMSER equalizers are clearly two different equalizers, as illustrated in Example 2-1. We further emphasize the differences between the two equalizers by evaluating their error-probability performance and by plotting their eye diagrams in the following examples.

Example 2-3: Consider a binary-signaling channel with transfer function $H(z) = 1.2 + 1.1z^{-1} - 0.2z^{-2}$. In Fig. 2-3, we plot BER versus SNR = $\sum_k h_k^2/\sigma^2$, for both the MMSE and EMSER equalizer with three and five taps. The figure shows that with three equalizer taps and a delay of $D = 2$. D is chosen to minimize MSE. The EMSER equalizer has a more than 6.5 dB gain over the MMSE equalizer. With 5 equalizer taps and a delay of $D = 4$, the EMSER equalizer has a nearly 2 dB gain over the MMSE equalizer. In Fig. 2-4, for the same channel, we present “artificial” noiseless eye patterns for 5-tap EMSER and MMSE equalizers, assuming SNR =

30 dB. These patterns were obtained by interpolating all possible noiseless equalizer outputs with a triangular pulse shape. Both equalizers were normalized to have identical norm (and thus identical noise enhancement). We see that the two eye diagrams are drastically different. The interesting difference between the two diagrams results from the MMSE equalizer's effort to force all possible equalizer outputs to the targets $\{\pm 1\}$, despite the benefits of sparing the outputs with large noise immunity. Although the MMSE equalizer achieves a lower mean-squared error, its error probability is more than a magnitude higher than the error probability of the EMSER equalizer.

Example 2-4: Consider a 4-PAM ISI channel with transfer function $H(z) = 0.66 + z^{-1} - 0.66\, z^{-2}$. In Fig. 2-5, we plot SER versus SNR = $\sum_k h_k^2/\sigma^2$, considering both MMSE and EMSER equalizers with five taps. The figure shows that with a delay of $D = 3$, the EMSER equalizer has a more than 16 dB gain over the MMSE equalizer. In Fig. 2-6, we again present "artificial" noiseless eye patterns for 5-tap EMSER and MMSE equalizers, assuming SNR = 30 dB. We observe that the eye patterns of the MMSE equalizer are somewhat uniform, whereas the eye patterns of the EMSER equalizer consist mainly of "sub-clusters." In a certain sense, the EMSER equalizer strives only to open the eye of the channel, and can be regarded as a somewhat "passive" equalization technique, where as the MMSE equalization is "aggressive" in that it pushes all equalizer outputs towards the desired constellation points. Again, we observe that the EMSER equalizer achieves a much lower error probability than the MMSE equalizer, even though it has a much higher MSE.

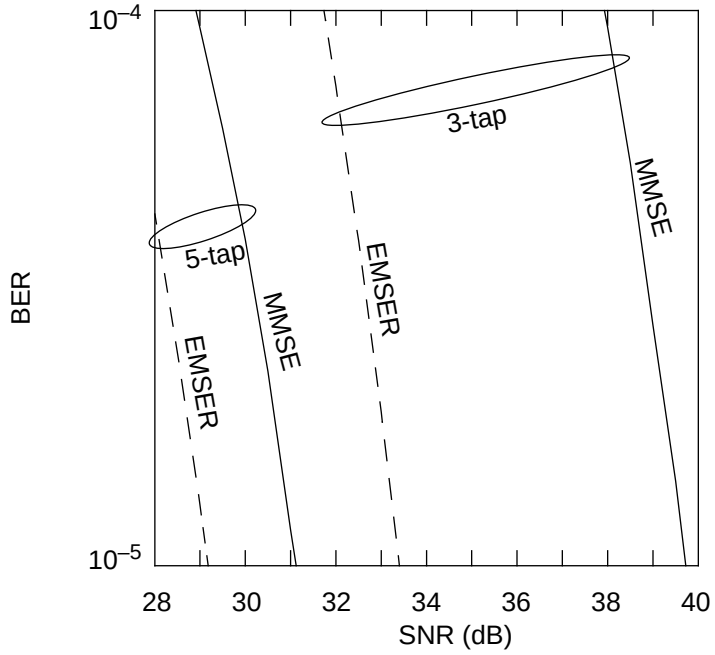

Fig. 2-3. The BER performance comparison of the EMSER and the MMSE equalizers for the 2-PAM system of Example 2-3.

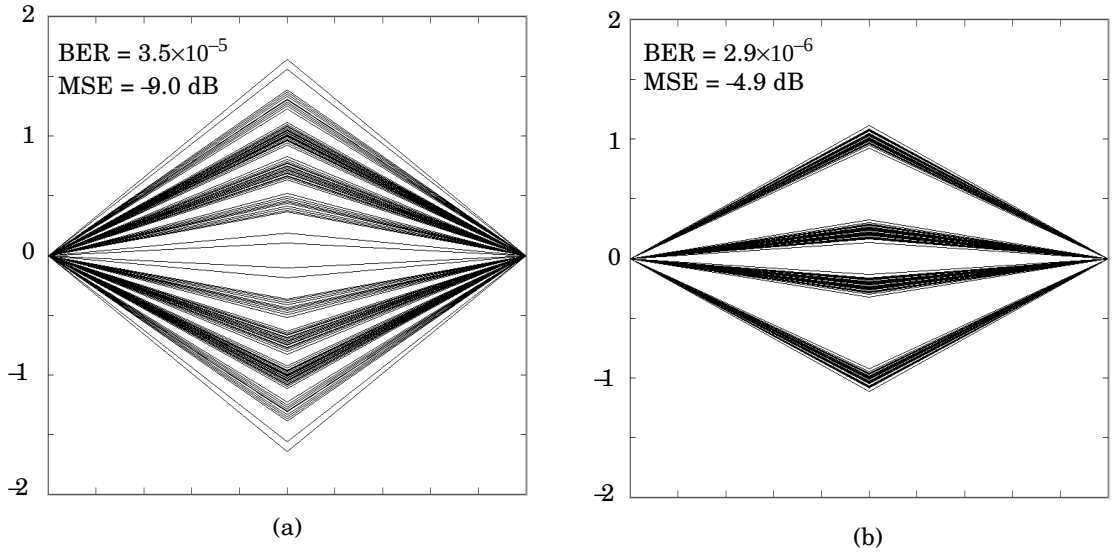

Fig. 2-4. Equalized noiseless eye diagrams of the (a) MMSE and (b) EMSER equalizers for the 2-PAM system of Example 2-3.

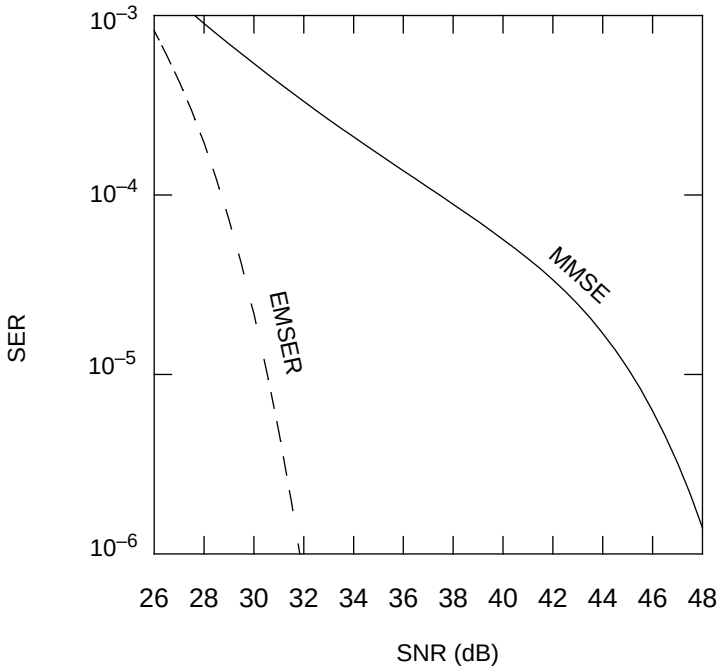

Fig. 2-5. The SER performance comparison of the 5-tap EMSER and MMSE equalizers for the 4-PAM system of Example 2-4.

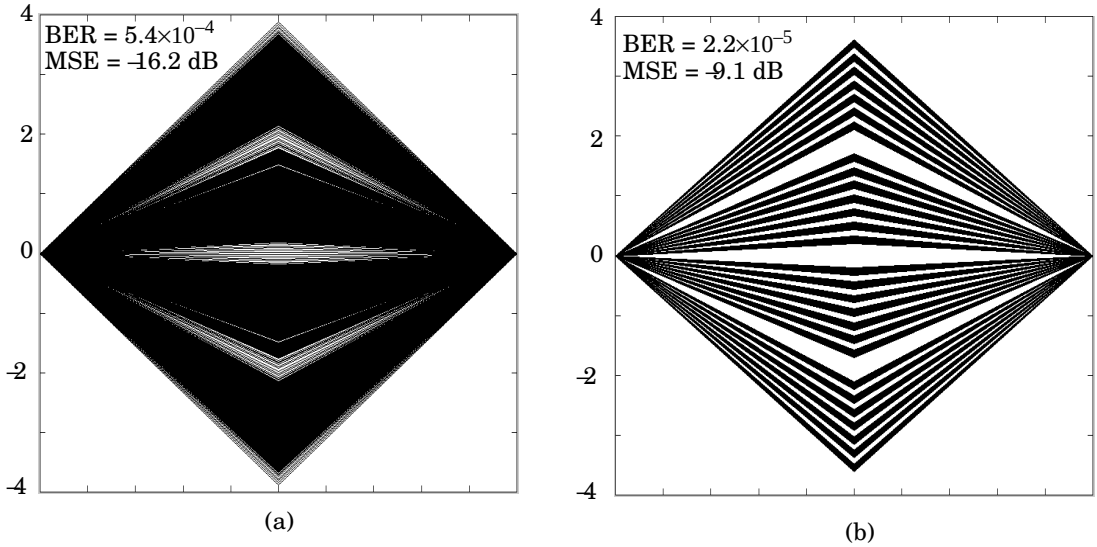

Fig. 2-6. Equalized noiseless eye diagrams of the (a) MMSE and (b) EMSER equalizers for the 4-PAM system of Example 2-4.

It is obvious from the above two examples that the finite-tap MMSE and the EMSER equalizers are different. Here we investigate the possibility that the infinite-tap MMSE and the EMSER equalizers are the same by proposing the following conjecture:

Conjecture: For any noise variance, the MMSE equalizer converges to the EMSER equalizer as the number of equalizer taps approaches infinity.

Example 2-5: Consider a binary-signaling system with transfer function $H(z) = 1.2 + 1.1\,z^{-1} - 0.2\,z^{-2}$. In Fig. 2-7, we plot SNR required to achieve BER = 10^{-5} versus the number of equalizer taps for the EMSER and MMSE equalizers. For each number of equalizer taps, the delay D is chosen to minimize MSE. We see that the SNR gain of the EMSER equalizer over the MMSE equalizer approaches zero as the number of equalizer taps increases.

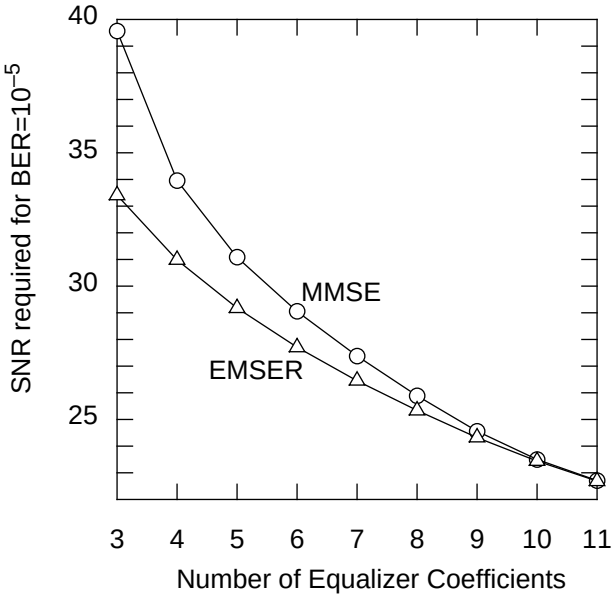

Fig. 2-7. SNR requirement vs. equalizer length for the binary signaling channel in Example 2-5.

Example 2-6: Consider another binary-signaling system with transfer function $H(z) = 1.2 + 0.7\,z^{-1} - 0.9\,z^{-2}$. In Fig. 2-8, we again plot SNR required to achieve BER = 10^{-5} versus the number of equalizer taps for the EMSER and MMSE equalizers. It is interesting to note that the required SNR for BER = 10^{-5} actually *increases* for the MMSE equalizer as we increase the number of taps from three to four. Although increasing the number of an MMSE equalizer taps strictly decrease MSE, it does not strictly decrease error probability. Again, the SNR gain of the EMSER equalizer over the MMSE equalizer approaches zero as the number of equalizer taps becomes large.

As the noise variance approaches zero, it is well known that the MMSE equalizer approaches the zero-forcing (ZF) equalizer. We note that the infinite-tap EMSER equalizer also approaches the infinite-tap ZF equalizer as the noise variance approaches zero by the

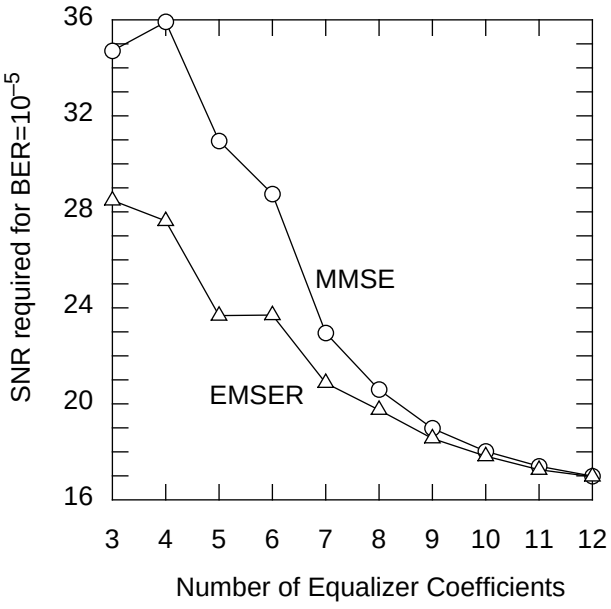

Fig. 2-8. SNR requirement vs. equalizer length for the binary signaling channel in Example 2-6.

following reasoning: If an equalizer $\boldsymbol{c}$ has an infinite number of taps, it can invert a FIR channel completely, *i.e.* there exists a zero-forcing vector $\boldsymbol{c}$ such that the inner products between $\boldsymbol{c}$ and all signal vectors $\boldsymbol{s}^{(i)}$ are unity. If the infinite-tap minimum-SER equalizer does not equal the zero-forcing vector, some inner products $\boldsymbol{c}^T\boldsymbol{s}^{(i)}$ are smaller than others and thus, as the noise variance approaches zero, the overall SER is solely dictated by the Q term associated with the smallest inner product. A lower SER can be obtained by adjusting $\boldsymbol{c}$ to increase the smallest inner product until it equals the largest inner product, or when the equalizer becomes the ZF equalizer.

It is not clear whether the infinite-tap MMSE equalizer equals the infinite-tap EMBER equalizer with an arbitrary noise variance. An interesting observation is that the MMSE linear equalizer with a large number of taps tends to make the residual ISI Gaussian-like, although this Gaussian-like distribution is bounded. A true Gaussian random variable is unbounded.

2.4 A NUMERICAL METHOD

In section 2.3, we have gained some good understanding of the EMSER equalizer by characterizing it with a fixed-point relationship. We now proceed to devise a numerical algorithm to actually compute the EMSER equalizer coefficients.

2.4.1 The Deterministic EMSER Algorithm

Example 2-1 in the previous section illustrates that the error probability function may not be convex. Nevertheless, a gradient algorithm may still be used to search for a local minimum. In particular, using the gradient (2-19) of the SER (2-16), we may form a gradient algorithm:

$$\begin{aligned}\boldsymbol{c}_{k+1} &= \boldsymbol{c}_k - \mu_1 \nabla_{\boldsymbol{c}_k} P_e \\ &= \left(1 - \mu \boldsymbol{c}_k^T f(\boldsymbol{c}_k)/\|\boldsymbol{c}_k\|^2\right)\boldsymbol{c}_k + \mu f(\boldsymbol{c}_k) \\ &= \left(1 - \mu \boldsymbol{c}_k^T f(\boldsymbol{c}_k)/\|\boldsymbol{c}_k\|^2\right)\left(\boldsymbol{c}_k + \frac{\mu}{1 - \mu \boldsymbol{c}_k^T f(\boldsymbol{c}_k)/\|\boldsymbol{c}_k\|^2} f(\boldsymbol{c}_k)\right),\end{aligned} \tag{2-25}$$

where the function $f(\cdot)$ is defined by (2-21). Recall that the norm of $\boldsymbol{c}$ has no impact on P_e, and observe that the first bracketed factor in (2-25) represents an adjustment of the norm of $\boldsymbol{c}_{k+1}$. Eliminating this factor leads to the following recursion, which we refer to as the *EMSER algorithm*:

$$\boldsymbol{c}_{k+1} = \boldsymbol{c}_k + \mu f(\boldsymbol{c}_k). \tag{2-26}$$

The transformation from (2-25) to (2-26) affects the convergence rate, the steady-state norm $\|\boldsymbol{c}_\infty\|$, and possibly the steady-state direction $\boldsymbol{c}_\infty/\|\boldsymbol{c}_\infty\|$, so it is no longer appropriate to call (2-26) a gradient search algorithm. The update equation (2-26) can be viewed as an iterative system designed to recover the solution to the fixed-point equation (2-24).

2.4.2 Convergence

Although the EMSER algorithm cannot in general be guaranteed to converge to the global SER minimum, it is guaranteed to converge to some local extremum solution within the signal cone generated by $\{\boldsymbol{s}^{(i)}\}$, as stated in the following theorem:

Theorem 2.2: Given an equalizable channel, the EMSER algorithm of (2-26) converges to a local extremum solution satisfying $\boldsymbol{c} = af(\boldsymbol{c})$ with $a > 0$.

Proof. The proof for Theorem 2.2 is in Appendix 2.1.

2.4.3 A Sufficiency Condition for Convergence to the Global Minimum

One general method for finding the EMSER equalizer is to find all solutions to the fixed-point equation $\boldsymbol{c} = a\boldsymbol{f}(\boldsymbol{c})$ with $a > 0$, and choose the solution that yields the smallest error probability. Fortunately, this brute-force method can be avoided in certain cases by taking advantage of the following sufficiency test:

Theorem 2.3: If $\boldsymbol{c} = a\boldsymbol{f}(\boldsymbol{c})$ for $a > 0$ and $P_e(\boldsymbol{c}) \le \frac{L-1}{LK}$, then $\boldsymbol{c}$ minimizes SER.

Proof. The proof for Theorem 2.3 is in Appendix 2.2.

This is a sufficient but not necessary condition for minimizing error probability because even the minimum error probability may exceed $\frac{L-1}{LK}$ when the SNR is sufficiently low. Note that the condition in Theorem 2.3 implies that the equalizer opens the eye diagram.

Taken together, Theorem 2.2 and Theorem 2.3 suggest the following strategy for finding the EMBER equalizer. First, iterate the deterministic EMSER algorithm of (2-26) until it converges. If the resulting SER $P_e \le \frac{L-1}{LK}$, stop. Otherwise, initialize the deterministic EMSER algorithm somewhere else and repeat the process. This is an effective strategy when the initial condition of the EMSER algorithm is chosen carefully (*e.g.* within the eye opening region) and when the SNR is not so small that $P_e \le \frac{L-1}{LK}$ is impossible.

2.5 EXTENSION TO QUADRATURE-AMPLITUDE MODULATION

Quadrature-amplitude modulation (QAM) is widely used on bandwidth-limited channels. Although thus far we have only discussed the EMSER equalizers for PAM systems, a QAM system can be thought as two PAM systems in parallel. The results of the EMSER

linear equalizer on the PAM system can be extended in a straightforward manner to the QAM system.

An L^2-QAM symbol is complex and consists two PAM symbols, one as its real part and the other as its imaginary part:

$$x = x^R + j x^I, \tag{2-27}$$

where x^R and x^I are two independent L-PAM symbols. To detect an QAM symbol, a 2-dimensional quantizer is used. However, the quantizer actually uses two 1-dimensional quantizers to separately detect x^R and x^I. In that sense, we can treat an L^2-QAM system as two L-PAM systems and thus, its error probability can be treated as

$$P_e = \frac{1}{2} P_e^R + \frac{1}{2} P_e^I \tag{2-28}$$

where P_e^R and P_e^I are the real and imaginary SER.

$$= \frac{L-1}{L}\left(\mathrm{E}\left[Q\left(\frac{(\boldsymbol{c}^T \boldsymbol{s}_1)^R}{\|\boldsymbol{c}\|\sigma} \right) \right] + \mathrm{E}\left[Q\left(\frac{(\boldsymbol{c}^T \boldsymbol{s}_j)^I}{\|\boldsymbol{c}\|\sigma} \right) \right] \right). \tag{2-29}$$

where we have introduced signal vectors $\boldsymbol{s}_1$ and $\boldsymbol{s}_j$ for a QAM system where

$$\boldsymbol{s}_{R_1} = \mathbf{H}\boldsymbol{x}_{R_1} \text{ and } \boldsymbol{s}_{I_1} = \mathbf{H}\boldsymbol{x}_{I_1} \tag{2-30}$$

where $\boldsymbol{s}_{R_1}$ is a random vector uniformly distributed over all noiseless QAM channel output vectors given that the real part of the desired symbol is 1, *i.e.* $x_{k-D}^R = 1$, whereas $\boldsymbol{s}_{I_1}$ is a random vector uniformly dis represent all possible noiseless QAM channel output vectors given that the quadrature part of the desired symbol is 1, *i.e.* $x_{k-D}^I = 1$.

To extend the EMSER algorithm to the QAM system, we take the derivative of the error probability of (2-29) with respect to the in-phase equalizer coefficient vector $\boldsymbol{c}^R$ and the quadrature equalizer coefficient vector $\boldsymbol{c}^I$. Following the derivation of (2-25), we obtain the EMSER algorithm for $\boldsymbol{c}^R$:

$$\boldsymbol{c}_{k+1}^R = \boldsymbol{c}_k^R + \mu f^R(\boldsymbol{c}_k), \tag{2-31}$$

and the EMSER algorithm for $\boldsymbol{c}^I$:

$$\boldsymbol{c}_{k+1}^I = \boldsymbol{c}_k^I + \mu f^I(\boldsymbol{c}_k), \tag{2-32}$$

where the driving vector term $f^R(\boldsymbol{c})$ is

$$f^R(\boldsymbol{c}) = \mathrm{E}\left[\exp\left(\frac{-[(\boldsymbol{c}^T \boldsymbol{s}_1)^R]^2}{2\|\boldsymbol{c}\|^2 \sigma^2} \right) \boldsymbol{s}_1^R \right] + \mathrm{E}\left[\exp\left(\frac{-[(\boldsymbol{c}^T \boldsymbol{s}_j)^I]^2}{2\|\boldsymbol{c}\|^2 \sigma^2} \right) \boldsymbol{s}_j^I \right] \tag{2-33}$$

and the driving vector term $f^I(\boldsymbol{c}_k)$ is:

$$f^I(\boldsymbol{c}) = -\mathrm{E}\left[\exp\left(\frac{-[(\boldsymbol{c}^T \boldsymbol{s}_1)^R]^2}{2\|\boldsymbol{c}\|^2 \sigma^2} \right) \boldsymbol{s}_1^I \right] + \mathrm{E}\left[\exp\left(\frac{-[(\boldsymbol{c}^T \boldsymbol{s}_j)^I]^2}{2\|\boldsymbol{c}\|^2 \sigma^2} \right) \boldsymbol{s}_j^R \right]. \tag{2-34}$$

Combining equations (2-31)-(2-34), the EMSER update equation for a QAM system is

$$\boldsymbol{c}_{k+1} = \boldsymbol{c}_k + \mu f_{\mathrm{QAM}}(\boldsymbol{c}_k) \tag{2-35}$$

where

$$f_{\mathrm{QAM}}(\boldsymbol{c}) = \mathrm{E}\left[\exp\left(\frac{-[(\boldsymbol{c}^T \boldsymbol{s}_1)^R]^2}{2\|\boldsymbol{c}\|^2 \sigma^2} \right) \boldsymbol{s}_1^* \right] + \mathrm{E}\left[\exp\left(\frac{-[(\boldsymbol{c}^T \boldsymbol{s}_j)^I]^2}{2\|\boldsymbol{c}\|^2 \sigma^2} \right) \boldsymbol{s}_j \right]. \tag{2-36}$$

2.6 EXTENSION TO DECISION-FEEDBACK EQUALIZATION

A decision-feedback equalizer is a straightforward extension of a linear equalizer. As mentioned in chapter 1, the feedback filter of an MMSE DFE subtracts off the post cursor ISI in order to minimize MSE. In this subsection, we show that similar to the MMSE DFE, the feedback filter of the EMSER DFE is also chosen to eliminate the post cursor ISI. In fact, we can show that if a forward filter of a DFE is fixed and opens the eye of a channel, then the feedback filter of a DFE need only eliminate the post cursor ISI in order to minimize error probability. In this subsection we concentrate the derivation of the minimum-SER DFE for the PAM systems. Its extension to QAM is straightforward.

Let $\boldsymbol{c} = [c_0 \ldots c_{N_1-1}]^T$ and $\boldsymbol{d} = [d_1 \ldots d_{N_2}]^T$ denote respectively the forward and the feedback filters of a DFE. Let $\boldsymbol{f}^T = \boldsymbol{c}^T\mathbf{H} = [f_0 \ldots f_D \ldots f_{M+N_1-1}]$ denote the impulse response of the convolution of the forward filter and the channel. The noiseless equalizer output prior to decision feedback subtraction is

$$\boldsymbol{f}^T\boldsymbol{x}_k = \sum_{i=0}^{D-1} f_i x_{k-i} + f_D x_{k-D} + \sum_{i=D+1}^{M+N_1-1} f_i x_{k-i}. \tag{2-37}$$

For now we assume that the length of the feedback filter is the same as the length of the postcursor residual ISI, *i.e.* $N_2 = M + N_1 - 1$. Observe that the error probability with correct decision feedback is

$$P_e(\boldsymbol{c}, \boldsymbol{d}) = \frac{2L-2}{L}\mathrm{E}\left[Q\left(\frac{\sum_{i=0}^{D-1} f_i x_{k-i} + f_D + \sum_{i=D+1}^{M+N_1-1}(f_i - d_{i-D})x_{k-i}}{\|\boldsymbol{c}\|\sigma}\right)\right], \tag{2-38}$$

where the expectation is over the L^{M+N_1-1} equally likely L-ary $\tilde{\boldsymbol{x}}$ vectors. For a given $\boldsymbol{f}$, we determine the coefficient vector $\boldsymbol{d}$ in order to minimize the error probability of (2-38).

We see that there are L^D possible points from $\sum_{i=0}^{D-1} f_i x_{k-i} + f_D$ which form a cloud centered at f_D. When we add $\sum_{i=D+1}^{M+N_1-1} (f_i - d_{i-D}) x_{k-i}$ to $\sum_{i=0}^{D-1} f_i x_{k-i} + f_D$ to form the noiseless equalizer output, we in a sense add a sub-cloud to each of the L^D points. Each sub-cloud disappears if $(f_i - d_{i-D}) = 0$ for $i = D+1 \ldots M + N_1 - 1$. However, if $(f_i - d_{i-D})$ is not zero for some i, the error probability becomes strictly greater than for $(f_i - d_{i-D}) = 0$ for all i. We explain this by constructing the following inequality:

$$2Q(A) \le Q(A+B) + Q(A-B), \tag{2-39}$$

where A is positive. This inequality is an immediate result from the fact that the Q function is a monotonously and exponentially decreasing function. The inequality in (2-39) becomes a strict equality only when B is zero. Thus we conclude that if the length is long enough, the feedback section of a EMSER DFE subtracts off the post-cursor ISI completely.

In the case when the length of the feedback filter is greater than the length of the post-cursor residual ISI (*i.e.* $N_2 > M + N_1 - 1$), the additional taps of the feedback filter will be zeros. On the other hand, when the length of the feedback filter is less than the length of the postcursor residual ISI (*i.e.* $N_2 < M + N_1 - 1$), based on the inequality of (2-39), the EMSER equalizer sets $d_{i-D} = f_i$ for $i = D+1 \ldots N_2$.

We now construct a numerical algorithm to recover the coefficients of a minimum-BER DFE. The numerical algorithm for the forward section of the DFE is

$$\boldsymbol{c}_{k+1} = \boldsymbol{c}_k + \mu f(\boldsymbol{c}_k, \boldsymbol{d}_k), \tag{2-40}$$

where

$$f(\boldsymbol{c}, \boldsymbol{d}) = \mathrm{E}\left[\exp\left(\frac{-(\boldsymbol{c}^T \boldsymbol{s} - \sum_{i=D+1}^{N_2} d_i x_{k-i})^2}{2\|\boldsymbol{c}\|^2 \sigma^2} \right) \boldsymbol{s} \right]. \tag{2-41}$$

We see that the forward filter is driven by its noiseless input vectors weighted by their conditional error probabilities. We can set the feedback section of the DFE to be the same as the post cursor ISI:

$$\boldsymbol{d} = [f_{D+1} \cdots f_{N_2}]. \tag{2-42}$$

2.7 SUMMARY AND CONCLUSIONS

In this chapter, we have introduced the concepts of the signal vectors and signal cone and used them to characterize the EMSER linear equalizer for the PAM ISI channel. We have shown that the EMSER equalizer must satisfy a particular fixed-point equation. We have shown that error probability function is generally not a convex function of the equalizer coefficients, and there are usually multiple solutions to the fixed-point equation. To find the EMSER equalizer, we have constructed a numerical algorithm based on the fixed-point equation. We have proved that the algorithm is guaranteed to converge to a solution to the fixed-point equation for any positive step size. Further, we have proposed a sufficiency condition for testing whether the algorithm has indeed converged to the global EMSER solution. In addition, we have extended the EMSER results on PAM to both QAM and DFE.

From our theoretical analysis and some numerical examples, we have concluded that the EMSER equalizer can be very different from the MMSE equalizer, depending on the ISI channel and the number of the equalizer taps. Some dramatical SNR gains of the EMSER equalizer over the MMSE equalizer found in this chapter have motivated us to proceed to finding an adaptive equalizer algorithm to minimize SER instead of MSE.

APPENDIX 2.1

PROOF OF THEOREM 2.2

In this appendix, we prove Theorem 2.2 on page 34: For any equalizable channel, the EMSER algorithm of (2-26) converges to a local extremum solution satisfying $\boldsymbol{c} = af(\boldsymbol{c})$ for $a > 0$.

Since the $\boldsymbol{s}^{(i)}$ vectors generate a signal cone, we can find a hyperplane P, containing the origin, such that all $\boldsymbol{s}^{(i)}$ vectors are strictly on one side of P. Every $\boldsymbol{s}^{(i)}$ makes an angle of $\theta_i \in [0, 90°)$ with the normal to P and consists of two components: one (with norm $\|\boldsymbol{s}^{(i)}\|\sin\theta_i$) parallel to P and the other (with norm $\|\boldsymbol{s}^{(i)}\|\cos\theta_i$) perpendicular to P. At each update, the correction vector $\mu f(\boldsymbol{c}_k)$ is strictly inside the signal cone and its norm is lower bounded by $\mu\exp(-\|\boldsymbol{s}\|_{\max}^2/2\sigma^2)\|\boldsymbol{s}\|_{\min}\cos\theta_{\max}$, where $\|\boldsymbol{s}\|_{\min} = \min_i\{\|\boldsymbol{s}^{(i)}\|\}$, $\|\boldsymbol{s}\|_{\max} = \max_i\{\|\boldsymbol{s}^{(i)}\|\}$, and $\theta_{\max} = \max_i\{\theta_i\}$. At iteration $M + 1$, the sum of the past M correction

vectors is a vector strictly inside the signal cone and has a norm lower bounded by $M\mu\exp(-\|\boldsymbol{s}\|_{\max}^2/2\sigma^2)\|\boldsymbol{s}\|_{\min}\cos\theta_{\max}$. We conclude that, for any initial $\boldsymbol{c}_0$ with a finite norm, there exists a finite M such that $\boldsymbol{c}_{M+1}$ is strictly inside the cone. In addition, we conclude that equalizer norm $\|\boldsymbol{c}_k\|$ grows without bound as k increases.

Showing that $\boldsymbol{c}_k$ converges to the direction of an extremum solution satisfying $\boldsymbol{c} = af(\boldsymbol{c})$ with $a > 0$ is equivalent to showing that the angle between $\boldsymbol{c}_k$ and $f(\tilde{\boldsymbol{c}}_k)$, where $\tilde{\boldsymbol{c}}_k$ equals $\boldsymbol{c}_k / \|\boldsymbol{c}_k\|$, approaches zero. First we observe that $\tilde{\boldsymbol{c}}_k$ must converge to some fixed vector $\tilde{\boldsymbol{c}}_\infty$, since $\|\boldsymbol{c}_k\|$ becomes arbitrarily large while the norm of the update, $\|\mu f(\tilde{\boldsymbol{c}}_k)\|$, is upper-bounded by $\mu\|\boldsymbol{s}\|_{\max}$. It follows that $f(\tilde{\boldsymbol{c}}_k)$ converges to $f(\tilde{\boldsymbol{c}}_\infty)$, and thus, for any $\varepsilon > 0$, there exists a finite $k(\varepsilon)$ such that for all $k > k(\varepsilon)$, $|\|f(\tilde{\boldsymbol{c}}_k)\| - \|f(\tilde{\boldsymbol{c}}_\infty)\|| \le \|f(\tilde{\boldsymbol{c}}_k) - f(\tilde{\boldsymbol{c}}_\infty)\| < \varepsilon$. Manipulating the inequalities yields that the angle between $f(\tilde{\boldsymbol{c}}_k)$ and $f(\tilde{\boldsymbol{c}}_\infty)$ is less than some $\theta(\varepsilon)$, where

$$\theta(\varepsilon) = \cos^{-1}\left[\frac{1 - \varepsilon/\|f(\tilde{\boldsymbol{c}}_\infty)\|}{1 + \varepsilon/\|f(\tilde{\boldsymbol{c}}_\infty)\|}\right]. \tag{2-43}$$

For any $M > 0$, $\sum_{j=0}^{M-1} f(\tilde{\boldsymbol{c}}_{k(\varepsilon)+j})$ is a vector strictly within the cone $W[f(\tilde{\boldsymbol{c}}_\infty); \theta(\varepsilon)]$ consisting of all vectors less than $\theta(\varepsilon)$ away from $f(\tilde{\boldsymbol{c}}_\infty)$. For a $\boldsymbol{c}_{k(\varepsilon)}$ with a finite norm, we can find a finite M such that $\boldsymbol{c}_{k(\varepsilon)+M} = \boldsymbol{c}_{k(\varepsilon)} + \mu\sum_{j=0}^{M-1} f(\tilde{\boldsymbol{c}}_{k(\varepsilon)+j})$ is strictly inside $W[f(\tilde{\boldsymbol{c}}_\infty); \theta(\varepsilon)]$. As ε approaches 0, $\theta(\varepsilon)$ approaches 0 and thus the angle between $\boldsymbol{c}_{k(\varepsilon)+M}$ and $f(\tilde{\boldsymbol{c}}_{k(\varepsilon)+M})$ approaches 0 as well. *Q.E.D.*

APPENDIX 2.2

PROOF OF THEOREM 2.3

In this appendix, we prove Theorem 2.3 on page 35: If $\boldsymbol{c} = af(\boldsymbol{c})$ for $a > 0$ and the error probability is less than $\frac{L-1}{LK}$, then $\boldsymbol{c}$ minimizes error probability.

Let $\mathbb{E} \subseteq \mathbb{R}^N$ denote the set of all eye-opening equalizers having unit length, *i.e.*, $\mathbb{E}$ is the set of unit-length vectors having positive inner product with all $\boldsymbol{s}^{(i)}$ signal vectors. This set is not empty when the channel is equalizable. We can write $\mathbb{E} = \bigcap_{i=1}^{K} \mathbb{E}_i$, where $\mathbb{E}_i = \{\boldsymbol{e}: \boldsymbol{e}^T\boldsymbol{s}^{(i)} > 0, \ \|\boldsymbol{e}\| = 1\}$. Observe from (2-18) that the condition $P_e(\boldsymbol{c}) \leq \frac{L-1}{LK}$ implies that the equalizer $\boldsymbol{c}$ opens the eye, $\frac{\boldsymbol{c}}{\|\boldsymbol{c}\|} \in \mathbb{E}$.

We now show that if $\boldsymbol{c} \in \mathbb{E}$ and $\boldsymbol{c} = af(\boldsymbol{c})$ with $a > 0$ then $\boldsymbol{c}$ globally minimizes error probability. First, observe from (2-18) that any equalizer not in $\mathbb{E}$ will have an error probability of $\frac{L-1}{LK}$ or greater, whereas at least one equalizer within $\mathbb{E}$ (namely $\boldsymbol{c}$) has an error probability $P_e \leq \frac{L-1}{LK}$, so that the global minimum must be in the eye-opening region $\mathbb{E}$.

However, as shown below, error probability has only one local minimum over $\mathbb{E}$; thus, the local extremum $\boldsymbol{c} = af(\boldsymbol{c})$ must be a local minimum and thus must be the global minimum.

It remains to show that error probability has only one local minimum over the eye-opening region $\mathbb{E}$. Let B be a map from the unit-radius hypersphere $\mathbb{B}$ to $\mathbb{R}^N$ according to $B(\boldsymbol{e}) = P(\boldsymbol{e})\boldsymbol{e}$. The function B shrinks each element of the unit-radius hypersphere by its corresponding error probability. Let $B(\mathbb{B}) \subseteq \mathbb{R}^N$ denote the resulting surface. Because $Q(\cdot) \leq 1$, the error probability surface $B(\mathbb{B})$ is wholly contained within the unit-radius hypersphere $\mathbb{B}$. Observe that $P(\boldsymbol{c})$ of (2-18) is the arithmetic average of K separate Q functions, so that $B(\boldsymbol{e}) = \frac{1}{K}\sum_{i=1}^{K} B_i(\boldsymbol{e})$, where $B_i(\boldsymbol{e}) = Q(\boldsymbol{e}^T\boldsymbol{s}^{(i)}/\sigma)\boldsymbol{e}$. Geometrically, each contributing surface $B_i(\mathbb{B}) \in \mathbb{R}^N$ has the approximate shape of a balloon when poked by a finger, with a global minimum in the direction of $\boldsymbol{s}^{(i)}$. In Fig. 2-9 we illustrate the four contributing surfaces $B_1(\mathbb{B})$ through $B_4(\mathbb{B})$ for the channel of Example 2-1. Although each surface $B_i(\mathbb{B})$ is not convex over the entire sphere $\mathbb{B}$, each is convex when restricted to the hemisphere $\mathbb{E}_i$, and hence so is $B_i(\mathbb{E})$. (A surface is convex if the line connecting any two points on the surface does not touch the surface.) Being the sum of convex functions, it follows that $B(\mathbb{E}) = \frac{1}{K}\sum_{i=1}^{K} B_i(\mathbb{E})$ is convex over the eye-opening region $\mathbb{E}$. But a convex function has at most one local minimum. *Q.E.D.*

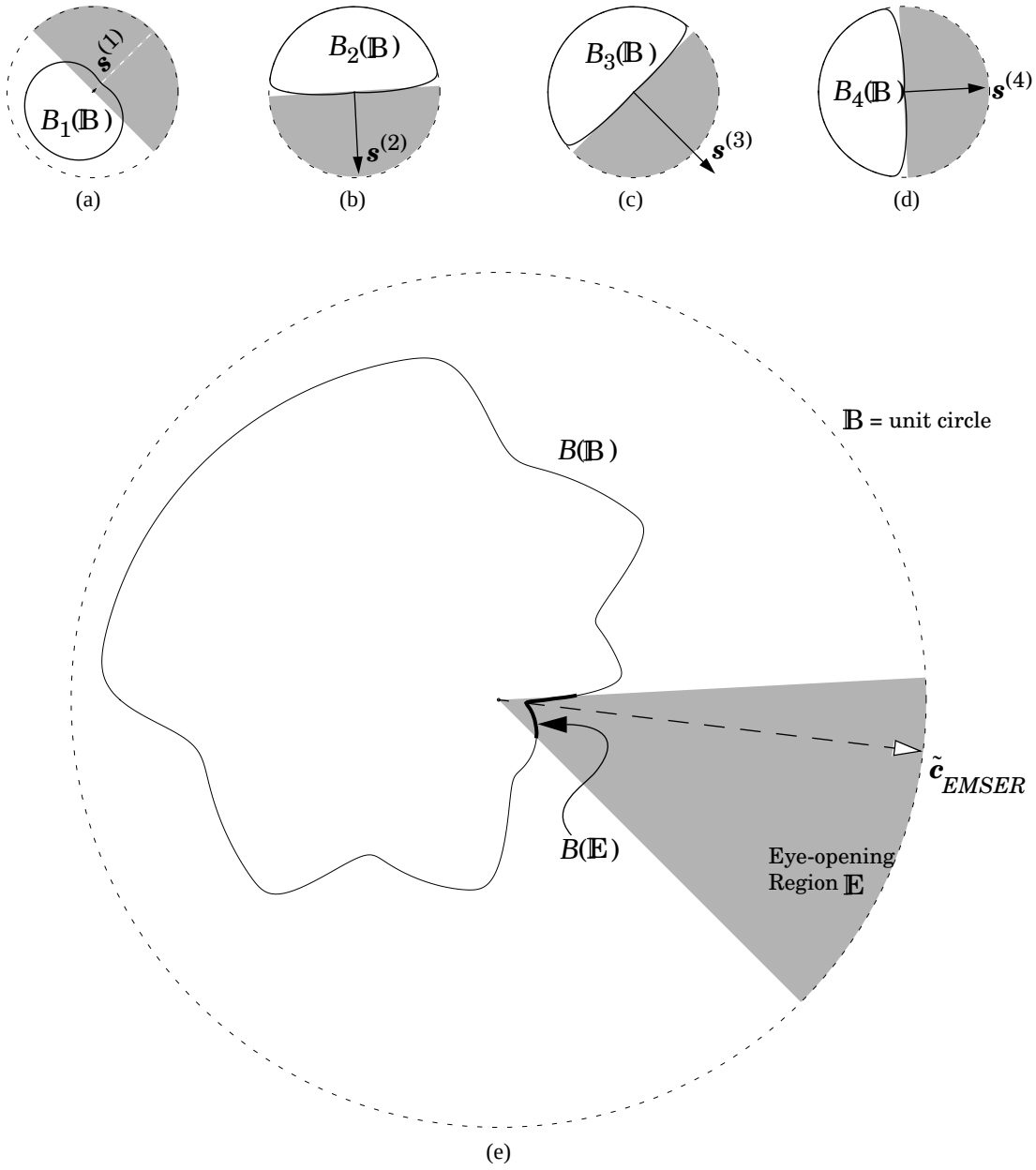

Fig. 2-9. Illustration for Proof of Theorem 2.3 based on the channel of Example 2-1. The BER surface $B(\mathbb{B})$ in (e) is the arithmetic average of the surfaces $B_1(\mathbb{B})$ through $B_4(\mathbb{B})$ in (a) through (d). The shaded regions in (a) through (d) are $\mathbb{E}_1$ through $\mathbb{E}_4$, respectively. The shaded region in (e) is the eye opening region $\mathbb{E}$, defined as the intersection of $\mathbb{E}_1$ through $\mathbb{E}_4$. Because each $B_i(\mathbb{E}_i)$ is convex, $B(\mathbb{E})$ is convex.

CHAPTER 3

ADAPTIVE EQUALIZATION USING THE AMBER ALGORITHM

3.1 INTRODUCTION

Although the EMSER algorithm of the previous chapter is useful for finding the minimum-SER equalizer of known channels, it is poorly suited for adaptive equalization. We now propose the *approximate minimum-bit-error-rate* (*AMBER*) algorithm for adapting the coefficients of an equalizer for both PAM and QAM channels. While less complex than the LMS algorithm, AMBER very nearly minimizes error probability in white Gaussian noise and can significantly outperform the MMSE equalizer when the number of equalizer coefficients is small relative to the severity of the intersymbol interference.

In section 3.2, we approximate the fixed-point relationship of the EMSER equalizer. In section 3.3, we propose a globally convergent numerical algorithm to recover the solution to the approximate fixed-point equation. In section 3.4, we transform the numerical algorithm into a stochastic equalizer algorithm, namely the AMBER algorithm. We discuss some key parameters, such as an error indicator function and an update threshold, of the AMBER algorithm. We then extend the AMBER algorithm to QAM and DFE. In section 3.5, we perform computer simulations to evaluate and compare the error probability performance of the MMSE, the EMSER, and the AMBER equalizers. In addition, we empirically characterize the ISI channels over which the EMSER and the AMBER equalizers are more beneficial than the MMSE equalizer. In section 3.6, we summarize our results.

3.2 FUNCTIONAL APPROXIMATION

As mentioned in chapter 2, by setting to zero the gradient of (2-12) with respect to the equalizer $\boldsymbol{c}$, we find that the $\boldsymbol{c}$ minimizing error probability must satisfy the EMSER fixed-point equation $\boldsymbol{c} = af(\boldsymbol{c})$ for some $a > 0$. For convenience, we again state $f(\boldsymbol{c})$ of (2-22) here:

$$f(\boldsymbol{c}) = \frac{1}{K}\left(e^{-\alpha_1^2/2}\boldsymbol{s}^{(1)} + e^{-\alpha_2^2/2}\boldsymbol{s}^{(2)} + \ldots + e^{-\alpha_K^2/2}\boldsymbol{s}^{(K)} \right), \tag{3-1}$$

where $\alpha_i = \boldsymbol{c}^T\boldsymbol{s}^{(i)}/(\|\boldsymbol{c}\|\,\sigma)$ is a normalized inner product of $\boldsymbol{s}^{(i)}$ with $\boldsymbol{c}$.

Instead of using the EMSER fixed-point relationship, we use an approximate fixed-point relationship for reasons that will become apparent later on. Recall that the error function $Q(\alpha)$ is upper bounded and approximated by $0.5\exp(\alpha^2/2)$, as shown in Fig. 3-1

[14]. Observe that the two functions have slopes close to each other. With this approximation, we can approximate $f(\boldsymbol{c})$ as follows:

$$f(\boldsymbol{c}) \approx \frac{\sqrt{2\pi}}{K}\left(\alpha_1 Q(\alpha_1)\boldsymbol{s}^{(1)} + \alpha_2 Q(\alpha_2)\boldsymbol{s}^{(2)} + \ldots + \alpha_L Q(\alpha_K)\boldsymbol{s}^{(K)}\right) \tag{3-2}$$

$$\approx \frac{\sqrt{2\pi}}{K}\alpha_{\min}\left(Q(\alpha_1)\boldsymbol{s}^{(1)} + Q(\alpha_2)\boldsymbol{s}^{(2)} + \ldots + Q(\alpha_K)\boldsymbol{s}^{(K)}\right) \tag{3-3}$$

$$= \sqrt{2\pi}\,\alpha_{\min} g(\boldsymbol{c}), \tag{3-4}$$

where $\alpha_{\min} = \min\{\alpha_i\}$, and where we have introduced the vector function $g : \mathbb{R}^N \to \mathbb{R}^N$:

$$g(\boldsymbol{c}) = \frac{1}{K}\left(Q(\alpha_1)\mathbf{s}^{(1)} + Q(\alpha_2)\boldsymbol{s}^{(2)} + \ldots + Q(\alpha_K)\boldsymbol{s}^{(K)}\right) \tag{3-5}$$

$$= \mathrm{E}\left[Q\left(\frac{\boldsymbol{c}^T\boldsymbol{s}}{\|\boldsymbol{c}\|\sigma}\right)\boldsymbol{s}\right]. \tag{3-6}$$

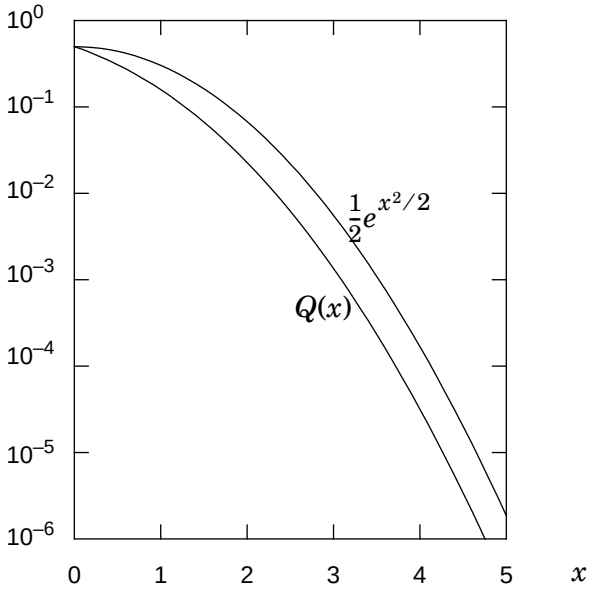

Fig. 3-1. A comparison of $Q(\alpha)$ and $\frac{1}{2}\exp(\alpha^2/2)$.

Comparing (3-1) and (3-5), we see that the vector function $g(\boldsymbol{c})$ has the same form as $f(\boldsymbol{c})$, but with $Q(\alpha)$ replacing $\exp(-\alpha^2/2)$. The approximation in (3-3) is valid because only the terms in (3-2) for which $\alpha_i \approx \alpha_{\min}$ are relevant, and the other terms have negligible impact. In analogy to the EMSER fixed-point relationship, we define the approximate minimum-bit-error-rate (AMBER) fixed-point relationship by:

$$\boldsymbol{c} = a g(\boldsymbol{c}), \text{ for some } a > 0. \tag{3-7}$$

We define that the equalizer satisfying (3-7) as the AMBER equalizer. Because $Q(\cdot)$ is also an exponentially decreasing function, (3-5) suggests that $g(\boldsymbol{c})$ is dictated by only these signal vectors whose inner products with $\boldsymbol{c}$ are relatively small. Thus, the AMBER equalizer will be very nearly a linear combination of the few signal vectors for which the eye diagram is most closed.

The following theorem shows that, although there may be numerous unit-length solutions to the EMSER fixed-point equation $\boldsymbol{c} = a f(\boldsymbol{c})$ for $a > 0$, there is only *one* unit-length solution to $\boldsymbol{c} = a g(\boldsymbol{c})$ for $a > 0$; call it $\tilde{\boldsymbol{c}}_{AMBER}$. This is one obvious advantage of this approximate fixed-point relationship (3-7) over the EMSER fixed-point relationship (2-24).

Theorem 3.1: For an equalizable channel there is a unique unit-length vector $\tilde{\boldsymbol{c}}_{AMBER}$ satisfying the AMBER fixed-point relationship of (3-7).

Proof. The proof of Theorem 3.1 is in Appendix 3.1.

We will learn in section 3.4 that a more important advantage of the approximate fixed-point relationship over the EMSER fixed-point relationship is its amenability to a simple stochastic implementation.

While the equalizer $\boldsymbol{c}_{AMBER}$ no longer minimizes error probability exactly, the accuracy with which $Q(x)$ approximates $\frac{1}{2}e^{-x^2/2}$ for large x suggests that $\boldsymbol{c}_{AMBER}$ closely approximates the EMSER equalizer at high SNR. The simulation results in section 3.5 will substantiate this claim.

3.3 A NUMERICAL METHOD

Recall that we constructed a numerical algorithm to recover solutions to the EMSER fixed-point relationship of (2-24). To recover solutions to the AMBER fixed-point relationship, we use a similar approach by proposing the following numerical algorithm:

$$\boldsymbol{c}_{k+1} = \boldsymbol{c}_k + \mu\, g(\boldsymbol{c}_k), \tag{3-8}$$

where μ is a positive step size.

Because there exists only one unique solution to $\boldsymbol{c} = ag(\boldsymbol{c})$ for $a > 0$, we can prove the global convergence of this numerical algorithm:

Theorem 3.2: If the channel is equalizable, the numerical algorithm of (3-8) is guaranteed to converge to the direction of the unique unit-length vector $\tilde{\boldsymbol{c}}_{AMBER}$ satisfying $\tilde{\boldsymbol{c}} = ag(\tilde{\boldsymbol{c}})$ for $a > 0$.

Proof. The proof of Theorem 3.2 is in Appendix 3.2.

3.4 STOCHASTIC IMPLEMENTATION

As mentioned before, the EMSER algorithm is useful only when the channel is known and thus is not suitable for stochastic implementation. The main advantage of the numerical algorithm of (3-8) is that there exists a simple stochastic implementation.

3.4.1 Error Indicator Function

At first glance, (3-8) is only more complicated than the EMSER algorithm of (2-26). However, the replacement of the exponential function with the Gaussian error function motivates a simplified adaptation algorithm. Let us first introduce an error indicator function $I(x_{k-D}, y_k)$ to indicate the *presence* and *sign* of an error: let $I = 0$ if no error occurs, let $I = 1$ if an error occurs because y_k is too negative, and let $I = -1$ if an error occurs because y_k is too positive. In other words:

$$I(x_{k-D}, y_k) = \begin{cases} 1, & \text{if } y_k < (x_{k-D} - 1)f_D \text{ and } x_{k-D} \neq -L + 1, \\ -1, & \text{if } y_k > (x_{k-D} + 1)f_D \text{ and } x_{k-D} \neq L - 1, \\ 0, & \text{otherwise.} \end{cases} \tag{3-9}$$

Thus, we see that the expectation of the squared error indicator function is simply the error probability:

$$\mathrm{E}[I^2] = \frac{2L-2}{L}\,\mathrm{E}\left[Q\left(\frac{\boldsymbol{c}^T\boldsymbol{s}}{\|\boldsymbol{c}\|\sigma}\right)\right]. \tag{3-10}$$

This equation suggests that there maybe a connection between the error indicator function and the numerical algorithm of (3-8), where the equalizer is adapted by signal vectors weighted by their conditional error probabilities. In fact, we can relate the error indicator function to $g(\boldsymbol{c})$ by the following theorem:

Theorem 3.3: The error indicator is related to $g(\boldsymbol{c})$ by

$$\mathrm{E}[I\,\boldsymbol{r}_k] = \frac{2L-2}{L}\left\{g(\boldsymbol{c}) - \varepsilon(\boldsymbol{c})\boldsymbol{c}\right\}, \tag{3-11}$$

where $\varepsilon(\boldsymbol{c})$ is a small positive constant.

Proof. The proof of Theorem 3.3 is in Appendix 3.3.

Theorem 3.3 allows us to use the error indicator function to simplify the numerical algorithm of (3-8) as follows:

$$\boldsymbol{c}_{k+1} = \boldsymbol{c}_k + \mu g(\boldsymbol{c}_k) \tag{3-12}$$

$$= \boldsymbol{c}_k + \mu(\mathrm{E}[I\,\boldsymbol{r}_k] + \varepsilon(\boldsymbol{c}_k)\boldsymbol{c}_k) \tag{3-13}$$

$$= (1 + \mu\varepsilon(\boldsymbol{c}_k))\boldsymbol{c}_k + \mu\mathrm{E}[I\,\boldsymbol{r}_k]. \tag{3-14}$$

$$\approx \boldsymbol{c}_k + \mu\mathrm{E}[I\,\boldsymbol{r}_k], \tag{3-15}$$

where the approximation in (3-15) is accurate when $\mu\varepsilon(\boldsymbol{c})$ is small.

When the step size μ is significantly small, an ensemble average can be well approximated by a time average, and we can remove the expectation in (3-15) to yield the following stochastic algorithm:

$$\boldsymbol{c}_{k+1} = \boldsymbol{c}_k + \mu\, I\,\boldsymbol{r}_k. \tag{3-16}$$

We refer to this stochastic update as the *approximate minimum-BER* (*AMBER*) algorithm. In chapter 4 we will address its convergence properties in details.

We remark that (3-16) has the same form as the LMS algorithm, except that the error indicator function of the LMS is $I_{LMS} = x_{k-D} - y_k$. Observe that AMBER is less complex than LMS because (3-16) does not require a floating-point multiplication. Recall that the sign-LMS algorithm is

$$\boldsymbol{c}_{k+1} = \boldsymbol{c}_k + \mu\, I_{sign\text{-}LMS}\,\boldsymbol{r}_k, \tag{3-17}$$

where $I_{sign\text{-}LMS} = \text{sgn}(I_{LMS})$. AMBER can be viewed as the sign LMS algorithm modified to update only when a symbol decision error is made.

3.4.2 Tracking of f_D

The LMS algorithm penalizes equalizer outputs for deviating away from constellation points and thus controls the norm of the equalizer so that the main tap of the overall impulse response is approximately unity, *e.g.* $f_D \approx 1$. On the other hand, f_D is not necessarily close to unity for the AMBER algorithm.

Knowledge of f_D is not needed for binary signaling since the decisions are made based on the sign of the equalizer outputs. However, for general L-PAM, the value of the indicator function I depends on f_D, which changes with time as $\boldsymbol{c}$ is being updated.

To estimate f_D, we propose an auxiliary update algorithm. First, we let $\hat{f}_D(k)$ denote the estimate of f_D at time k. For a given x_{k-D}, the equalizer output y_k equals the sum of $f_D x_{k-D}$ and a perturbation term resulting from residual ISI and Gaussian noise. Since the perturbation term has zero mean, the mean of the equalizer output is $f_D x_{k-D}$, and that y_k / x_{k-D} has a mean of f_D. We can thus track f_D using a simple moving average as follows:

$$\hat{f}_D(k+1) = (1-\lambda)\hat{f}_D(k) + \lambda \frac{y_k}{x_{k-D}}, \tag{3-18}$$

where λ is a small positive step size. The estimated detection thresholds are then $\{0, \pm 2\hat{f}_D(k), \ldots, \pm(L-2)\hat{f}_D(k)\}$.

3.4.3 Update Threshold

Because the AMBER algorithm of (3-16) updates only when an error occurs, *i.e.* when the error indicator $I \neq 0$, the convergence rate will be slow when the error rate is low. To

increase convergence speed, we can modify AMBER so that the equalizer updates not only when an error is made, but also when an error is *almost* made, *i.e.* when the distance between the equalizer output and the nearest decision threshold is less than some small positive constant τ. Mathematically, the modified indicator function is

$$I_\tau(x_{k-D}, y_k) = \begin{cases} 1, & \text{if } y_k < (x_{k-D} - 1)f_D + \tau \text{ and } x_{k-D} \neq -L + 1, \\ -1, & \text{if } y_k > (x_{k-D} + 1)f_D - \tau \text{ and } x_{k-D} \neq L - 1, \\ 0, & \text{otherwise.} \end{cases} \tag{3-19}$$

Observe that when $\tau = 0$, the modified AMBER algorithm reverts back to (3-16).

We note that the expectation of the squared modified-error-indicator function is no longer the error probability, but rather

$$\mathrm{E}[I_\tau^2] = \frac{2L-2}{L}\,\mathrm{E}\left[Q\left(\frac{\boldsymbol{c}^T\boldsymbol{s} - \tau}{\|\boldsymbol{c}\|\sigma}\right)\right]. \tag{3-20}$$

The original AMBER algorithm ($\tau = 0$) requires knowledge of x_{k-D}; In other words, it requires a training sequence. When a training sequence is not available, the original AMBER algorithm cannot be operated in a decision-directed manner: if decisions are used in place of actual symbols, the indicator function would be identically zero since it is not possible for AMBER to tell whether an error has occurred, and hence the equalizer would never escape from its initial condition. Fortunately, the threshold modification has a second advantage: besides increasing the convergence speed, the modified algorithm can also be implemented in a decision-directed manner by using $\hat{x}_{k-D}$ in place of x_{k-D} in (3-19). Because a decision-directed algorithm cannot recognize when an error is made, the modified algorithm in decision-directed mode updates only when an error is *almost* made. We can expect that the impact of decision errors on this decision-directed algorithm will be negligible when the error probability is reasonably small, perhaps 10^{-2} or less.

3.4.4 Extension to the QAM Channel

Extending the AMBER equalizer to L^2-QAM is straightforward since the in-phase and quadratic components of a QAM system can be viewed as two parallel PAM systems. Replacing the exponential function by the Gaussian error function in equations (2-35)-(2-35), we obtain the deterministic AMBER algorithm for QAM as

$$\boldsymbol{c}_{k+1} = \boldsymbol{c}_k + \mu g_{\mathrm{QAM}}(\boldsymbol{c}_k) \tag{3-21}$$

where

$$g_{\mathrm{QAM}}(\boldsymbol{c}_k) = \mathrm{E}\left[Q\left(\frac{(\boldsymbol{c}_k^T \boldsymbol{s}_1)^R}{\|\boldsymbol{c}_k\| \sigma} \right) \boldsymbol{s}_1^* \right] + \mathrm{E}\left[Q\left(\frac{(\boldsymbol{c}_k^T \boldsymbol{s}_j)^I}{\|\boldsymbol{c}_k\| \sigma} \right) \boldsymbol{s}_j \right]. \tag{3-22}$$

Once again, if we assume the effect of noise on the received channel output vector is not significant, we can replace the ensemble averages in (3-21)-(3-22) by the following simple stochastic update for the complex QAM equalizer:

$$\boldsymbol{c}_{k+1} = \boldsymbol{c}_k + \mu I_\tau \boldsymbol{r}_k^*, \tag{3-23}$$

where $I_\tau = I_\tau(x_{k-D}^R, y_k^R) + jI_\tau(x_{k-D}^I, y_k^I)$ and where the superscripts R and I are used to denote real (or in-phase) and imaginary (or quadrature) parts, respectively.

3.4.5 Extension to Decision-Feedback Equalizer

A decision-feedback equalizer is basically a cascade of a linear equalizer and a decision-feedback device, where the forward section of a DFE is the linear equalizer. We replace the exponential function by the Gaussian error function in the EMSER update equation (2-40) for the forward filter of a DFE as follows:

$$\boldsymbol{c}_{k+1} = \boldsymbol{c}_k + \mu g_{fwd}(\boldsymbol{c}_k, \boldsymbol{d}_k), \tag{3-24}$$

where

$$g_{fwd}(\boldsymbol{c}, \boldsymbol{d}) = \mathrm{E}\left[Q\left(\frac{(\boldsymbol{c}^T \boldsymbol{s} - \sum_{i=D}^{N2} d_i x_{k-i})}{\|\boldsymbol{c}\| \sigma} \right) \boldsymbol{s} \right]. \tag{3-25}$$

Based on the deterministic AMBER update of (3-24), we can then form an almost identical stochastic update for the forward filter:

$$\boldsymbol{c}_{k+1} = \boldsymbol{c}_k + \mu I_\tau \boldsymbol{r}_k, \tag{3-26}$$

where I_τ is the error indicator function evaluating the equalizer outputs after decision feedback and $\boldsymbol{r}_k$ is the equalizer inputs for the forward filter of the DFE.

As mentioned in section 2.6, the feedback filters of both the MMSE and the EMBER DFEs are to eliminate post-cursor ISI and we can update the feedback filter of the AMBER DFE with the LMS algorithm:

$$\boldsymbol{d}_{k+1} = \boldsymbol{d}_k - \mu e_k \boldsymbol{x}_{k-D-1}, \tag{3-27}$$

where e_k is the difference between the DFE output and the desired signal, and where $\boldsymbol{x}_{k-D-1}^T = [x_{k-D-1} \ \ldots \ x_{k-N_2}]$ is the past data vector and is replaced by the data decision vector $\hat{\boldsymbol{x}}_{k-D-1}^T = [\hat{x}_{k-D-1} \ \ldots \ \hat{x}_{k-N_2}]$ in the decision-directed mode.

3.5 NUMERICAL RESULTS

3.5.1 SER Simulation

In this subsection, we consider several examples to compare the SER performance of the EMSER, AMBER, and MMSE equalizers. We also plot some eye diagrams of equalizer outputs to illustrate the difference between the MMSE and the AMBER equalizers.

Example 3-1: We first consider linear equalization for a binary signaling channel $H(z) = 1.2 + 1.1z^{-1} - 0.2z^{-2}$. In Fig. 3-2 we plot BER versus SNR $= \sum_k h_k^2/\sigma^2$, considering the MMSE, EMSER, and AMBER equalizers of length three and five. With three equalizer taps and a delay of $D = 2$, the AMBER equalizer has a more than 6.5 dB gain over the MMSE equalizer. With five taps and $D = 4$, the AMBER equalizer has a nearly 2 dB gain over MMSE. Observe that the AMBER (solid) and EMSER (dashed) curves are nearly indistinguishable. In Fig. 3-3, we present "artificial" noiseless eye patterns for the EMSER, AMBER, and MMSE equalizers, assuming five equalizer taps and SNR = 30 dB. These patterns are obtained by interpolating all possible noiseless equalizer outputs with a triangular pulse shape. All equalizers are normalized to have identical norm (and thus identical noise enhancement). The EMSER and AMBER eye patterns are virtually identical, whereas the MMSE eye pattern is drastically different. The interesting difference between the MMSE and AMBER equalizers results from the MMSE equalizer's effort to force all possible equalizer outputs to $\{\pm 1\}$, despite the benefits of sparing the outputs with large noise immunity.

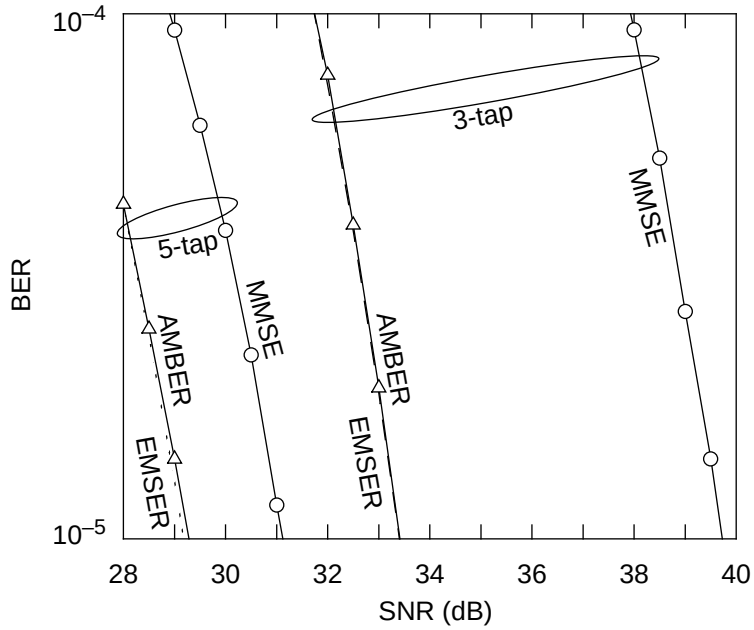

Fig. 3-2. Performance of linear equalization for the channel $H(z) = 1.2 + 1.1z^{-1} - 0.2\,z^{-2}$.

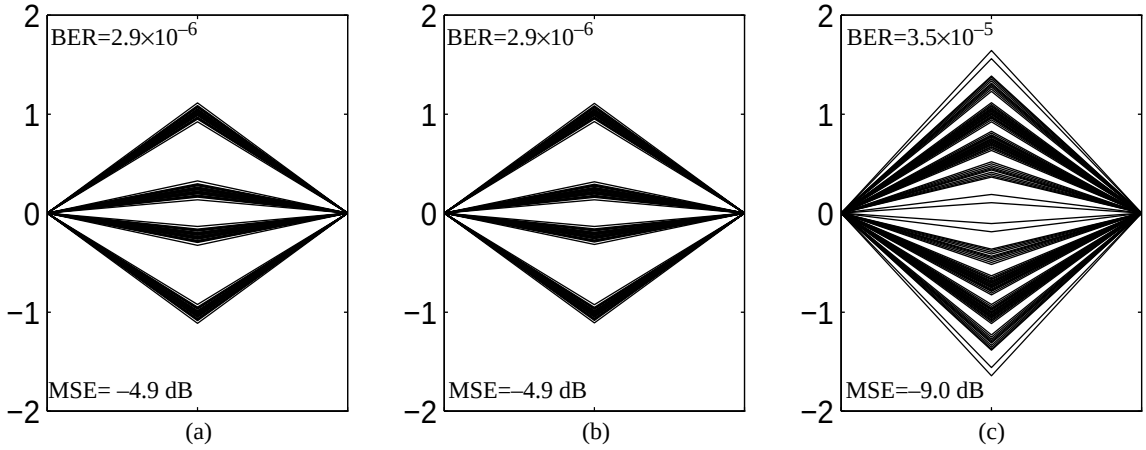

Fig. 3-3. Equalized noiseless eye patterns for 5-tap (a) EMSER; (b) AMBER; and (c) MMSE for the channel $H(z) = 1.2 + 1.1z^{-1} - 0.2\,z^{-2}$.

Example 3-2: We now consider a 4-PAM channel with transfer function $H(z) = 0.66 + z^{-1} - 0.66z^{-2}$. In Fig. 3-4 we plot error probability versus SNR = $\sum_k |h_k|^2/\sigma^2$ for three different five-tap linear equalizers: MMSE, EMSER, and AMBER. The delay is $D = 3$, which is optimal for the MMSE equalizer. The coefficients of the MMSE and EMSER equalizers are calculated exactly, whereas the AMBER coefficients were obtained via the stochastic AMBER update (3-16), with $\mu = 0.0002$, $\tau = 0.05$, and 10^6 training symbols. The error probability for all three equalizers is then evaluated using (2-16). Observe from Fig. 3-4 that the performance of AMBER is virtually indistinguishable from that of EMSER, and that the AMBER equalizer outperforms the MMSE equalizer by over 14 dB at SER = 10^{-5}.

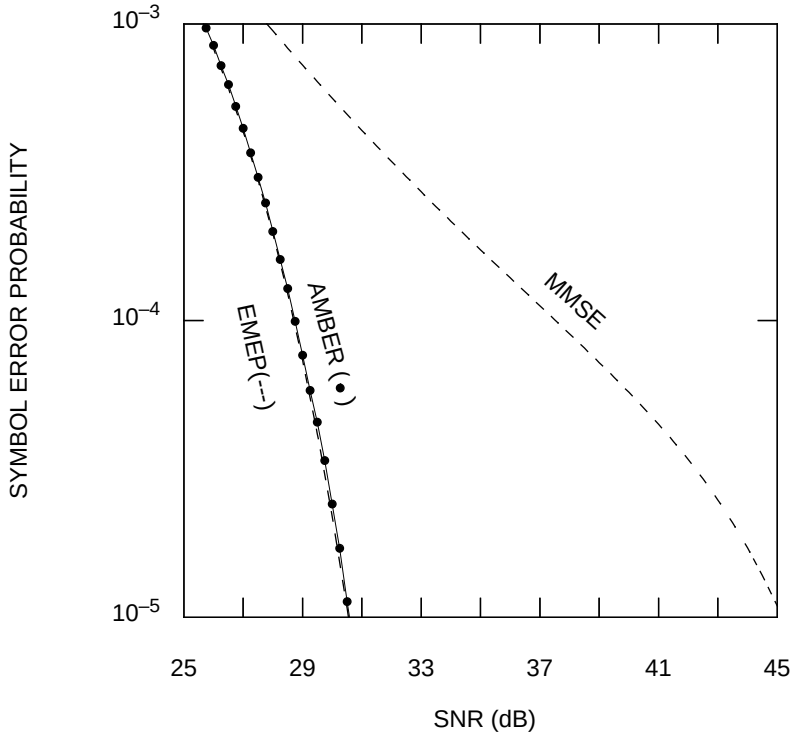

Fig. 3-4. Error-probability comparison for the 4-PAM channel with $H(z) = 0.66 + z^{-1} - 0.66z^{-2}$.

Example 3-3: Here we consider a 4-QAM channel with linear equalization and $H(z) = (0.7 - 0.2j) + (0.4 - 0.5j)z^{-1} + (-0.2 + 0.3j)z^{-2}$, and SNR $= \sum_k |h_k|^2 / \sigma^2$. As shown in Fig. 3-5, the 4-tap ($D = 3$) AMBER linear equalizer outperforms MMSE equalizer by about 18 dB. With five taps, the gain drops to slightly more than 2 dB. In Fig. 3-6 we present the noiseless constellation diagrams for the 4-tap AMBER and MMSE linear equalizers. Observe the interesting structure of the AMBER constellation clouds; they result in a higher MSE than the MMSE clouds (which appear roughly Gaussian), but the edges of the AMBER clouds are further apart.

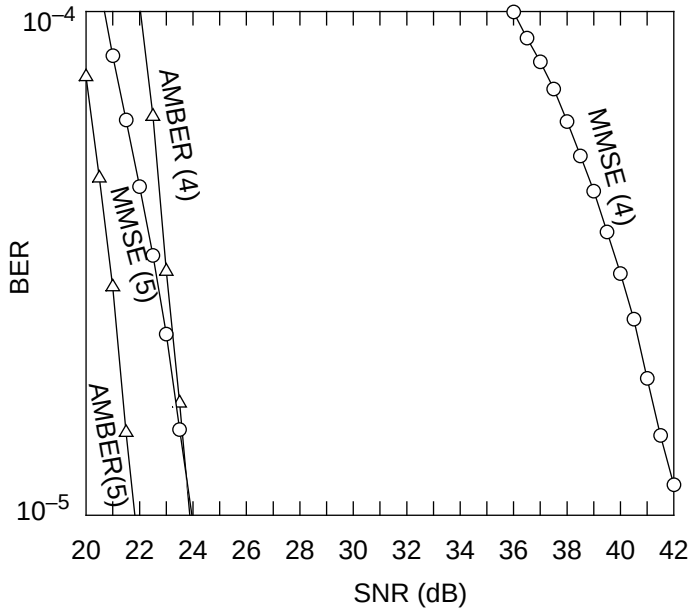

Fig. 3-5. BER comparison for linear equalizer on the 4-QAM channel with $H(z) = (0.7 - 0.2j) + (0.4 - 0.5j)z^{-1} + (-0.2 + 0.3j)z^{-2}$.

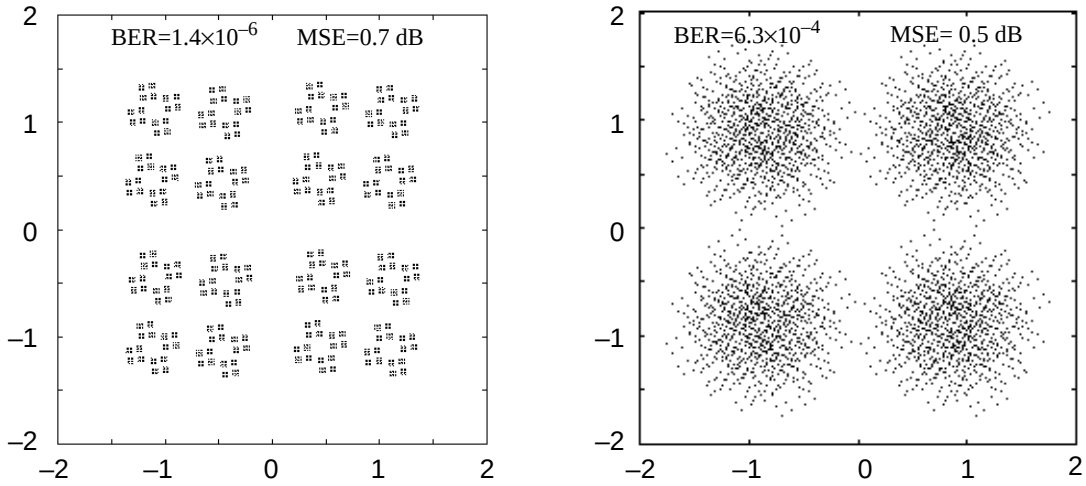

Fig. 3-6. Noiseless equalized constellations of 4-tap (a) AMBER and (b) MMSE equalizers at 25 dB SNR on the 4-QAM channel with $H(z) = (0.7 - 0.2j) + (0.4 - 0.5j)z^{-1} + (-0.2 + 0.3j)z^{-2}$.

Example 3-4: We now consider a 16-QAM system with channel $H(z) = (0.5 + 0.3j) + (1.2 + 0.9j)z^{-1} - (0.6 + 0.4j)z^{-2}$. In Fig. 3-7 we plot symbol-error probability versus SNR for a four-tap linear MMSE equalizer and a four-tap linear AMBER equalizer. The MMSE delay $D = 3$ is used on both cases. The coefficients of the MMSE equalizer are exact, whereas the AMBER coefficients are obtained via (3-16) with $\mu = 0.0002$, $\tau = 0.05$, and 10^6 training symbols. Both curves are obtained using Monte-Carlo techniques, averaged over 30×10^6 trials. Observe that AMBER outperforms MMSE by more than 6 dB. In Fig. 3-8 we plot the first quadrant of the noiseless 16-QAM constellation diagrams after the AMBER and MMSE equalizers. The equalizers are scaled to have the same norm and therefore the same noise enhancement. Observe that the distance between the AMBER

clouds is greater than the distance between the MMSE clouds. Thus, although the MSE of the AMBER equalizer is 0.5 dB higher than the MSE of the MMSE equalizer, the error probability is smaller by a factor of 17.

Example 3-5: Here we consider a binary signaling channel with a transfer function of $H(z) = 0.35 + 0.8z^{-1} + z^{-2} + 0.8z^{-3}$, but this time with decision-feedback equalization. In Fig. 3-9 we compare the BER performance of AMBER to MMSE. For a five-tap DFE (3 forward and 2 feedback taps), AMBER has a more than 5 dB gain over MMSE at $\mathrm{BER} = 10^{-5}$. For a seven-tap DFE (4 forward and 3 feedback taps), AMBER outperforms MMSE by about 1.8 dB. Observe that the 5-tap AMBER DFE outperforms the 7-tap MMSE DFE.

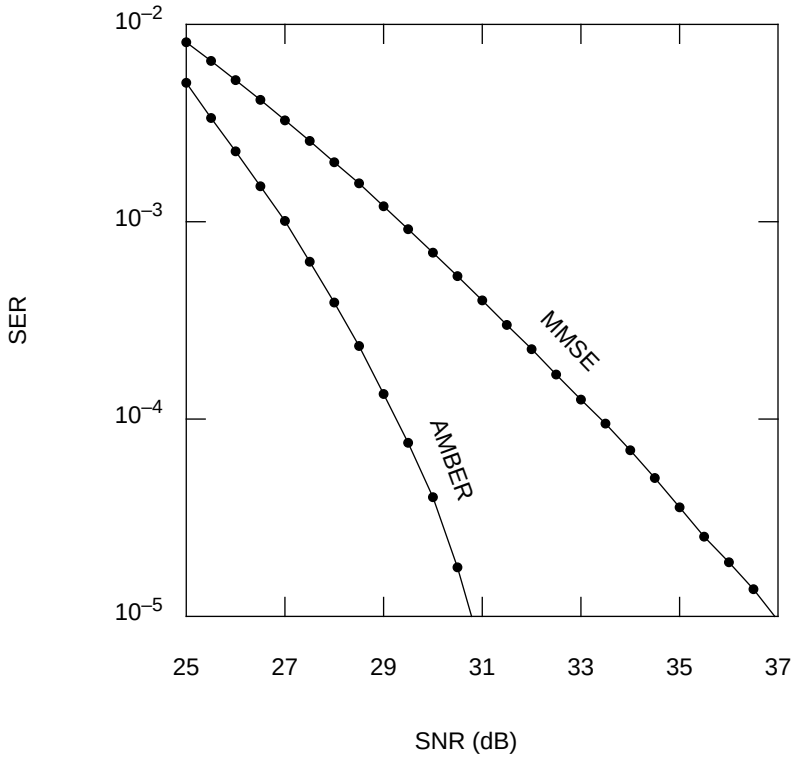

Fig. 3-7. Error probability performance comparison for the 16-QAM channel with $H(z) = (0.5 + 0.3j) + (1.2 + 0.9j)z^{-1} - (0.6 + 0.4j)z^{-2}$.

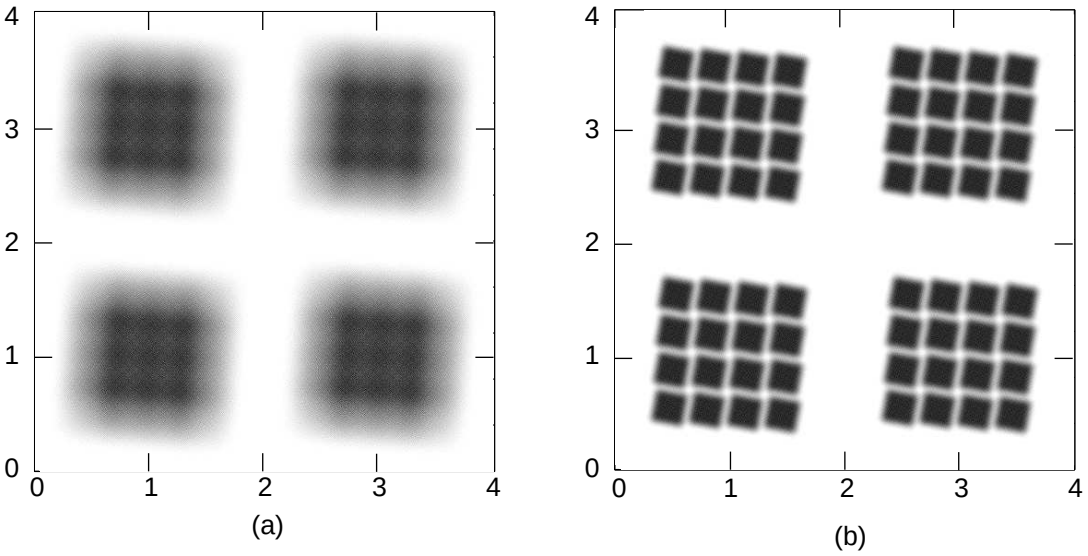

Fig. 3-8. Noiseless constellations (first quadrant only) of the 16-QAM channel with $H(z) = (0.5 + 0.3j) + (1.2 + 0.9j)z^{-1} - (0.6 + 0.4j)z^{-2}$: (a) after MMSE (MSE = -5.9 dB, $P_e = 69.6 \times 10^{-5}$); (b) after AMBER (MSE = -5.4 dB, $P_e = 4.0 \times 10^{-5}$).

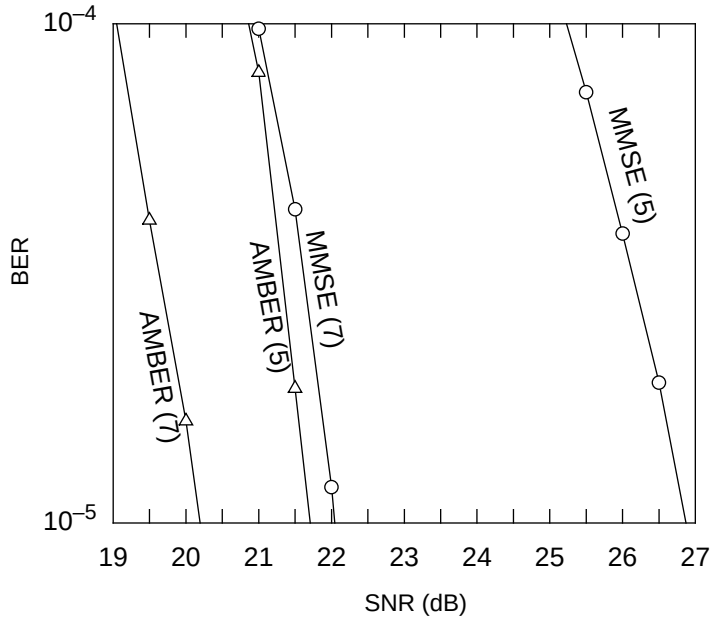

Fig. 3-9. BER comparison of DFE for the binary channel with $H(z) = 0.35 + 0.8z^{-1} + z^{-2} + 0.8z^{-3}$.

3.5.2 ISI Channel Characterization

Based on our simulation results in the previous subsection, we suspect that without enough equalizer taps, the AMBER (and the EMSER) equalizers are likely to significantly outperform the MMSE equalizers on severe ISI channels. However, the above claim is rather vague and more concrete scenarios are needed to quantify the claim. In this subsection we devise an ISI channel characterization procedure to identify scenarios in which the AMBER and the EMSER equalizers significantly outperform the MMSE equalizer.

We have realized from our previous simulation results that drastically different error-probability performances are reflected in the eye diagrams. More specifically, the more the MMSE eye pattern is closed, the more potential is the AMBER equalizer to improve error probability performance. As we have mentioned earlier, the noiseless eye pattern is formed by plotting the noiseless equalizer outputs and equivalently, the inner products between the equalizer and the signal vectors. We will now give two rules-of-thumb based on our empirical observations.

Rule 1. For an MMSE equalizer, if its smallest output is significantly less than the desired signal (*e.g.* the smallest noiseless equalizer output is 0.1 and the desired signal is 1), then it is *possible* to have the AMBER and the EMSER equalizers significantly outperform the MMSE equalizer.

Rule 2. If some MMSE equalizer outputs, which significantly close the eye of the channel, have large dispersion, then the AMBER and the EMSER equalizers are *possible* to have large SNR gains over the MMSE equalizer.

Of course the above rules do not always hold, but they are in general good. We now design a crude characterization procedure to predict the SNR gains of the n-tap AMBER and EMSER equalizers over the n-tap MMSE equalizer.

Step 1. Given a channel, compute the n-tap MMSE equalizer at a high SNR. Obtain noiseless equalizer outputs by convolving the channel and the MMSE equalizer.

Step 2. Of all the MMSE equalizer outputs corresponding to $x_{k-D} = 1$, pick one tenth with smallest values and average them. The predicted SNR gain of the AMBER and the EMSER equalizers over the MMSE equalizer is

$$\mathrm{SNR}_{\mathrm{gain}} = 20 \log_{10}\left(\frac{\mathrm{OUT}_{\mathrm{avg}}}{\mathrm{OUT}_{\mathrm{smallest}}}\right), \tag{3-28}$$

where $\mathrm{OUT}_{\mathrm{avg}}$ is the average of the one tenth MMSE equalizer outputs with the smallest values and $\mathrm{OUT}_{\mathrm{smallest}}$ is the smallest MMSE equalizer output. At very high SNR, the smallest of equalizer outputs dictates the error probability performance; Thus $\mathrm{OUT}_{\mathrm{smallest}}$ is the effective signal strength for the MMSE equalizer at high SNR. On the other hand, we have observed that both the AMBER and the EMSER equalizers tend to passively "cluster" equalizer output into sub-clusters, and $\mathrm{OUT}_{\mathrm{avg}}$ is used to roughly estimate the mean of the sub-cluster that nearly closes the eye of the channel. The predicted SNR gains of the AMBER and the EMSER equalizers over the MMSE equalizer are thus the ratios of $\mathrm{OUT}_{\mathrm{avg}}$ over $\mathrm{OUT}_{\mathrm{smallest}}$ in decibels.

In Fig. 3-10, we plot the actual versus the predicted SNR gains of the EMSER equalizers over the MMSE equalizer. With various equalizer taps and two hundred equalizable 3-tap and 4-tap channels, we perform simulations to find the actual SNR gains of the EMSER equalizer over the MMSE equalizer at error probability less than 10^{-6}. In general,

the characterization procedure predicts well whether an EMSER equalizer is likely to significantly outperform an MMSE equalizer. In Fig. 3-11, we plot the actual versus the predicted SNR gains of the AMBER equalizers over the MMSE equalizer.

3.6 SUMMARY AND CONCLUSION

We have derived the approximate minimum-BER (AMBER) equalization algorithm for both PAM and QAM. The stochastic AMBER algorithm for adaptive equalization has the following attributes: it closely approximates the minimum-error-probability equalizer; it does not require knowledge of the noise variance; it has low complexity, even lower than the LMS algorithm; and simulation results suggest that the algorithm is globally convergent. We also have carried out a simple ISI channel characterization procedure to predict SNR gains of the EMSER and AMBER equalizers over the MMSE equalizer.

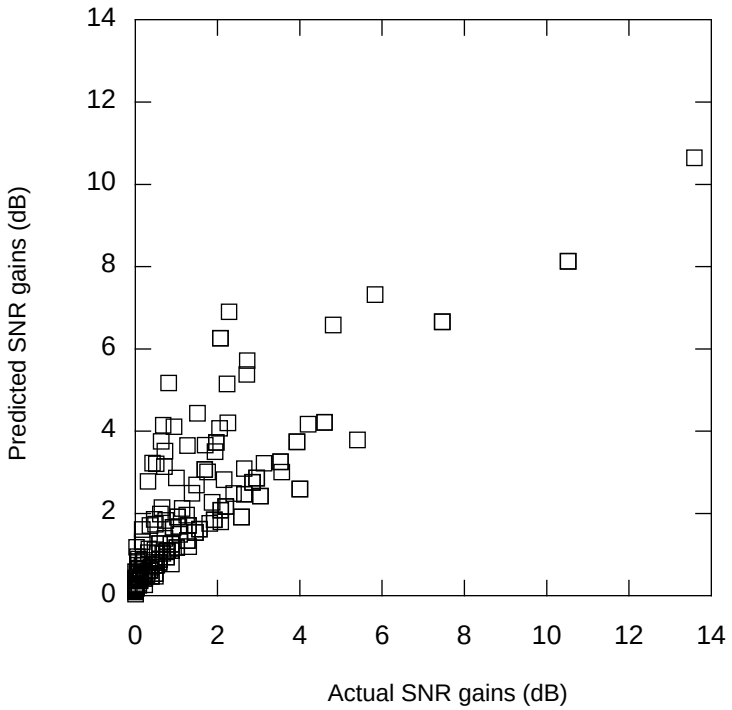

Fig. 3-10. The actual vs. the predicted SNR gains of the EMBER equalizers over the MMSE equalizers.

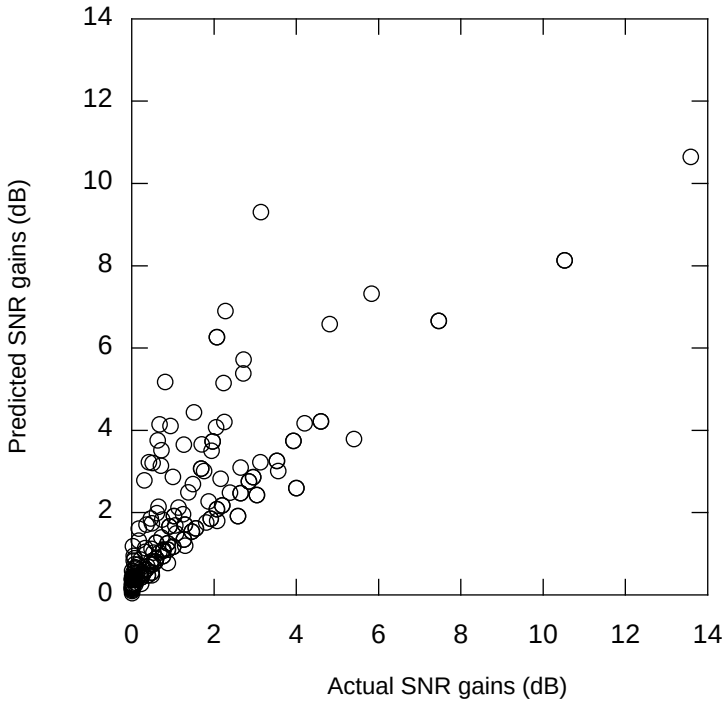

Fig. 3-11. The actual vs. the predicted SNR gains of the AMBER equalizers over the MMSE equalizers.

APPENDIX 3.1

PROOF OF THEOREM 3.1

In this appendix, we prove Theorem 3.1: For any equalizable channel there is a unique unit-length vector, $\tilde{\boldsymbol{c}}_{AMBER}$, satisfying the fixed-point relationship $\tilde{\boldsymbol{c}} = ag(\tilde{\boldsymbol{c}})$ for $a > 0$.

By contradiction: suppose both $\tilde{\boldsymbol{c}}_1$ and $\tilde{\boldsymbol{c}}_2$ satisfy $\tilde{\boldsymbol{c}} = ag(\tilde{\boldsymbol{c}})$, $a > 0$, where $\| \tilde{\boldsymbol{c}}_1 \| = \| \tilde{\boldsymbol{c}}_2 \| = 1$. Let P denote the plane containing the origin and the perpendicular bisector of $\tilde{\boldsymbol{c}}_1$ and $\tilde{\boldsymbol{c}}_2$, as shown in Fig. 3-12 for a three-tap equalizer. This plane bisects the signal cone $S = \{\Sigma_i a_i \boldsymbol{s}^{(i)} : a_i \geq 0\}$ into two subcones A and B, so that $S = A \cup B$, where A is the intersection of S with the set of vectors on the $\tilde{\boldsymbol{c}}_1$ side of P, excluding P, and B is the intersection of S with the set of vectors on the $\tilde{\boldsymbol{c}}_2$ side of P, including P. Observe that $\tilde{\boldsymbol{c}}_1 \in A$ and $\tilde{\boldsymbol{c}}_2 \in B$ and that A and B are disjoint, $A \cap B = \varnothing$.

From (3-5), $g(\tilde{\boldsymbol{c}}_1)$ can be decomposed into two summations over signal vectors from A and B:

$$g(\boldsymbol{c}_1) = \sum_{s^{(i)} \in A} Q\left(\frac{\tilde{\boldsymbol{c}}_1^T \boldsymbol{s}^{(i)}}{\sigma}\right)\boldsymbol{s}^{(i)} + \sum_{s^{(j)} \in B} Q\left(\frac{\tilde{\boldsymbol{c}}_1^T \boldsymbol{s}^{(j)}}{\sigma}\right)\boldsymbol{s}^{(j)} \quad . \tag{3-29}$$

Now consider $g(\tilde{\boldsymbol{c}}_2)$; it too can be expressed using (3-29), but with different weights. Compared with $\tilde{\boldsymbol{c}}_1$, the vector $\tilde{\boldsymbol{c}}_2$ forms a larger angle $\cos^{-1}(\tilde{\boldsymbol{c}}_2{}^T \boldsymbol{s}^{(i)} / \| \boldsymbol{s}^{(i)} \|)$ with all vectors $\boldsymbol{s}^{(i)}$ from A, while it forms a smaller or equal angle with all vectors from B. Thus, compared with the weights for $g(\tilde{\boldsymbol{c}}_1)$, the weights $Q(\tilde{\boldsymbol{c}}_2{}^T \boldsymbol{s}^{(i)} / \sigma)$ for $g(\tilde{\boldsymbol{c}}_2)$ in (3-29) strictly *increase* for the $\boldsymbol{s}^{(i)}$ vectors in A, while they either *decrease* or remain the same for vectors in B. Since $g(\tilde{\boldsymbol{c}}_1) = \tilde{\boldsymbol{c}}_1 \in A$, it follows that $g(\tilde{\boldsymbol{c}}_2)$ is also in A. But this contradicts $\tilde{\boldsymbol{c}}_2 = g(\tilde{\boldsymbol{c}}_2)$, since $\tilde{\boldsymbol{c}}_2 \in B$. *Q.E.D.*

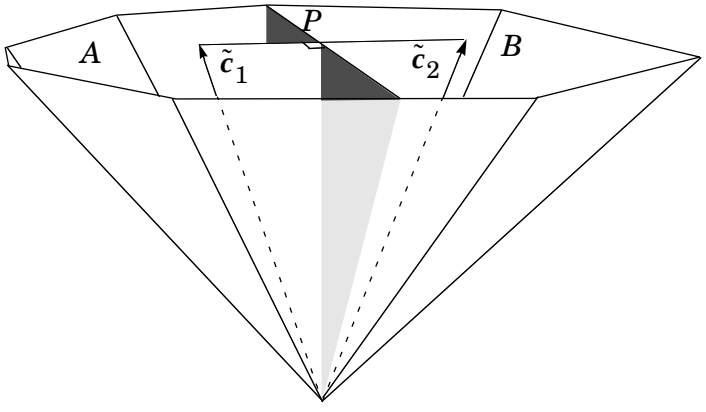

Fig. 3-12. Dividing the signal cone into two subcones A and B with the plane P.

APPENDIX 3.2

PROOF OF THEOREM 3.2

In this appendix, we prove Theorem 3.2. Let $\boldsymbol{s}^{(i)}$ be the i-th of the L^{M+N-1} possible signal vectors. Since the channel is equalizable, all $\boldsymbol{s}^{(i)}$ vectors form a cone such that we can find a vector having an angle of strictly less than 90° with all $\boldsymbol{s}^{(i)}$ vectors. Because the $\boldsymbol{s}^{(i)}$ vectors form a cone, we can find a hyperplane P, containing the origin, such that all $\boldsymbol{s}^{(i)}$ vectors are strictly on one side of P. Every $\boldsymbol{s}^{(i)}$ makes an angle $\theta_i \in [0, 90°)$ with the normal to P and consists of two components: one (with norm $||\boldsymbol{s}^{(i)}||\sin\theta$) parallel to P and the other (with norm $||\boldsymbol{s}^{(i)}||\cos\theta$) perpendicular to P. At each update, the correction vector $\mu g(\boldsymbol{c}_k)$ is strictly inside the cone and its norm is lower bounded by $\mu Q(||\boldsymbol{s}||_{\max}/\sigma)||\boldsymbol{s}||_{\min}\sin\theta_{\min}$, where $||\boldsymbol{s}||_{\min} = \min_i\{||\boldsymbol{s}^{(i)}||\}$, $||\boldsymbol{s}||_{\max} = \max_i\{||\boldsymbol{s}^{(i)}||\}$, and $\theta_{\max} = \max_i\{\theta_i\}$. At iteration $M + 1$, the sum of the past M correction vectors is a vector strictly inside the cone and has a norm of at least $M\mu Q(||\boldsymbol{s}||_{\max}/\sigma)||\boldsymbol{s}||_{\min}\sin\theta_{\min}$. We conclude that, for any initial $\boldsymbol{c}_0$ with a finite

norm, there exists a finite M such that $\boldsymbol{c}_{M+1}$ is strictly inside the cone. In addition, we conclude that $\| \boldsymbol{c}_k \|$ grows without bound as k increases.

Showing that $\boldsymbol{c}_k$ converges to the direction of a solution satisfying $\boldsymbol{c} = ag(\boldsymbol{c})$ for $a > 0$ is equivalent to showing that the angle between $\boldsymbol{c}_k$ and $g(\tilde{\boldsymbol{c}}_k)$ approaches zero, where $\tilde{\boldsymbol{c}}_k = \boldsymbol{c}_k / \| \boldsymbol{c}_k \|$. Because $\|\boldsymbol{c}_k\|$ grows without bound while the norm of the update, $\| \mu g(\tilde{\boldsymbol{c}}_k)\|$, is upper-bounded by $\mu \| \boldsymbol{s} \|_{\max}$, it follows that $\tilde{\boldsymbol{c}}_k$ must converge to some fixed vector $\tilde{\boldsymbol{c}}_\infty$, so that $g(\tilde{\boldsymbol{c}}_k)$ converges to $g(\tilde{\boldsymbol{c}}_\infty)$. Thus, for any $\varepsilon > 0$, there exists a finite $k(\varepsilon)$ such that for all $k > k(\varepsilon)$, $| \|g(\tilde{\boldsymbol{c}}_k)\| - \|g(\tilde{\boldsymbol{c}}_\infty)\| | \leq \|g(\tilde{\boldsymbol{c}}_k) - g(\tilde{\boldsymbol{c}}_\infty)\| < \varepsilon$. Manipulating the inequalities yields that the angle between $g(\tilde{\boldsymbol{c}}_k)$ and $g(\tilde{\boldsymbol{c}}_\infty)$ is less than some $\theta(\varepsilon)$, where

$$\theta(\varepsilon) = \cos^{-1}\left[\frac{1 - \varepsilon / \left\|q(\tilde{\boldsymbol{c}}_\infty)\right\|}{1 + \varepsilon / \left\|q(\tilde{\boldsymbol{c}}_\infty)\right\|}\right]. \tag{3-30}$$

For any $M > 0$, $\sum_{j=0}^{M-1} g(\tilde{\boldsymbol{c}}_{k(\varepsilon)+j})$ is a vector strictly within the cone $W[g(\tilde{\boldsymbol{c}}_\infty); \theta(\varepsilon)]$ consisting of all vectors forming an angle of less than $\theta(\varepsilon)$ with $g(\tilde{\boldsymbol{c}}_\infty)$. For a $\boldsymbol{c}_{k(\varepsilon)}$ with finite norm, we can find a finite $\boldsymbol{M}$ such that $\boldsymbol{c}_{k(\varepsilon)+M}$ is strictly inside $W[g(\tilde{\boldsymbol{c}}_\infty); \theta(\varepsilon)]$. As ε approaches 0, $\theta(\varepsilon)$ approaches 0 and thus the angle between $\boldsymbol{c}_{k(\varepsilon)+M}$ and $g(\tilde{\boldsymbol{c}}_{k(\varepsilon)+M})$ approaches 0 as well. *Q.E.D.*

APPENDIX 3.3

PROOF OF THEOREM 3.3

This appendix proves Theorem 3.3: The ensemble average $\mathrm{E}[I\boldsymbol{s}_k]$ is the same as $\mathrm{E}[I\mathbf{H}\boldsymbol{x}_k]$ or $\mathbf{H}\mathrm{E}[I\boldsymbol{x}_k]$. We equivalently derive the ensemble average $\mathrm{E}[I\boldsymbol{x}_k]$ by finding the scalar $\mathrm{E}[Ix_{k-D}]$ and the vector $\mathrm{E}[I\boldsymbol{z}]$ where we have defined the vector $\boldsymbol{z} = [x_k, \ldots, x_{k-D+1}, x_{k-D-1}, \ldots, x_{k-M-N+1}]^T$ by discarding the $(D + 1)$-st component of $\boldsymbol{x}_k$.

Let "left", "right", and "inner" denote the events of $x_{k-D} = -L + 1$, $x_{k-D} = L - 1$, and $x_{k-D} \in \{\pm 1, \pm 3, \ldots, \pm(L-3)\}$, respectively. (If $L = 2$, "inner" is the null event.) Then:

$$\mathrm{E}[Ix_{k-D}] = \mathrm{E}[Ix_{k-D} \mid \text{left}]\mathrm{P}[\text{left}] + \mathrm{E}[Ix_{k-D} \mid \text{right}]\mathrm{P}[\text{right}] + \mathrm{E}[Ix_{k-D} \mid \text{inner}]\mathrm{P}[\text{inner}] \tag{3-31}$$

$$= \frac{-L+1}{L}\mathrm{E}[I \mid \text{left}] + \frac{L-1}{L}\mathrm{E}[I \mid \text{right}] + \frac{L-2}{L}\mathrm{E}[Ix_{k-D} \mid \text{inner}]. \tag{3-32}$$

But I is independent of x_{k-D} when x_{k-D} is an inner point, so that the last term is zero:

$$\mathrm{E}[I\, x_{k-D} \mid \text{inner}] = \mathrm{E}[I \mid \text{inner}]\mathrm{E}[x_{k-D} \mid \text{inner}] = \mathrm{E}[I \mid \text{inner}] \times 0 = 0. \tag{3-33}$$

Thus, (3-32) reduces to:

$$\mathrm{E}[I\, x_{k-D}] = \frac{L-1}{L}\left\{\mathrm{E}[I \mid \text{left}] + \mathrm{E}[I \mid \text{right}]\right\} \tag{3-34}$$

$$= \frac{L-1}{L}\left\{(\mathrm{P}[\boldsymbol{b}^T\boldsymbol{z} + \boldsymbol{c}^T\boldsymbol{n}_k > f_D]) + \mathrm{P}[\boldsymbol{b}^T\boldsymbol{z} + \boldsymbol{c}^T\boldsymbol{n}_k < -f_D]\right\} \tag{3-35}$$

$$= \frac{L-1}{L}\left\{\mathrm{E}\left[Q\left(\frac{f_D - \boldsymbol{b}^T\boldsymbol{z}}{\|\boldsymbol{c}\|\sigma}\right)\right] + \mathrm{E}\left[Q\left(\frac{f_D + \boldsymbol{b}^T\boldsymbol{z}}{\|\boldsymbol{c}\|\sigma}\right)\right]\right\} \tag{3-36}$$

$$= \frac{2L-2}{L}\mathrm{E}\left[Q\left(\frac{f_D + \boldsymbol{b}^T\boldsymbol{z}}{\|\boldsymbol{c}\|\sigma}\right)\right]. \tag{3-37}$$

We thus have the surprising result that the ensemble average $\mathrm{E}[I\, x_{k-D}]$ does not depend on x_{k-D}! We have defined the vector $\boldsymbol{b} = [f_0, \ldots, f_{D-1}, f_{D+1}, \ldots, f_{M+N-1}]^T$ by discarding the $(D+1)$-st component of $\boldsymbol{f}$. The last equality follows because $\boldsymbol{z}$ and $-\boldsymbol{z}$ have the same distribution. The derivation of $\mathrm{E}[I\boldsymbol{z}]$ is as follows:

$$\mathrm{E}[I\boldsymbol{z}] = \frac{1}{L}\mathrm{E}[I\boldsymbol{z} \mid \text{left}] + \frac{1}{L}\mathrm{E}[I\boldsymbol{z} \mid \text{right}] + \frac{L-2}{L}\mathrm{E}[I\boldsymbol{z} \mid \text{inner}] \tag{3-38}$$

$$= \frac{1}{L}\mathrm{E}\left[\mathrm{E}[I \mid \boldsymbol{z}, \text{left}]\boldsymbol{z} + \mathrm{E}[I \mid \boldsymbol{z}, \text{right}]\boldsymbol{z} + (L-2)\mathrm{E}[I \mid \boldsymbol{z}, \text{inner}]\boldsymbol{z}\right] \tag{3-39}$$

$$= \frac{1}{L}\mathrm{E}\left[-Q\left(\frac{f_D - \boldsymbol{b}^T\boldsymbol{z}}{\|\boldsymbol{c}\|\sigma}\right)\boldsymbol{z} + Q\left(\frac{f_D + \boldsymbol{b}^T\boldsymbol{z}}{\|\boldsymbol{c}\|\sigma}\right)\boldsymbol{z} + (L-2)\left\{Q\left(\frac{f_D + \boldsymbol{b}^T\boldsymbol{z}}{\|\boldsymbol{c}\|\sigma}\right) - Q\left(\frac{f_D - \boldsymbol{b}^T\boldsymbol{z}}{\|\boldsymbol{c}\|\sigma}\right)\right\}\boldsymbol{z}\right] \tag{3-40}$$

$$= \frac{L-1}{L}\mathrm{E}\left[Q\left(\frac{f_D + \boldsymbol{b}^T\boldsymbol{z}}{\|\boldsymbol{c}\|\sigma}\right)\boldsymbol{z}\right] - \frac{L-1}{L}\mathrm{E}\left[Q\left(\frac{f_D - \boldsymbol{b}^T\boldsymbol{z}}{\|\boldsymbol{c}\|\sigma}\right)\boldsymbol{z}\right] \tag{3-41}$$

$$= \frac{2L-2}{L}\mathrm{E}\left[Q\left(\frac{f_D + \boldsymbol{b}^T\boldsymbol{z}}{\|\boldsymbol{c}\|\sigma}\right)\boldsymbol{z}\right]. \tag{3-42}$$

The ensemble $\mathrm{E}[I\boldsymbol{z}]$ does not depend on x_{k-D} either. Combining (3-37) and (3-42), we have

$$\mathrm{E}[I\boldsymbol{x}_k] = \frac{2L-2}{L}\mathrm{E}\left[Q\left(\frac{\boldsymbol{c}^T\mathbf{H}\tilde{\boldsymbol{x}}}{\|\boldsymbol{c}\|\sigma}\right)\tilde{\boldsymbol{x}}\right] \tag{3-43}$$

and

$$\mathrm{E}[I\boldsymbol{s}_k] = \mathrm{E}[I\mathbf{H}\boldsymbol{x}_k] = \frac{2L-2}{L}\mathrm{E}\left[Q\left(\frac{\boldsymbol{c}^T\tilde{\boldsymbol{s}}}{\|\boldsymbol{c}\|\sigma}\right)\tilde{\boldsymbol{s}}\right] \tag{3-44}$$

where $\tilde{\boldsymbol{x}}$ is a random vector with distribution $p(\tilde{\boldsymbol{x}}) = p(\boldsymbol{x}_k \mid x_{k-D} = 1)$, *i.e.*, $\tilde{\boldsymbol{x}}$ is uniformly distributed over the set of L^{M+N-1} L-ary $\boldsymbol{x}_k$ vectors for which $x_{k-D} = 1$ and $\tilde{\boldsymbol{s}} = \mathbf{H}\tilde{\boldsymbol{x}}$.

We now derive the ensemble average $\mathrm{E}[I\boldsymbol{n}_k]$. We first partition $\mathrm{E}[I\boldsymbol{n}_k]$ into three conditional expectation terms as follows:

$$\begin{aligned}\mathrm{E}[I\boldsymbol{n}_k] = &\sum_l \mathrm{E}[I\boldsymbol{n}_k \mid I = 1,\ \boldsymbol{z} = \boldsymbol{z}^l]\ \mathrm{P}[I = 1,\ \boldsymbol{z} = \boldsymbol{z}^l] + \\ &\sum_l \mathrm{E}[I\boldsymbol{n}_k \mid I = -1,\ \boldsymbol{z} = \boldsymbol{z}^l]\ \mathrm{P}[I = -1,\ \boldsymbol{z} = \boldsymbol{z}^l] + \\ &\sum_l \mathrm{E}[I\boldsymbol{n}_k \mid I = 0,\ \boldsymbol{z} = \boldsymbol{z}^l]\ \mathrm{P}[I = 0,\ \boldsymbol{z} = \boldsymbol{z}^l],\end{aligned} \tag{3-45}$$

where each term is summed over L^{M+N-1} possible $\boldsymbol{z}$ vectors. Note that the last summation term in (3-45) is a zero vector since $I = 0$ and $I\boldsymbol{n}_k = \mathbf{0}$. We first concentrate on the first summation term in (4-18) by finding the conditional expectation $\mathrm{E}[I\boldsymbol{n}_k \mid I = 1,\ \boldsymbol{z} = \boldsymbol{z}^l]$ and the joint probability $\mathrm{P}[I = 1,\ \boldsymbol{z} = \boldsymbol{z}^l]$. Here we determine $\mathrm{E}[I\boldsymbol{n}_k \mid I = 1,\ \boldsymbol{z} = \boldsymbol{z}^l]$:

$$\mathrm{E}[I\boldsymbol{n}_k \mid I = 1,\ \boldsymbol{z} = \boldsymbol{z}^l] = \mathrm{E}[\boldsymbol{n}_k \mid I = 1,\ \boldsymbol{z} = \boldsymbol{z}^l] \tag{3-46}$$

$$= \mathrm{E}[\boldsymbol{n}_k \mid \boldsymbol{c}^T\boldsymbol{n}_k < -f_D - \boldsymbol{b}^T\boldsymbol{z}^l,\ x_{k-D} \neq -L + 1] \tag{3-47}$$

$$= \mathrm{E}[\boldsymbol{n}_k \mid \boldsymbol{c}^T\boldsymbol{n}_k < -f_D - \boldsymbol{b}^T\boldsymbol{z}^l]. \tag{3-48}$$

Let $\mathbf{U}$ be any unitary matrix with first column equal to the unit-norm equalizer vector $\boldsymbol{c}/\|\boldsymbol{c}\|$. Then $\tilde{\boldsymbol{n}} = \mathbf{U}^T\boldsymbol{n}_k$ has the same statistics as $\boldsymbol{n}_k$, namely, the components of $\tilde{\boldsymbol{n}}$ are *i.i.d.* zero-mean Gaussian with variance σ^2. Furthermore, $\boldsymbol{c}^T\mathbf{U} = \|\boldsymbol{c}\|\boldsymbol{e}_1$, where $\boldsymbol{e}_1 = [1\ 0\ 0\ \ldots\ 0]$, and $\boldsymbol{n}_k = \mathbf{U}\tilde{\boldsymbol{n}}$. Continuing on (3-48), we have

$$\mathrm{E}[I\boldsymbol{n}_k \mid I = 1,\ \boldsymbol{z} = \boldsymbol{z}^l] = \mathrm{E}[\mathbf{U}\tilde{\boldsymbol{n}} \mid \boldsymbol{c}^T\mathbf{U}\tilde{\boldsymbol{n}} < -f_D - \boldsymbol{b}^T\boldsymbol{z}^l] \tag{3-49}$$

$$= \mathbf{U}\mathrm{E}[\tilde{\boldsymbol{n}} \mid \|\boldsymbol{c}\|\tilde{n}_1 < -f_D - \boldsymbol{b}^T\boldsymbol{z}^l] \tag{3-50}$$

$$= \mathbf{U}\mathrm{E}\left[\tilde{\boldsymbol{n}} \mid \frac{-\tilde{n}_1}{\sigma} > \frac{f_D + \boldsymbol{b}^T\boldsymbol{z}^l}{\|\boldsymbol{c}\|\sigma}\right] \tag{3-51}$$

$$= -\sigma\mathbf{U}\mathrm{E}\left[\frac{-\tilde{n}_1}{\sigma} \mid \frac{-\tilde{n}_1}{\sigma} > \frac{f_D + \boldsymbol{b}^T\boldsymbol{z}^l}{\|\boldsymbol{c}\|\sigma}\right]\boldsymbol{e}_1 \tag{3-52}$$

$$= -\sigma\mathrm{E}\left[m\left(\frac{f_D + \boldsymbol{b}^T\boldsymbol{z}^l}{\|\boldsymbol{c}\|\sigma}\right)\right]\boldsymbol{c}/\|\boldsymbol{c}\|, \tag{3-53}$$

where we have introduced the function

$$m(\eta) = \frac{e^{-\eta^2/2}}{\sqrt{2\pi}Q(\eta)} \triangleq \mathrm{E}[X \mid X \geq \eta], \tag{3-54}$$

where X is a zero-mean unit-variance Gaussian random variable. We now derive the joint probability $\mathrm{P}[I = 1,\ \boldsymbol{z} = \boldsymbol{z}^l]$:

$$\mathrm{P}[I = 1,\ \boldsymbol{z} = \boldsymbol{z}^l] = \mathrm{P}[I = 1 \mid \boldsymbol{z} = \boldsymbol{z}^l]\ \mathrm{P}[\boldsymbol{z} = \boldsymbol{z}^l] \tag{3-55}$$

$$= \frac{L-1}{L} Q\left(\frac{f_D + \boldsymbol{b}^T \boldsymbol{z}^l}{\|\boldsymbol{c}\|\sigma}\right) \frac{1}{L^{M+N-1}}. \tag{3-56}$$

Combining (3-53) and (3-56), the first summation term in (3-45) becomes

$$\sum_l \mathrm{E}[I\boldsymbol{n}_k \mid I = 1, \boldsymbol{z} = \boldsymbol{z}^l]\, \mathrm{P}[I = 1, \boldsymbol{z} = \boldsymbol{z}^l]$$

$$= \sum_l \frac{-(L-1)\sigma}{L^{M+N}\sqrt{2\pi}} \exp\left(\frac{-(f_D + \boldsymbol{b}^T \boldsymbol{z}^l)^2}{2\|\boldsymbol{c}\|^2\sigma^2}\right) \frac{\boldsymbol{c}}{\|\boldsymbol{c}\|} \tag{3-57}$$

$$= \frac{-(L-1)\sigma}{L\sqrt{2\pi}} \mathrm{E}\left[\exp\left(\frac{-(f_D + \boldsymbol{b}^T \boldsymbol{z})^2}{2\|\boldsymbol{c}\|^2\sigma^2}\right)\right] \frac{\boldsymbol{c}}{\|\boldsymbol{c}\|} \tag{3-58}$$

$$= \frac{-(L-1)\sigma}{L\sqrt{2\pi}} \mathrm{E}\left[\exp\left(\frac{-(\boldsymbol{c}^T \tilde{\boldsymbol{s}})^2}{2\|\boldsymbol{c}\|^2\sigma^2}\right)\right] \frac{\boldsymbol{c}}{\|\boldsymbol{c}\|}. \tag{3-59}$$

It is not hard to show that

$$\sum_l \mathrm{E}[I\boldsymbol{n}_k \mid I = 1, \boldsymbol{z} = \boldsymbol{z}^l]\, \mathrm{P}[I = 1, \boldsymbol{z} = \boldsymbol{z}^l]$$

$$= \sum_l \mathrm{E}[I\boldsymbol{n}_k \mid I = -1, \boldsymbol{z} = \boldsymbol{z}^l]\, \mathrm{P}[I = -1, \boldsymbol{z} = \boldsymbol{z}^l], \tag{3-60}$$

and therefore, we conclude that

$$\mathrm{E}[I\boldsymbol{n}_k] = -\frac{2L-2}{L} \frac{\sigma}{\sqrt{2\pi}} \mathrm{E}\left[\exp\left(\frac{-(\boldsymbol{c}^T \tilde{\boldsymbol{s}})^2}{2\|\boldsymbol{c}\|^2\sigma^2}\right)\right] \frac{\boldsymbol{c}}{\|\boldsymbol{c}\|}. \tag{3-61}$$

Q.E.D.

CHAPTER 4

CONVERGENCE ANALYSIS

4.1 INTRODUCTION

In the previous chapter, we proposed a low-complexity stochastic equalizer algorithm (AMBER) that very nearly minimizes error probability. In this chapter, we discuss its global convergence properties and propose a variant to increase its convergence speed.

Assuming the equalizer coefficients vary slowly (which is true for a sufficiently small step size), a stochastic equalizer update can then be expected to follow a deterministic trajectory [15]. In this chapter, we first derive the ensemble average of the stochastic AMBER algorithm to approximate its time average in order to study its mean convergence behavior. Because of the highly complicated and nonlinear nature of the update dynamics, instead of a rigorous mathematical proof, we describe the likely global convergence property of the AMBER algorithm and propose a global convergence conjecture based on sim-

ulation results and some analytical understanding on the update dynamics. Finally, we propose a variant with faster convergence speed.

4.2 ENSEMBLE AVERAGE OF AMBER

The AMBER algorithm proposed in the previous chapter is

$$\boldsymbol{c}_{k+1} = \boldsymbol{c}_k + \mu I_\tau \boldsymbol{r}_k, \tag{4-1}$$

whose ensemble average can be derived by taking expectation of both sides of (4-1). The deterministic trajectory of the equalizer coefficients is described by

$$\boldsymbol{c}_{k+1} = \boldsymbol{c}_k + \mu \mathrm{E}[I_\tau \boldsymbol{r}_k] \tag{4-2}$$

$$= \boldsymbol{c}_k + \mu \mathrm{E}[I_\tau \boldsymbol{s}_k] + \mu \mathrm{E}[I_\tau \boldsymbol{n}_k], \tag{4-3}$$

where we separate the noisy channel output vector $\boldsymbol{r}_k$ into the noiseless channel output vector $\boldsymbol{s}_k$ and the noise vector $\boldsymbol{n}_k$. We now find the ensemble averages $\mathrm{E}[I_\tau \boldsymbol{s}_k]$ and $\mathrm{E}[I_\tau \boldsymbol{n}_k]$.

Theorem 4.1: The ensemble average of the AMBER algorithm of (4-2) is

$$\boldsymbol{c}_{k+1} = \boldsymbol{c}_k + \mu \mathrm{E}\left[Q\left(\frac{\boldsymbol{c}_k^T \tilde{\boldsymbol{s}} - \tau}{\|\boldsymbol{c}_k\| \sigma} \right) \tilde{\boldsymbol{s}} \right] - \mu \frac{\sigma}{\sqrt{2\pi}} \mathrm{E}\left[\exp\left(\frac{-(\boldsymbol{c}_k^T \tilde{\boldsymbol{s}} - \tau)^2}{2\|\boldsymbol{c}_k\|^2 \sigma^2} \right) \right] \frac{\boldsymbol{c}_k}{\|\boldsymbol{c}_k\|}. \tag{4-4}$$

Proof. The proof of Theorem 4.1 is in Appendix 4.1.

4.3 GLOBAL CONVERGENCE PROPERTY

Having derived the ensemble average of the AMBER algorithm in the previous section, we now discuss the global convergence property of AMBER by analyzing the deter-

ministic trajectory of the equalizer coefficient vector. From the results of the previous section, the ensemble average of the stochastic AMBER algorithm is

$$\begin{aligned}\boldsymbol{c}_{k+1} &= \boldsymbol{c}_k + \mu_1 \mathrm{E}[I_\tau \boldsymbol{r}_k] \\ &= \boldsymbol{c}_k + \mu_1 \mathrm{E}[I_\tau \boldsymbol{s}_k] + \mu_1 \mathrm{E}[I_\tau \boldsymbol{n}_k] \\ &= \boldsymbol{c}_k + \mu \mathrm{E}\left[Q\left(\frac{\boldsymbol{c}_k^T \tilde{\boldsymbol{s}} - \tau}{\|\boldsymbol{c}_k\| \sigma} \right) \tilde{\boldsymbol{s}} \right] - \mu \frac{\sigma}{\sqrt{2\pi}} \mathrm{E}\left[\exp\left(\frac{-(\boldsymbol{c}_k^T \tilde{\boldsymbol{s}} - \tau)^2}{2\|\boldsymbol{c}_k\|^2 \sigma^2} \right) \right] \frac{\boldsymbol{c}_k}{\|\boldsymbol{c}_k\|},\end{aligned} \tag{4-5}$$

where $\mu = \frac{2L-2}{L}\mu_1$. Rearranging (4-5), we get

$$\boldsymbol{c}_{k+1} = \left\{ 1 - \frac{\mu\sigma}{\sqrt{2\pi}\|\boldsymbol{c}_k\|} \mathrm{E}\left[\exp\left(\frac{-(\boldsymbol{c}_k^T \tilde{\boldsymbol{s}} - \tau)^2}{2\|\boldsymbol{c}_k\|^2 \sigma^2} \right) \right] \right\} \boldsymbol{c}_k + \mu \mathrm{E}\left[Q\left(\frac{\boldsymbol{c}_k^T \tilde{\boldsymbol{s}} - \tau}{\|\boldsymbol{c}_k\| \sigma} \right) \tilde{\boldsymbol{s}} \right]. \tag{4-6}$$

By inspection, we see that when the step size μ is chosen sufficiently small, the norm of the equalizer in (4-6) is shrunk by some positive factor (less than 1) before the equalizer vector is adjusted by the steering term $\mathrm{E}\left[Q\left(\frac{\boldsymbol{c}_k^T \tilde{\boldsymbol{s}} - \tau}{\|\boldsymbol{c}_k\| \sigma} \right) \tilde{\boldsymbol{s}} \right]$. We denote the vector term $\frac{\sigma}{\sqrt{2\pi}} \mathrm{E}\left[\exp\left(\frac{-(\boldsymbol{c}_k^T \tilde{\boldsymbol{s}} - \tau)^2}{2\|\boldsymbol{c}_k\|^2 \sigma^2} \right) \right] \frac{\boldsymbol{c}_k}{\|\boldsymbol{c}_k\|}$ as the shrinking vector since it reduces the equalizer norm.

Before we analyze the convergence property, we would like to point out from (4-5) that the equalizer update stops, or $\boldsymbol{c}_{k+1} = \boldsymbol{c}_k$, when the steering term equals the shrinking term:

$$\mathrm{E}\left[Q\left(\frac{\boldsymbol{c}_k^T \tilde{\boldsymbol{s}} - \tau}{\|\boldsymbol{c}_k\| \sigma} \right) \tilde{\boldsymbol{s}} \right] = \frac{\sigma}{\sqrt{2\pi}} \mathrm{E}\left[\exp\left(\frac{-(\boldsymbol{c}_k^T \tilde{\boldsymbol{s}} - \tau)^2}{2\|\boldsymbol{c}_k\|^2 \sigma^2} \right) \right] \frac{\boldsymbol{c}_k}{\|\boldsymbol{c}_k\|}. \tag{4-7}$$

The equilibrium condition of (4-7) directly implies: (1) the steering vector points in the same direction as the equalizer vector when the equalizer converges, and (2) the magnitudes (or norms) of the steering vector and the shrinking vector are the same.

4.3.1 The Locus

Recall that the original AMBER ($\tau = 0$) equalizer is uniquely characterized by the fixed-point relationship $\boldsymbol{c} = ag(\boldsymbol{c})$ for some $a > 0$, where only the direction of $\boldsymbol{c}$ matters. However, for $\tau > 0$, the norm of $\boldsymbol{c}$ matters as well. We now define a new fixed-point relationship:

$$\boldsymbol{c} = \frac{\|\boldsymbol{c}\|}{\|g_\tau(\boldsymbol{c})\|} g_\tau(\boldsymbol{c}) \tag{4-8}$$

where

$$g_\tau(\boldsymbol{c}) = \mathrm{E}\left[Q\left(\frac{\boldsymbol{c}^T \tilde{\boldsymbol{s}} - \tau}{\|\boldsymbol{c}\|\sigma} \right) \tilde{\boldsymbol{s}} \right]. \tag{4-9}$$

Following the proof in Appendix 3.1 which shows that there is a unique unit-length vector satisfying the fixed-point relationship $\boldsymbol{c} = ag(\boldsymbol{c})$ for some $a > 0$, it is not hard to show that for a positive number M, there exists a unique equalizer with equalizer norm M satisfying the new fixed-point relationship of (4-8).

When the norm of $\boldsymbol{c}$ is very small relative to τ, the term $\mathrm{E}\left[Q\left(\frac{\boldsymbol{c}^T \tilde{\boldsymbol{s}} - \tau}{\|\boldsymbol{c}\|\sigma} \right) \tilde{\boldsymbol{s}} \right]$ is essentially $\mathrm{E}\left[Q\left(\frac{-\tau}{\|\boldsymbol{c}\|\sigma} \right) \tilde{\boldsymbol{s}} \right]$, or $\mathrm{E}[\tilde{\boldsymbol{s}}]$ ($Q(w) \approx 1$ when $w << 0$). $\boldsymbol{c} = \mathrm{E}[\tilde{\boldsymbol{s}}]$ simply means that $\boldsymbol{c}$ is the average of all signal vectors. On the other hand, when the norm of $\boldsymbol{c}$ is very large relative to τ, we have $g_\tau(\boldsymbol{c}) \approx g(\boldsymbol{c})$ since the effect of τ in (4-9) is effectively eliminated by the large denominator.

Geometrically, the new fixed-point relationship defines a locus of equalizer vector $\boldsymbol{c}$ parameterized by τ. Given a channel, a noise variance σ^2, and an update threshold τ, we can form a locus realizing (4-8) by plotting the norm and the direction of $\boldsymbol{c}$ for all values of $\|\boldsymbol{c}\| \geq 0$.

Example 4-1: Here we use a two-tap equalizer to illustrate a locus. We consider a two-tap binary-signaling channel where the channel has a transfer function $H(z) = -0.6 + z^{-1}$. In this example, we use SNR = 10 dB and $\tau = 0.1$. In Fig. 4-1, we plot three different-norm equalizer vectors satisfying (4-8). The dashed circles are circles whose radii are the norms of the equalizers. We see these vectors point in three different directions. In Fig. 4-2, we plot the locus by connecting all equalizers (with norms from 0.001 to 2.0) satisfying (4-8). We see that the portion on locus corresponding to large equalizer norms is nearly a straight line, whereas when the equalizer norm is small, the effect of τ makes the initial curvy segment of the locus.

It is harder to visualize a locus when we consider equalizers with more than two taps since the locus would then live in a higher dimensional space. We now attempt to describe a locus in an intuitive way: A N-dimensional space is occupied by a N-dimensional onion with the center of the onion at the origin of the space. The onion has infinite layers of skin, each skin layer is a hollow hypersphere with a certain radius. In Fig. 4-1 and Fig. 4-2, the dashed circles are the onion skin layers in the two-dimensional space. As demonstrated Fig. 4-1, for each skin layer, there is a hole pierced by a unique vector whose norm is the radius of the layer and whose direction is characterized by (4-8). The locus is like a thread passing through the holes of all skin layers of the onion as seen in Fig. 4-2.

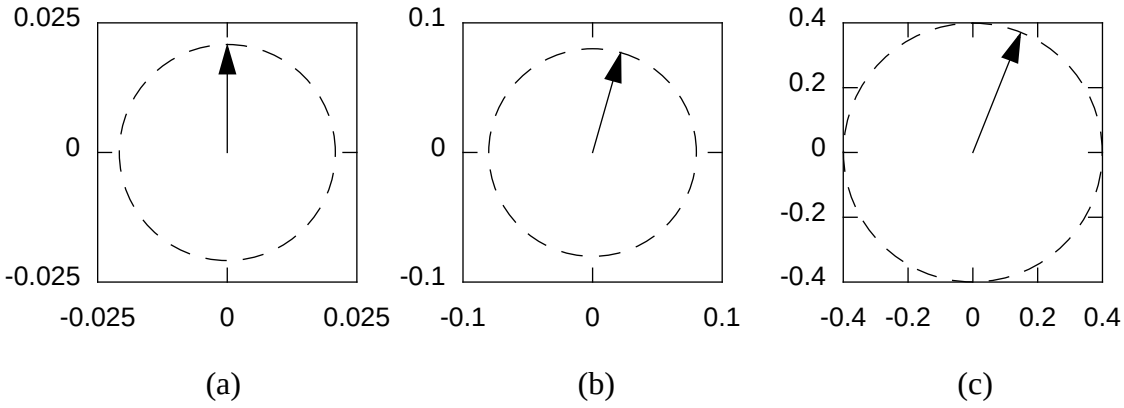

Fig. 4-1. Equalizer vectors satisfying the locus equation of (4-8) with norms (a) 0.02, (b) 0.06, and (c) 0.4.

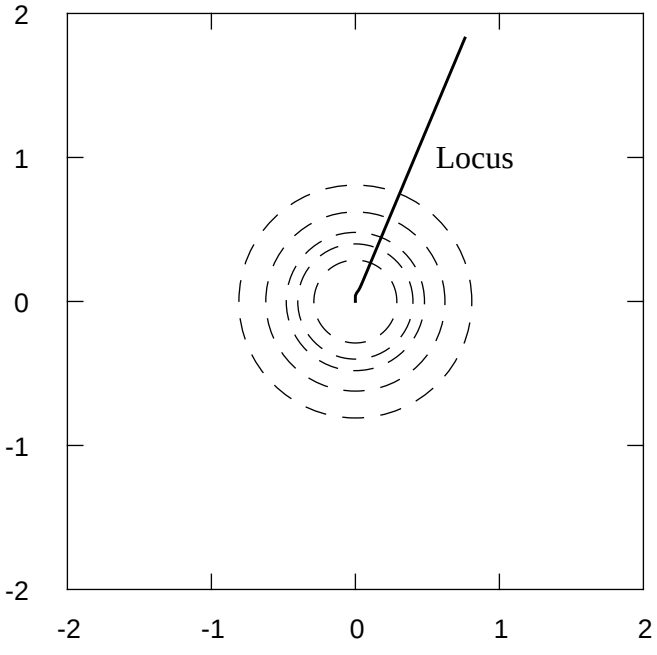

Fig. 4-2. The locus for a 2-tap equalizer for the channel in Example 4-1.

4.3.2 Global Convergence

In this subsection, we conjecture that the AMBER algorithm converges globally with a sufficiently small step size. To substantiate our conjecture, we first study the equilibrium state of AMBER with the following claim:

Lemma 4-1: The equilibrium state described by (4-7) cannot be true for a $\boldsymbol{c}$ with an arbitrary large or small norm. In addition, there exists some $\boldsymbol{c}$ with a finite non-zero norm satisfying the equilibrium state.

Proof. The proof for Lemma 4-1 is in Appendix 4.2.

We now investigate whether the AMBER algorithm indeed converges globally. We start with the concept of the hyperspace onion. For any positive number M, there exists a hollow hypersphere (onion skin layer) with radius M and there exists a unique vector $\boldsymbol{c}^*(M)$ with norm M satisfying the fixed-point relationship of (4-8). We now make the claim that the locus acts as an "attractor" which attracts the update towards it, starting with the following lemma:

Lemma 4-2: If $\boldsymbol{c}_k$ and $\boldsymbol{c}^*(||\boldsymbol{c}_k||)$ form an angle ϕ, there exists a sufficiently small step size μ such that the angle between $\boldsymbol{c}_{k+1}$ and $\boldsymbol{c}^*(||\boldsymbol{c}_k||)$ is strictly smaller then ϕ.

Proof. The proof for Lemma 4-2 is in Appendix 4.3.

Conjecture: In order to formally claim that the update becomes asymptotically closer to the locus, we need to show that the angle between $\boldsymbol{c}_{k+1}$ and $\boldsymbol{c}^*(||\boldsymbol{c}_{k+1}||)$ is less than the angle between $\boldsymbol{c}_k$ and $\boldsymbol{c}^*(||\boldsymbol{c}_k||)$**.** Although it hasn't been rigorously proved, simulation results in section 4.5 have shown that the rate of change of the enclosed angle between $\boldsymbol{c}^*(||\boldsymbol{c}_k||)$ and $\boldsymbol{c}^*(||\boldsymbol{c}_{k+1}||)$ is slower than the rate of change

of the enclosed angle between $\boldsymbol{c}_k$ and $\boldsymbol{c}_{k+1}$ and thus we conjecture that the update trajectory gets closer to the locus for a sufficiently small update step size.

We observe that once the update trajectory gets close enough to the locus, the equalizer update process is more norm adjusting (expanding or shrinking the equalizer norm to reach the equilibrium state) than direction adjustment. We will substantiate our claim with computer simulation results in section 4.5.

4.4 MULTI-STEP ALGORITHMS

The update frequency, and consequently the convergence speed, of the original AMBER ($\tau = 0$) is proportional to error probability. Although we have incorporated an update threshold τ to increase its convergence speed, a further increase in convergence speed may still be possible.

It is well known that the recursive least-squared (RLS) algorithm [7] yields the fastest convergence speed and the best steady-state MSE performance. One may be tempted to ask this question: what is the *best* algorithm in terms of convergence speed and steady-state error-probability performance (closest to the minimum error probability)?

Unfortunately, the counterpart of the RLS algorithm in the minimum error probability criterion is difficult to find. Nevertheless, we recognize that by simply varying the step size of an update algorithm, we can increase the convergence speed. Instead of finding the *best* error-probability-based algorithm to maximize speed of convergence, here we attempt to give a reasonably good step size function to improve convergence speed.

Recall that the error indicator function of AMBER is binary (either there is an update or there is no update), and the expectation of the error indicator function is the Gaussian error function. It relies on a long training sequence in order to approach its expectation.

Thus, we predict that if the error indicator function of the stochastic update is the Gaussian error function, then the update frequency, and consequently the convergence speed, should become higher. Assuming that the noise variance is known or can be estimated, we can form a update algorithm by using the noisy, instead of the noiseless, channel output vector:

$$\boldsymbol{c}_{k+1} = \boldsymbol{c}_k + \mu I_{\text{fast}} \boldsymbol{r}_k, \tag{4-10}$$

where the update decision I_{fast} is

$$I_{\text{fast}} = \begin{cases} Q\left(\dfrac{\text{sgn}(x_{k-D})y_k - (|x_{k-D}| - 1)f_D}{\|\boldsymbol{c}_k\|\sigma}\right), & \text{if } y_k < x_{k-D}f_D \text{ and } x_{k-D} \neq -L+1, \\ -Q\left(\dfrac{\text{sgn}(x_{k-D})y_k - (|x_{k-D}| - 1)f_D}{\|\boldsymbol{c}_k\|\sigma}\right), & \text{if } y_k > x_{k-D}f_D \text{ and } x_{k-D} \neq L-1, \\ 0, & \text{otherwise,} \end{cases} \tag{4-11}$$

where y_k is the noisy equalizer output and the term $[\text{sgn}(x_{k-D})y_k - (|x_{k-D}| - 1)f_D]$ is a noisy inner product between $\boldsymbol{c}$ and a signal vector $\boldsymbol{s}$. With some increased complexity, *i.e.* noise variance estimation and calculation of equalizer norm, we have devised a new update algorithm approximating the ensemble average of the AMBER algorithm. The convergence behavior of (4-10) is numerically studied in the next section.

We can apply the dual-sign concept in [19] to obtain an update algorithm with a complexity lower than the algorithm of (4-10) but with a faster convergence performance than that of (4-1). Instead of a single step size, we may use multiple step sizes so that updates

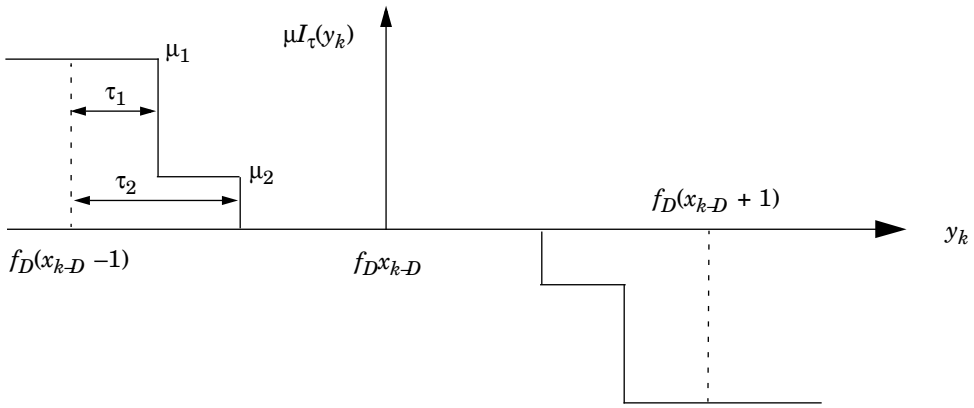

Fig. 4-3. Illustration of a 2-step AMBER algorithm.

occur more frequently. For example, a 2-step AMBER uses μ_1 and μ_2 for thresholds τ_1 and τ_2, as illustrated in Fig. 4-3. The 2-step AMBER algorithm adjusts an equalizer with a larger increment when the equalizer output is further away from the desired signal $f_D x_{k-D}$. Higher-step AMBER algorithms can be constructed likewise.

4.5 NUMERICAL RESULTS

In this section, we first use computer simulation results to substantiate our claim that the AMBER algorithm converges globally. We then compare the convergence speed of the AMBER algorithm and its variants. Finally, we investigate the decision-directed mode performance of the AMBER algorithm.

4.5.1 Global Convergence

In this subsection, we first plot the loci of two simple equalizable channels and the deterministic AMBER trajectories to confirm our analytical predications. We then perform simulations on channels to investigate the global convergence property of the stochastic AMBER algorithm.

We first use the simple channel $H(z) = -0.6 + z^{-1}$ from Example 4-1. For visualization purpose, we update a two-tap equalizer so that we can plot the update trajectory in a two-dimensional space. We use SNR = 10 dB and $\tau = 0.1$. In Fig. 4-4, we plot the locus and the trajectory with the initial condition [–2, 1]. In Fig. 4-5, we plot the locus and the trajectory with the initial condition [–1, –1]. The equilibrium point is [0.2031, 0.5014].

We substantiate our claim with another simple channel: $H(z) = 0.4 + z^{-1} - 0.2z^{-2}$. With SNR = 10 dB and $\tau = 0.1$. In Fig. 4-6, we plot the locus and the update trajectory with the initial condition [–1, –1]. In Fig. 4-7, we plot the locus and the trajectory with the initial condition [1, 1]. The equilibrium point is [-0.2278, 0.6629] .

As predicted by our analytical reasoning in section 4.3, the deterministic trajectories from above two examples first approach the loci and then “slide” along the loci to reach the equilibrium points.

Besides observing the deterministic trajectories of the ensemble averaged AMBER algorithm, we also perform computer simulations to substantiate our claim on the global convergence property of the stochastic AMBER algorithm. We pick one hundred equalizable three-tap ISI channels, whose taps are distributed uniformly between -1 and 1, and apply three-tap equalizers. All equalizers are initialized with small random numbers. All equalizers converge closely to their minimum-error-probability solutions. For each channel, we first find the EMSER solution and thus find the minimum-SER value. Each equalizer learning curve is plotted with time k versus $\mathrm{SER}_k/\mathrm{SER}_{min}$. Instead of plotting one hundred different equalizer learning curves, we average the one hundred learning curves and plot the averaged learning curve in Fig. 4-8. All equalizers use a step size of $\mu = 0.0001$ and a threshold of $\tau = 0.1$.

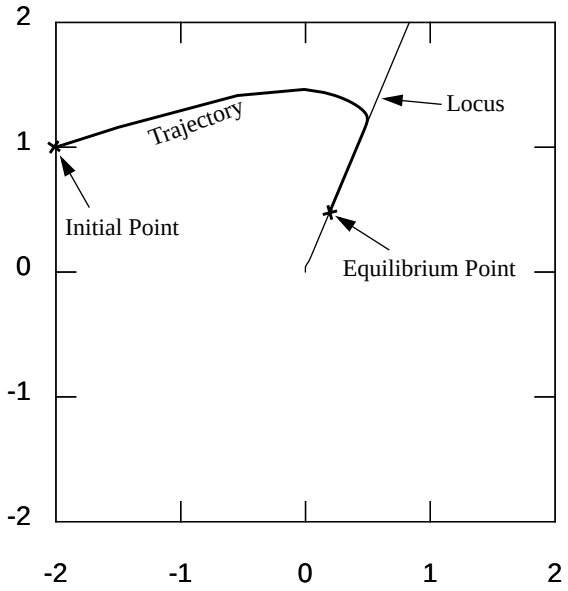

Fig. 4-4. The locus and the 2-tap equalizer trajectory (with initial condition [-2, 1]) for the channel $H(z) = -0.6 + z^{-1}$.

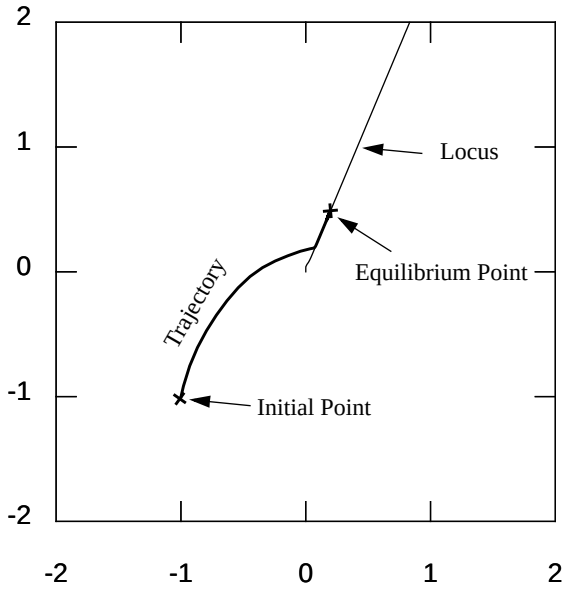

Fig. 4-5. The locus and the trajectory (with initial condition [–1, –1]) for the channel $H(z) = -0.6 + z^{-1}$.

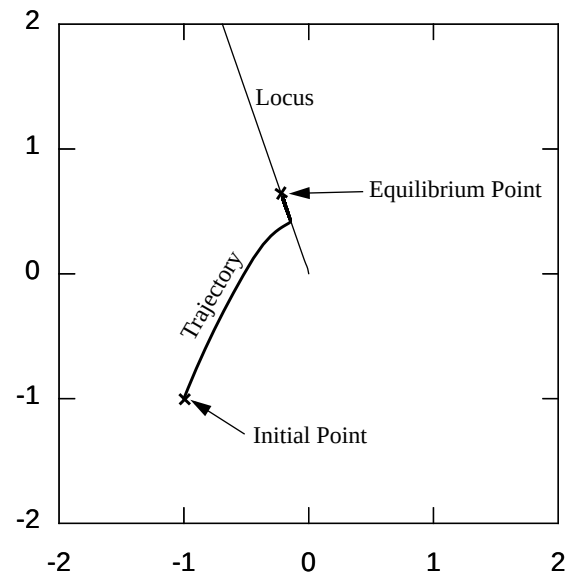

Fig. 4-6. The locus and the 2-tap equalizer trajectory (with initial condition [–1, –1]) for the channel $H(z) = 0.4 + z^{-1} - 0.2z^{-2}$.

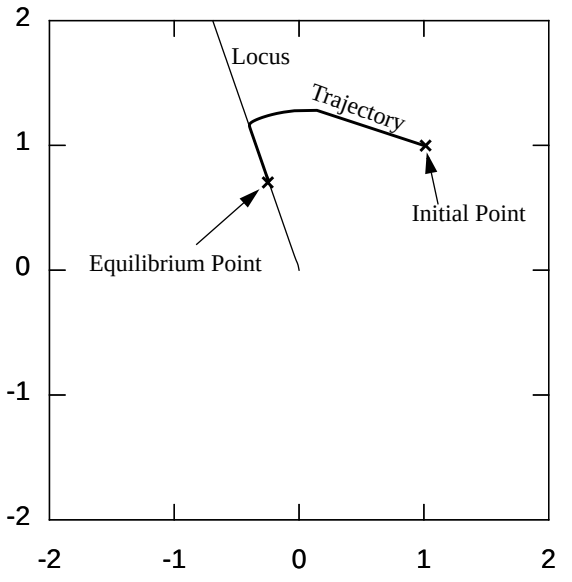

Fig. 4-7. The locus and the 2-tap equalizer trajectory (with initial condition [1, 1]) for the channel $H(z) = 0.4 + z^{-1} - 0.2z^{-2}$.

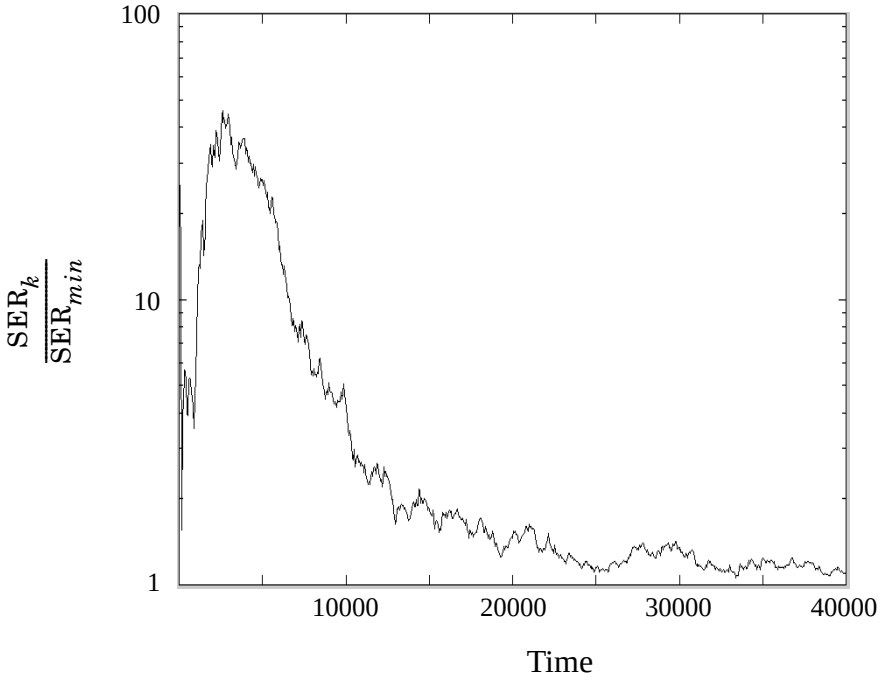

Fig. 4-8. The averaged learning curve of 3-tap equalizers over 100 3-tap channels.

4.5.2 Convergence Speed

In this subsection, we compare convergence speed of the AMBER algorithm, the 3-step AMBER algorithm, and the "infinite-step" AMBER algorithm of (4-10) on one hundred 3-tap 2-PAM channels with SNR = 20 dB. All equalizers have three taps and the delays *D*s are chosen to minimize MSE. We use $\mu = 0.0001$ and $\tau = 0.1$ for the AMBER algorithm. For the 3-step AMBER, we use parameters $\mu_1 = 0.0004$, $\mu_2 = 0.0002$, $\mu_3 = 0.0001$, $\tau_1 = 0$, $\tau_2 = 0.05$, and $\tau_3 = 0.1$. For the "infinite-step" AMBER algorithm, we use $\mu = 0.01$. In Fig. 4-9, we see that the "infinite-step" AMBER algorithm has the best convergence performance, the 3-step AMBER algorithm is next, while the 1-step AMBER algorithm has the worst convergence performance.

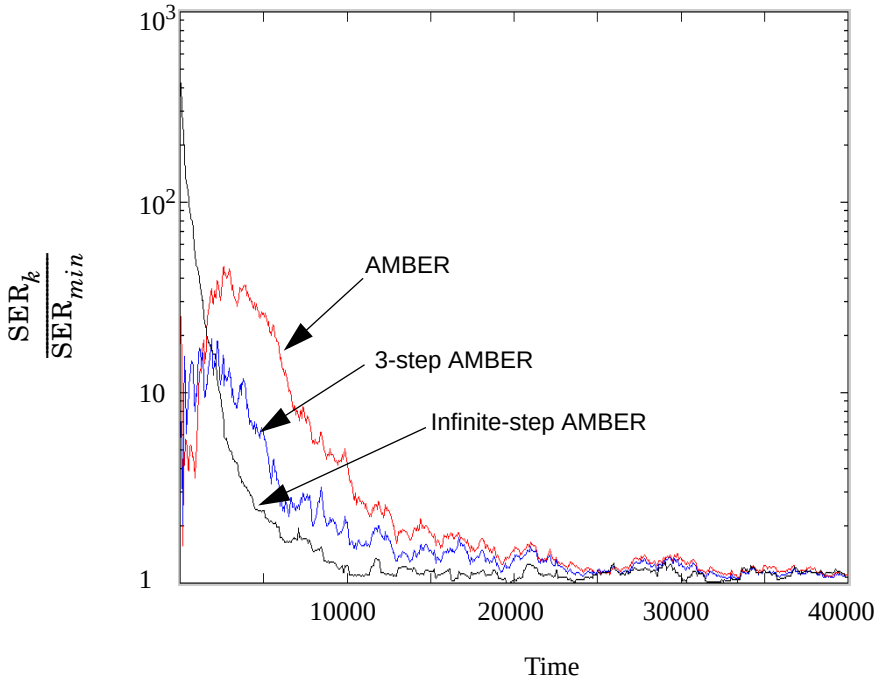

Fig. 4-9. Averaged convergence comparison of the AMBER, 3-step AMBER, and infinite-step AMBER algorithms.

4.5.3 Decision-Directed Adaptation

In this subsection, we evaluate the decision-directed mode of the AMBER algorithm. After using a training sequence to initialize the equalizer with some acceptable error probability, we switch the adaptation to a decision-directed mode to see whether the algorithm is able to converge closely to the minimum error-probability performance.

In Fig. 4-10, we plot the learning curve of a 3-tap AMBER algorithm on the 4-PAM channel $H(z) = 1 + 1.67z^{-1}$. We use $\mu = 0.0005$, $\tau = 0.1$, and SNR = 30 dB. After 2500 training data, we switch the adaptation to a decision-directed mode. Observe that the algo-

rithm continues to converge closely to the minimum error-probability state. In addition, we add the learning curve obtained with training data and observe that it behaviors closely to the decision-directed learning curve.

4.6 SUMMARY AND CONCLUSIONS

In this chapter, we have obtained the deterministic trajectory equation of the AMBER algorithm by taking expectation of the stochastic update algorithm. We found that the expectation of the noise component term of the received channel output vector constituted a shrinking term which is always in the opposite direction of the equalizer. Based on the deterministic trajectory of AMBER, we have gained some understanding of its update dynamics. Because of its highly nonlinear and complicated dynamical behavior, we have

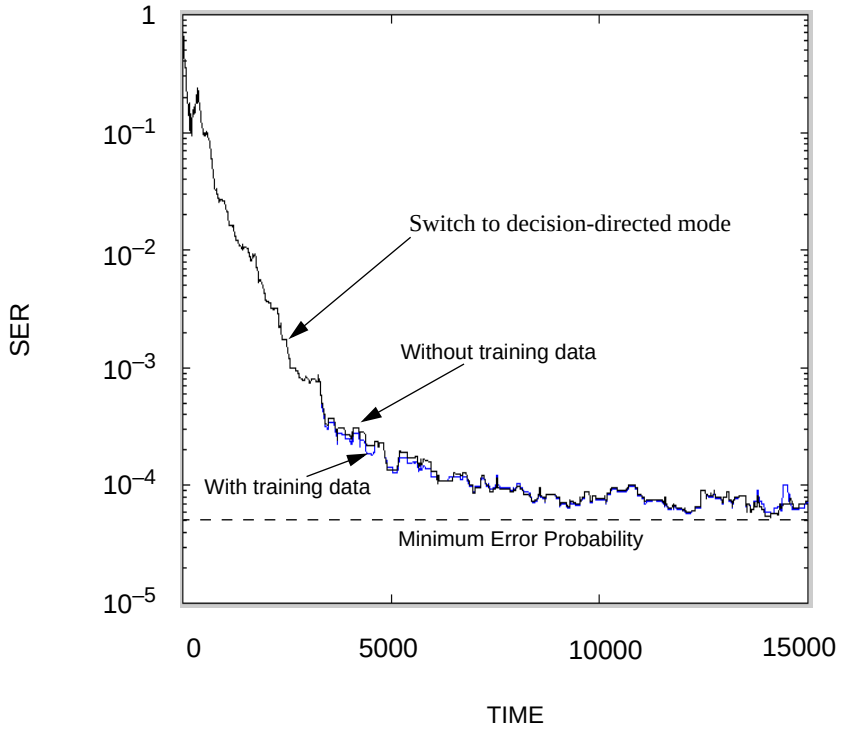

Fig. 4-10. Learning curve comparison of a 3-tap AMBER equalizer with and without training data after 2500 iterations.

not been able to rigorously prove global convergence. However, we can qualitatively predict the nonlinear dynamics. Further, we have substantiated our claim of the global convergence property with computer simulation results.

In addition to the discussion on the global convergence, we have proposed a multi-step variant of AMBER to increase convergence speed. We have shown that the “infinite-tap” AMBER equalizer converges rather quickly at a cost of some complexity increase. By incorporating the ideas of the dual-sign algorithm and the continuous function of the expected error indicator function, we have used variable step sizes to increase update frequency and convergence speed.

APPENDIX 4.1

PROOF OF THEOREM 4.1

In this appendix, we prove Theorem 4.1. This proof closely follows the proof in Appendix 3.3 and will only be sketched here.

We first find the ensemble average $\mathrm{E}[I_\tau \boldsymbol{x}_k]$ by finding the scalar $\mathrm{E}[I_\tau x_{k-D}]$ and the vector $\mathrm{E}[I_\tau \boldsymbol{z}]$ where $\boldsymbol{z} = [x_k, \ldots, x_{k-D+1}, x_{k-D-1}, \ldots, x_{k-M-N+1}]^T$.

Following the notations in Appendix 3.3, we have:

$$\mathrm{E}[I_\tau x_{k-D}] = \frac{-L+1}{L}\mathrm{E}[I_\tau \mid \text{left}] + \frac{L-1}{L}\mathrm{E}[I_\tau \mid \text{right}] \tag{4-12}$$

$$= \frac{L-1}{L}\left\{\mathrm{E}\left[Q\left(\frac{f_D - \boldsymbol{b}^T\boldsymbol{z} - \tau}{\|\boldsymbol{c}\|\sigma}\right)\right] + \mathrm{E}\left[Q\left(\frac{f_D + \boldsymbol{b}^T\boldsymbol{z} - \tau}{\|\boldsymbol{c}\|\sigma}\right)\right]\right\} \tag{4-13}$$

$$= \frac{2L-2}{L}\mathrm{E}\left[Q\left(\frac{f_D + \boldsymbol{b}^T\boldsymbol{z} - \tau}{\|\boldsymbol{c}\|\sigma}\right)\right], \tag{4-14}$$

where $\boldsymbol{b} = [f_0, \ldots, f_{D-1}, f_{D+1}, \ldots, f_{M+N-1}]^T$. The derivation of $\mathrm{E}[I_\tau \boldsymbol{z}]$ is similar to the derivation of $\mathrm{E}[I \boldsymbol{z}]$ in Appendix 3.3 and is:

$$\mathrm{E}[I_\tau \boldsymbol{z}] = \frac{2L-2}{L} \mathrm{E}\left[Q\left(\frac{f_D + \boldsymbol{b}^T \boldsymbol{z} - \tau}{\|\boldsymbol{c}\| \sigma} \right) \boldsymbol{z} \right]. \tag{4-15}$$

Combining (4-14) and (4-15), we have

$$\mathrm{E}[I_\tau \boldsymbol{x}_k] = \frac{2L-2}{L} \mathrm{E}\left[Q\left(\frac{\boldsymbol{c}^T \mathbf{H} \tilde{\boldsymbol{x}} - \tau}{\|\boldsymbol{c}\| \sigma} \right) \tilde{\boldsymbol{x}} \right] \tag{4-16}$$

and

$$\mathrm{E}[I_\tau \boldsymbol{s}_k] = \mathrm{E}[I_\tau \mathbf{H} \boldsymbol{x}_k] = \frac{2L-2}{L} \mathrm{E}\left[Q\left(\frac{\boldsymbol{c}^T \tilde{\boldsymbol{s}} - \tau}{\|\boldsymbol{c}\| \sigma} \right) \tilde{\boldsymbol{s}} \right] \tag{4-17}$$

where $\tilde{\boldsymbol{x}}$ is a random vector with distribution $p(\tilde{\boldsymbol{x}}) = p(\boldsymbol{x}_k \mid x_{k-D} = 1)$, *i.e.*, $\tilde{\boldsymbol{x}}$ is uniformly distributed over the set of L^{M+N-1} L-ary $\boldsymbol{x}_k$ vectors for which $x_{k-D} = 1$ and $\tilde{\boldsymbol{s}} = \mathbf{H} \tilde{\boldsymbol{x}}$.

Again, following the derivation of $\mathrm{E}[I \boldsymbol{n}_k]$ in Appendix 3.3, the ensemble average $\mathrm{E}[I_\tau \boldsymbol{n}_k]$ is

$$\begin{aligned} \mathrm{E}[I_\tau \boldsymbol{n}_k] = & \sum_l \mathrm{E}[I_\tau \boldsymbol{n}_k \mid I_\tau = 1, \boldsymbol{z} = \boldsymbol{z}^l] \, \mathrm{P}[I_\tau = 1, \boldsymbol{z} = \boldsymbol{z}^l] + \\ & \sum_l \mathrm{E}[I_\tau \boldsymbol{n}_k \mid I_\tau = -1, \boldsymbol{z} = \boldsymbol{z}^l] \, \mathrm{P}[I_\tau = -1, \boldsymbol{z} = \boldsymbol{z}^l], \end{aligned} \tag{4-18}$$

where the conditional expectation $\mathrm{E}[I_\tau \boldsymbol{n}_k \mid I_\tau = 1, \boldsymbol{z} = \boldsymbol{z}^l]$ is:

$$\mathrm{E}[I_\tau \boldsymbol{n}_k \mid I_\tau = 1, \boldsymbol{z} = \boldsymbol{z}^l] = -\sigma \mathrm{E}\left[m\left(\frac{f_D + \boldsymbol{b}^T \boldsymbol{z}^l - \tau}{\|\boldsymbol{c}\| \sigma} \right) \right] \boldsymbol{c} / \| \boldsymbol{c} \|, \tag{4-19}$$

where the function $m(\eta)$ is defined in (3-54).

We now derive the joint probability $\mathrm{P}[I_\tau = 1,\ \boldsymbol{z} = \boldsymbol{z}^l]$:

$$\mathrm{P}[I_\tau = 1,\ \boldsymbol{z} = \boldsymbol{z}^l] = \mathrm{P}[I_\tau = 1 \mid \boldsymbol{z} = \boldsymbol{z}^l]\ \mathrm{P}[\boldsymbol{z} = \boldsymbol{z}^l] \tag{4-20}$$

$$= \frac{L-1}{L} Q\left(\frac{f_D + \boldsymbol{b}^T \boldsymbol{z}^l - \tau}{\|\boldsymbol{c}\|\sigma}\right) \frac{1}{L^{M+N-1}}. \tag{4-21}$$

Combining (4-19) and (4-21), the first summation term in (4-18) becomes

$$\sum_l \mathrm{E}[I_\tau \boldsymbol{n}_k \mid I_\tau = 1,\ \boldsymbol{z} = \boldsymbol{z}^l]\ \mathrm{P}[I_\tau = 1,\ \boldsymbol{z} = \boldsymbol{z}^l] = \frac{-(L-1)\sigma}{L\sqrt{2\pi}} \mathrm{E}\left[\exp\left(\frac{-(\boldsymbol{c}^T \tilde{\boldsymbol{s}} - \tau)^2}{2\|\boldsymbol{c}\|^2 \sigma^2}\right)\right] \frac{\boldsymbol{c}}{\|\boldsymbol{c}\|}. \tag{4-22}$$

It is not hard to show that

$$\sum_l \mathrm{E}[I_\tau \boldsymbol{n}_k \mid I_\tau = 1,\ \boldsymbol{z} = \boldsymbol{z}^l]\ \mathrm{P}[I_\tau = 1,\ \boldsymbol{z} = \boldsymbol{z}^l]$$

$$= \sum_l \mathrm{E}[I_\tau \boldsymbol{n}_k \mid I_\tau = -1,\ \boldsymbol{z} = \boldsymbol{z}^l]\ \mathrm{P}[I_\tau = -1,\ \boldsymbol{z} = \boldsymbol{z}^l], \tag{4-23}$$

and thus

$$\mathrm{E}[I_\tau \boldsymbol{n}_k] = -\frac{2L-2}{L} \frac{\sigma}{\sqrt{2\pi}} \mathrm{E}\left[\exp\left(\frac{-(\boldsymbol{c}^T \tilde{\boldsymbol{s}} - \tau)^2}{2\|\boldsymbol{c}\|^2 \sigma^2}\right)\right] \frac{\boldsymbol{c}}{\|\boldsymbol{c}\|}. \tag{4-24}$$

Q.E.D.

APPENDIX 4.2

PROOF OF LEMMA 4-1

In this appendix, we prove Lemma 4-1: The equilibrium state described by (4-7) cannot be true for a $\boldsymbol{c}$ with an arbitrary large or small norm. In addition, there exists some $\boldsymbol{c}$ with a finite non-zero norm satisfying (4-7).

Recall that a locus depicts norms and directions of equalizers satisfying the fixed-point relationship of (4-8). However, not all equalizers on the locus satisfy (4-7). For referencing convenience, here we again state the equilibrium condition of (4-7):

$$\mathrm{E}\left[Q\left(\frac{\boldsymbol{c}^T\tilde{\boldsymbol{s}}-\tau}{\|\boldsymbol{c}\|\sigma}\right)\tilde{\boldsymbol{s}}\right] = \frac{\sigma}{\sqrt{2\pi}}\mathrm{E}\left[\exp\left(\frac{-(\boldsymbol{c}^T\tilde{\boldsymbol{s}}-\tau)^2}{2\|\boldsymbol{c}\|^2\sigma^2}\right)\right]\frac{\boldsymbol{c}}{\|\boldsymbol{c}\|}. \tag{4-25}$$

Here we show that an equalizer $\boldsymbol{c}$ (on the locus) with an arbitrary large or small norm cannot satisfy (4-25). In order for (4-25) to be true, the norms of both sides have to be

equal. We see that when an equalizer satisfies (4-25), the norm of the left hand side term in (4-25) is

$$\left\| \mathrm{E}\left[Q\left(\frac{\boldsymbol{c}^T \tilde{\boldsymbol{s}} - \tau}{\|\boldsymbol{c}\|\sigma} \right) \tilde{\boldsymbol{s}} \right] \right\| = \frac{\boldsymbol{c}^T}{\|\boldsymbol{c}\|} \mathrm{E}\left[Q\left(\frac{\boldsymbol{c}^T \tilde{\boldsymbol{s}} - \tau}{\|\boldsymbol{c}\|\sigma} \right) \tilde{\boldsymbol{s}} \right] = \mathrm{E}\left[Q\left(\frac{\boldsymbol{c}^T \tilde{\boldsymbol{s}} - \tau}{\|\boldsymbol{c}\|\sigma} \right) \frac{\boldsymbol{c}^T \tilde{\boldsymbol{s}}}{\|\boldsymbol{c}\|} \right]. \tag{4-26}$$

since the vector $\mathrm{E}\left[Q\left(\frac{\boldsymbol{c}^T \tilde{\boldsymbol{s}} - \tau}{\|\boldsymbol{c}\|\sigma} \right) \tilde{\boldsymbol{s}} \right]$ and the unit-norm vector $\frac{\boldsymbol{c}^T}{\|\boldsymbol{c}\|}$ are in the same direction and their inner product equals the norm of $\mathrm{E}\left[Q\left(\frac{\boldsymbol{c}^T \tilde{\boldsymbol{s}} - \tau}{\|\boldsymbol{c}\|\sigma} \right) \tilde{\boldsymbol{s}} \right]$. The norm of the right hand side term in (4-25) is simply

$$\left\| \frac{\sigma}{\sqrt{2\pi}} \mathrm{E}\left[\exp\left(\frac{-(\boldsymbol{c}^T \tilde{\boldsymbol{s}} - \tau)^2}{2\|\boldsymbol{c}\|^2 \sigma^2} \right) \right] \frac{\boldsymbol{c}}{\|\boldsymbol{c}\|} \right\| = \frac{\sigma}{\sqrt{2\pi}} \mathrm{E}\left[\exp\left(\frac{-(\boldsymbol{c}^T \tilde{\boldsymbol{s}} - \tau)^2}{2\|\boldsymbol{c}\|^2 \sigma^2} \right) \right]. \tag{4-27}$$

Thus, the equilibrium point(s) on a locus needs to satisfies both (4-25) and the following norm equality:

$$\mathrm{E}\left[Q\left(\frac{\boldsymbol{c}^T \tilde{\boldsymbol{s}} - \tau}{\|\boldsymbol{c}\|\sigma} \right) \frac{\boldsymbol{c}^T \tilde{\boldsymbol{s}}}{\|\boldsymbol{c}\|} \right] = \frac{\sigma}{\sqrt{2\pi}} \mathrm{E}\left[\exp\left(\frac{-(\boldsymbol{c}^T \tilde{\boldsymbol{s}} - \tau)^2}{2\|\boldsymbol{c}\|^2 \sigma^2} \right) \right]. \tag{4-28}$$

Now if $\|\boldsymbol{c}\|$ is arbitrarily large, the effect of τ in (4-28) is zero and the left hand side term of (4-28) effectively becomes $\mathrm{E}\left[Q\left(\frac{\boldsymbol{c}^T \tilde{\boldsymbol{s}}}{\|\boldsymbol{c}\|\sigma} \right) \frac{\boldsymbol{c}^T \tilde{\boldsymbol{s}}}{\|\boldsymbol{c}\|} \right]$, and the right hand side term of (4-28) becomes $\frac{\sigma}{\sqrt{2\pi}} \mathrm{E}\left[\exp\left(\frac{-(\boldsymbol{c}^T \tilde{\boldsymbol{s}})^2}{2\|\boldsymbol{c}\|^2 \sigma^2} \right) \right]$, and we will show that the two terms cannot be equal under the assumption that $\boldsymbol{c}$ opens the eye of the channel (*i.e.* the inner products $\boldsymbol{c}^T \tilde{\boldsymbol{s}} > 0$).

Let $\frac{\boldsymbol{c}^T \tilde{\boldsymbol{s}}}{\|\boldsymbol{c}\|\sigma} = w$ and use the fact that $\frac{1}{\sqrt{2\pi} w} \exp\left(\frac{-w^2}{2} \right)$ is strictly a upper bound for $Q(w)$, we prove the following inequality:

$$\mathrm{E}\left[Q\left(\frac{\boldsymbol{c}^T \tilde{\boldsymbol{s}}}{\|\boldsymbol{c}\|\sigma} \right) \frac{\boldsymbol{c}^T \tilde{\boldsymbol{s}}}{\|\boldsymbol{c}\|\sigma} \right] = \mathrm{E}[Q(w)w] \tag{4-29}$$

$$< \frac{1}{\sqrt{2\pi}} \mathrm{E}\left[\exp\left(\frac{-w^2}{2} \right) \right] \tag{4-30}$$

$$= \frac{1}{\sqrt{2\pi}} \mathrm{E}\left[\exp\left(\frac{-(\boldsymbol{c}^T \tilde{\boldsymbol{s}})^2}{2\|\boldsymbol{c}\|^2 \sigma^2} \right) \right]. \tag{4-31}$$

Thus, the existence of an equalizer with an arbitrarily large norm is not possible at equilibrium. We now show the existence of an equalizer with an arbitrarily small norm is not possible at equilibrium. As $\|\boldsymbol{c}\| \to 0$, the effect of τ in (4-28) dominates the term $\boldsymbol{c}^T \tilde{\boldsymbol{s}}$ and the left hand side of (4-28) effectively becomes $\mathrm{E}\left[Q\left(\frac{-\tau}{\|\boldsymbol{c}\|\sigma} \right) \frac{\boldsymbol{c}^T \tilde{\boldsymbol{s}}}{\|\boldsymbol{c}\|} \right]$, or $\mathrm{E}\left[\frac{\boldsymbol{c}^T \tilde{\boldsymbol{s}}}{\|\boldsymbol{c}\|} \right]$ ($Q(w) \approx 1$ if w << 0), and the right hand side of (4-28) effectively becomes $\frac{\sigma}{\sqrt{2\pi}} \mathrm{E}\left[\exp\left(\frac{-\tau^2}{2\|\boldsymbol{c}\|^2 \sigma^2} \right) \right]$ or 0 ($\exp(w) \approx 0$ if w << 0).

We now prove that there exists some $\boldsymbol{c}$ satisfying (4-25). Let Z be the difference between the two norms of (4-28):

$$Z = \mathrm{E}\left[Q\left(\frac{\boldsymbol{c}^T \tilde{\boldsymbol{s}} - \tau}{\|\boldsymbol{c}\|\sigma} \right) \frac{\boldsymbol{c}^T \tilde{\boldsymbol{s}}}{\|\boldsymbol{c}\|} \right] - \frac{\sigma}{\sqrt{2\pi}} \mathrm{E}\left[\exp\left(\frac{-(\boldsymbol{c}^T \tilde{\boldsymbol{s}} - \tau)^2}{2\|\boldsymbol{c}\|^2 \sigma^2} \right) \right]. \tag{4-32}$$

We see that Z is a continuous function of $\boldsymbol{c}$. Since $Z < 0$ when $\|\boldsymbol{c}\|$ is arbitrarily large and $Z > 0$ when $\|\boldsymbol{c}\|$ is arbitrarily small, we conclude that there exists some $\boldsymbol{c}$ with a finite non-zero norm which yields $Z = 0$ and thus, satisfies the equilibrium state. *Q.E.D.*

APPENDIX 4.3

PROOF OF LEMMA 4-2

In this appendix, we prove Lemma 4-2: There exists a sufficiently small step size such that if $\boldsymbol{c}_k$ and $\boldsymbol{c}^*(||\boldsymbol{c}_k||)$ form an angle ϕ, then the angle between $\boldsymbol{c}_{k+1}$ and $\boldsymbol{c}^*(||\boldsymbol{c}_k||)$ is strictly smaller then ϕ.

Without loss of generality, we sketch a three-dimensional space example (a 3-tap equalizer) in Fig. 4-11 and Fig. 4-12. The sphere in Fig. 4-11 has a radius of $\|\boldsymbol{c}_k\|$ and $\boldsymbol{c}^*(||\boldsymbol{c}_k||)$ is the unique vector, with the norm $\|\boldsymbol{c}_k\|$, satisfying (4-8). The darker shaded circular cone has a base angle of ϕ, and has $\boldsymbol{c}^*(||\boldsymbol{c}_k||)$ at its center and $\boldsymbol{c}_k$ at its perimeter. The lighter shaded irregular cone is the signal cone as discussed in chapter 2.

In Fig. 4-12, we plot the top cross-sectional view of the cones. Let P denote the plane containing the origin and the perpendicular bisector of $\boldsymbol{c}_k$ and $\boldsymbol{c}^*(||\boldsymbol{c}_k||)$. This plane divides the signal cone $S = \{\Sigma_i\, a_i \tilde{\boldsymbol{s}}^{(i)} : a_i \geq 0\}$ into two subcones A and B, so that $S = A \cup B$,

where A is the intersection of S with the set of vectors on the $\boldsymbol{c}^*(||\boldsymbol{c}_k||)$ side of P, excluding P, and B is the intersection of S with the set of vectors on the $\boldsymbol{c}_k$ side of P, including P. Observe that $\boldsymbol{c}^*(||\boldsymbol{c}_k||) \in A$ and $\boldsymbol{c}_k \in B$ and that A and B are disjoint, $A \cap B = \varnothing$.

The function $g_\tau(\boldsymbol{c}^*(||\boldsymbol{c}_k||))$ can be decomposed into two weighted summations over signal vectors from A and B:

$$g_\tau(\boldsymbol{c}^*(||\boldsymbol{c}_k||)) \propto \sum_{s^{(i)} \in A} Q\left(\frac{\boldsymbol{c}^*(\|\boldsymbol{c}_k\|)^T \tilde{\boldsymbol{s}}^{(i)} - \tau}{\|\boldsymbol{c}_1\|\sigma}\right)\tilde{\boldsymbol{s}}^{(i)} + \sum_{s^{(j)} \in B} Q\left(\frac{\boldsymbol{c}^*(\|\boldsymbol{c}_k\|)^T \tilde{\boldsymbol{s}}^{(j)} - \tau}{\boldsymbol{c}_1\sigma}\right)\tilde{\boldsymbol{s}}^{(j)}. \quad (4\text{-}33)$$

Instead of $g_\tau(\boldsymbol{c}^*(||\boldsymbol{c}_k||))$, we look at $g_\tau(\boldsymbol{c}_k)$; it too can be expressed using (4-33), but with different weights. Compared with $\boldsymbol{c}^*(||\boldsymbol{c}_k||)$, the vector $\boldsymbol{c}_k$ forms a larger angle with all vectors $\boldsymbol{s}^{(i)}$ from A, while it forms a smaller or equal angle with all vectors from B. Thus, compared with the weights for $g_\tau(\boldsymbol{c}^*(||\boldsymbol{c}_k||))$, the weights for $g_\tau(\boldsymbol{c}_k)$ in (4-33) strictly *increase* for the $\boldsymbol{s}^{(i)}$ vectors in A, while they either *decrease* or remain the same for vectors in B. Since $g_\tau(\boldsymbol{c}^*(||\boldsymbol{c}_k||)) \propto \boldsymbol{c}^*(||\boldsymbol{c}_k||) \in A$, it follows that $g_\tau(\boldsymbol{c}_k)$ is also in A as shown in Fig. 4-12. The vector $\boldsymbol{c}_{k+1}$ is a linear combination of $\boldsymbol{c}_k$ and $g_\tau(\boldsymbol{c}_k)$ and can be made inside the circular cone if the step size is sufficiently small. Thus, the angle between $\boldsymbol{c}_{k+1}$ and $\boldsymbol{c}^*(||\boldsymbol{c}_k||)$ is less than the angle between $\boldsymbol{c}_k$ and $\boldsymbol{c}^*(||\boldsymbol{c}_k||)$. *Q.E.D.*

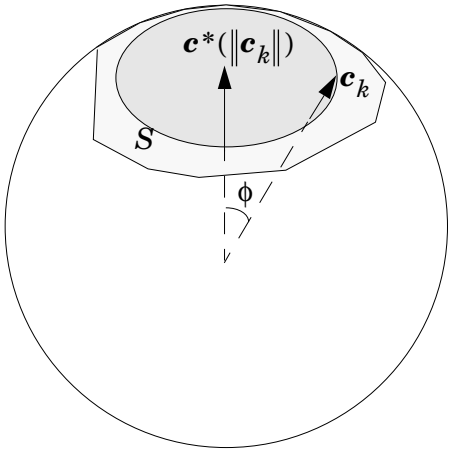

Fig. 4-11. A three-dimensional sphere with radius $\|\boldsymbol{c}_k\|$, a circular cone, and the signal cone.

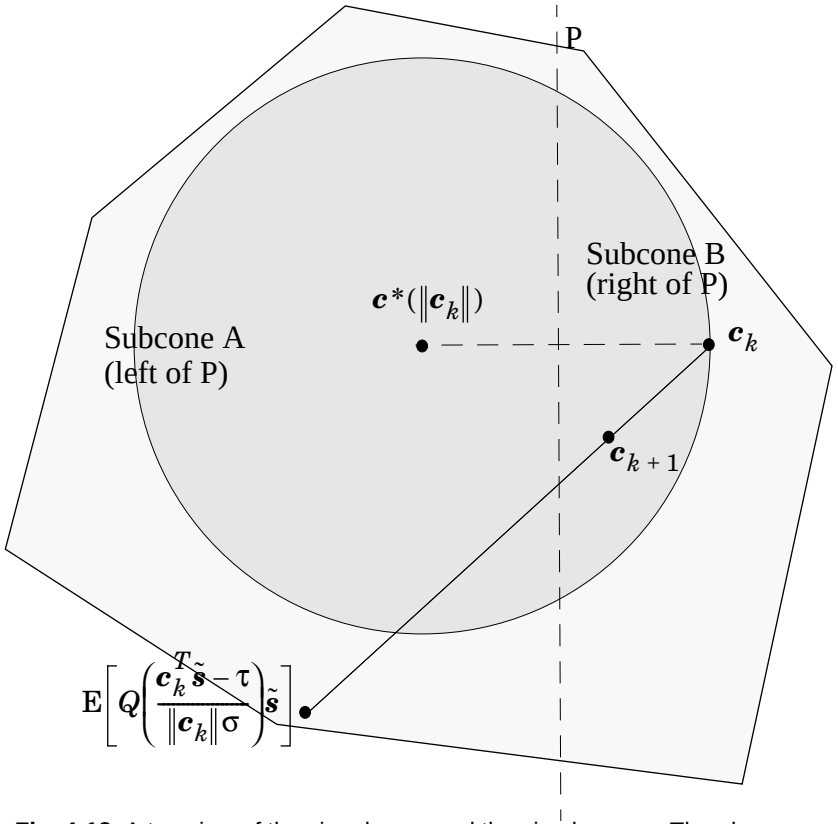

Fig. 4-12. A top view of the signal cone and the circular cone. The plane P bisects the segment connecting $\boldsymbol{c}_{k+1}$ and $\boldsymbol{c}^*(\|\boldsymbol{c}_k\|)$.

CHAPTER 5

APPROXIMATE MINIMUM-BER MULTIUSER DETECTION

5.1 INTRODUCTION

Previous chapters have been devoted to deriving and evaluating the minimum error-probability equalizers. In this chapter, we will extend the results on minimum-error-probability equalization to multiuser detection.

The class of linear multiuser detectors (which includes the conventional matched filter (MF), decorrelator, and MMSE detectors) is particularly attractive because it offers the advantages of low complexity, ease of adaptation, and the ability to operate in a decentralized fashion, meaning that only a single user of interest need be demodulated. While the

MMSE detector is widely regarded as a good multiuser detector, a better — indeed, the best — linear multiuser detector would choose its coefficients so as to minimize the resulting error probability.

Lupas and Verdú [4] proposed the maximum asymptotic-multiuser-efficiency (MAME) linear detector which minimizes BER in the limit as the noise approaches zero. An adaptive algorithm for realizing the MAME detector is not yet available. Adaptive algorithms for realizing the minimum-BER multiuser detector were proposed in [5] and [6], but they are either high in complexity or require knowledge of the signature sequence of the user of interest. The AMBER multiuser detector proposed here has low complexity and does not require knowledge of the signature sequence of user of interest.

This chapter is organized as follows. In section 5.2, we present the problem statement. In section 5.3, we discuss the exact minimum-BER (EMBER) multiuser detection. In section 5.4, we propose the approximate minimum-BER (AMBER) multiuser detector. In section 5.5, we present numerical results comparing the AMBER, MMSE, decorrelator, and MF detectors.

5.2 MEMORYLESS MULTIUSER CHANNELS

The essential features of the multiuser detection problem are captured by the synchronous CDMA channel model in which the receiver observation waveform is given by

$$r(t) = \sum_{i=1}^{N} A_i \sum_{k=-\infty}^{\infty} b_k^{(i)} s_i(t - kT) + n(t), \tag{5-1}$$

where N is the number of active users, $s_i(t)$ is the unit-energy received signature sequence for user i, A_i is the received amplitude for user i, $b_k^{(i)} \in \{\pm 1\}$ is the information bit for user

i during bit-epoch k, and $n(t)$ is additive white Gaussian noise with PSD σ^2. Assume that the signature sequence for user i is of the direct-sequence form

$$s_i(t) = \sum_{j=1}^{M} d_i^{(j)} p(t - jT/m), \tag{5-2}$$

where M is the number of chips per baud, $p(t)$ is a unit-energy Nyquist chip pulse-shape, and $\boldsymbol{d}_i = [d_i^{(1)} \ldots d_i^{(M)}]^T$ is a unit-norm vector representing the spreading code for user i.

The receiver may generate sufficient statistics by passing $r(t)$ through a filter matched to the chip-pulse shape and sampling the output at the chip rate, which leads to the following equivalent discrete-time memoryless model:

$$\boldsymbol{r}_k = \mathbf{H}\boldsymbol{b}_k + \boldsymbol{n}_k, \tag{5-3}$$

where $\mathbf{H} = [\boldsymbol{d}_1\ \boldsymbol{d}_2 \ldots \boldsymbol{d}_N]\mathbf{A}$ has dimension $M \times N$, $\mathbf{A} = \text{diag}(A_i)$, $\boldsymbol{b}_k = [b_k^{(1)} \ldots b_k^{(N)}]^T$, and $\boldsymbol{n}_k$ is white Gaussian noise with PSD $\sigma^2\mathbf{I}$. A decentralized linear multiuser detector for user i is then characterized by an M-vector $\boldsymbol{c}$ and the decision rule:

$$\hat{b}_k^{(i)} = \text{sgn}\{\boldsymbol{c}^T\boldsymbol{r}_k\}. \tag{5-4}$$

5.3 EXACT MINIMUM-BER MULTIUSER DETECTION

Based on (5-3), the probability that the decision of (5-4) for user i is erroneous is then

$$\begin{aligned} P[\hat{b}_k^{(i)} \neq b_k^{(i)}] &= P[b_k^{(i)}\boldsymbol{c}^T\boldsymbol{r}_k < 0] \\ &= P[b_k^{(i)}\boldsymbol{c}^T\mathbf{H}\boldsymbol{b}_k + b_k^{(i)}\boldsymbol{c}^T\boldsymbol{n}_k < 0] \end{aligned}$$

$$= \mathrm{E}\left[P[b_k^{(i)} \boldsymbol{c}^T \mathbf{H} \boldsymbol{b}_k + b_k^{(i)} \boldsymbol{c}^T \boldsymbol{n}_k < 0 \mid \boldsymbol{b}_k] \right]$$
$$= \mathrm{E}\left[Q\left(\frac{\boldsymbol{c}^T \mathbf{H} \boldsymbol{b}_k b_k^{(i)}}{\|\boldsymbol{c}\| \sigma} \right) \right], \tag{5-5}$$

where the expectations are over the 2^N equally likely binary bit vectors $\boldsymbol{b}_k \in \{\pm 1\}^N$. Observe that the product $\boldsymbol{b}_k b_k^{(i)}$ is a binary vector with a one in the i-th component (corresponding to the user of interest). Let $\boldsymbol{b}^{(1)}, \ldots, \boldsymbol{b}^{(K)}$ denote any ordering of the $K = 2^{N-1}$ such distinct vectors. Similar to the signal vectors defined by (2-17), the signal vectors for this multiuser setup are:

$$\boldsymbol{s}^{(l)} = \mathbf{H} \boldsymbol{b}^{(l)}, \; l = 1 \ldots K. \tag{5-6}$$

These $\boldsymbol{s}^{(l)}$ vectors represent the K possible noiseless channel output vectors given that the k-th bit from the desired user is unity, $b_k^{(i)} = 1$. With this definition, (5-5) simplifies to

$$\mathrm{BER} = \frac{1}{K} \sum_{l=1}^{K} Q\left(\frac{\boldsymbol{c}^T \boldsymbol{s}^{(l)}}{\|\boldsymbol{c}\| \sigma} \right). \tag{5-7}$$

Again, the BER depends on the direction $\boldsymbol{c} / \| \boldsymbol{c} \|$ of $\boldsymbol{c}$ only, and that the norm of $\boldsymbol{c}$ is irrelevant; this is because the receiver decisions are determined by the sign of the detector output only.

Similar to the assumption of the channel being equalizable in chapter 2, in this chapter we assume that user i is *linearly detectable*, by which we mean that the signature $\boldsymbol{d}_i$ of user i does not lie within the interference subspace spanned by $\{\boldsymbol{d}_{j \neq i}\}$.

Let $\boldsymbol{c}_{EMBER}$ denote a linear multiuser detector that achieves the exact minimum-BER (EMBER) performance, minimizing (5-7). Unlike $\boldsymbol{c}_{MMSE} = A_i (\mathbf{H}\mathbf{H}^* + \sigma^2 \mathbf{I})^{-1} \boldsymbol{d}_i$ that minimizes $\mathrm{MSE} = \mathrm{E}[(\boldsymbol{c}^T \boldsymbol{r}_k - b_k^{(i)})^2]$, there is no closed-form expression for $\boldsymbol{c}_{EMBER}$. However,

by setting to zero the gradient of (5-7) with respect to the multiuser detector $\boldsymbol{c}$, we find that $\boldsymbol{c}_{EMBER}$ must also satisfy:

$$\boldsymbol{c} = af(\boldsymbol{c}) \quad \text{for some } a > 0, \tag{5-8}$$

as seen for the equalization problem, where $f(\boldsymbol{c})$ is the function defined by (2-21). Similar to its role in equalization, the fixed-point relationship of (5-8) characterizes local maxima as well as local minima for the BER cost function, and hence (5-8) is a necessary but not sufficient criterion for the global minimum as illustrated by the following example.

Example 5-1: Consider the simplest nontrivial two-user system described by (5-3) with $\boldsymbol{d}_1=[1, 0]^T$, $\boldsymbol{d}_2 = [\rho, \sqrt{1-\rho^2}]^T$, normalized correlation $\rho = 0.9$, $\text{SNR}_1= A_1^2/\sigma^2 = 18$ dB, and $\text{SNR}_2 = 14.6$ dB. In Fig. 2-2 we present a polar plot of BER for user 1 versus θ for the unit-norm detector $\boldsymbol{c} = [\cos\theta, \sin\theta]^T$. Superimposed on this plot are the $K = 2$ signal vectors $\boldsymbol{s}^{(1)}$ and $\boldsymbol{s}^{(2)}$, depicted by solid lines. Also superimposed are the coefficient vectors of four detectors: the minimum-BER detector at an angle of $\theta = -36.9^\circ$; the MMSE detector at $\theta = -60.2^\circ$; the MF detector at $\theta = 0^\circ$; and the decorrelator at $\theta = -64.2^\circ$. Observe that none of the traditional detectors, not even the MMSE detector, are colinear with the minimum-BER detector. We should point out that the minimum-BER detector is not always colinear with the worst-case signal vector, but rather satisfies (5-8) in the general case.

While (5-8) is a necessary condition for minimum-BER performance, the previous example illustrates that the BER surface is not convex, and that there may exist solutions to (5-8) that are non-global local minima. One general method for finding the minimum-

BER solution (hence the EMBER detector) is to find all solutions to (5-8), and choose the solution that yields the smallest BER. However, we can avoid this brute-force method by using this simple sufficiency test which has been employed in equalization setup: If $\boldsymbol{c} = af(\boldsymbol{c})$ and $\text{BER} \leq 2^{-N}$, then $\boldsymbol{c}$ minimizes BER. This test is based on the observation that the eye diagram is open when the condition is satisfied, and that local minima arise only when there exist certain combinations of interfering bits that close the eye.

To recover a solution to (5-8), we can use the *EMSER algorithm* proposed in 2.4:

$$\boldsymbol{c}_{k+1} = \boldsymbol{c}_k + \mu f(\boldsymbol{c}_k). \tag{5-9}$$

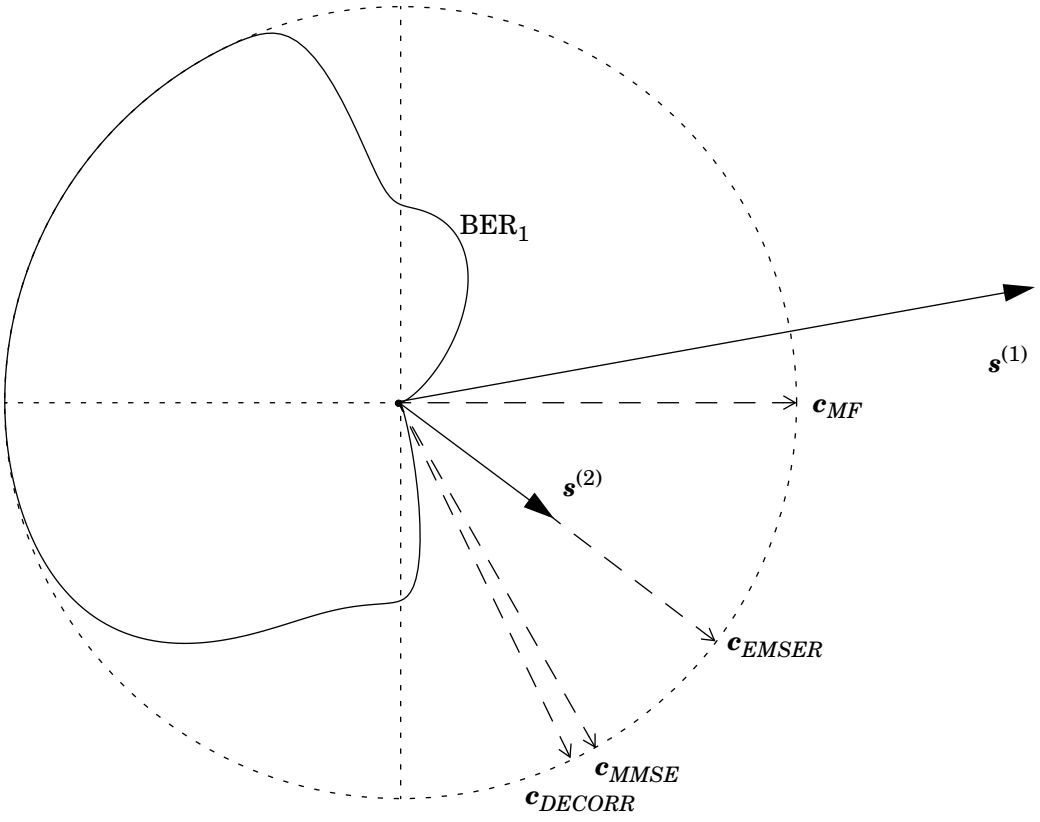

Fig. 5-1. A polar plot of BER_1 versus θ for a two-user system with correlation $\rho = 0.9$. Superimposed are the signal vectors (scaled by a factor of 0.5) and the MMSE, decorrelating, MF, and minimum-BER detectors.

It has been shown that the EMSER algorithm is guaranteed to converge to a solution satisfying (5-8). However, convergence of the EMSER algorithm to the global minimum-BER detector cannot in general be guaranteed.

Similar to the strategy for finding the EMSER equalizer, we use the following strategy for finding the EMBER linear multiuser detector. First, iterate the EMSER algorithm of (5-9) until it converges. If the resulting BER $\leq 2^{-N}$, stop. Otherwise, initialize the EMSER algorithm somewhere else and repeat the process. This is an effective strategy when the initial condition of the EMSER algorithm is chosen carefully and when the SNR is sufficiently large that BER $\leq 2^{-N}$ is possible.

5.4 APPROXIMATE MINIMUM-BER MULTIUSER DETECTION

Although the EMSER algorithm is useful for finding the minimum-BER detector of known channels, it is poorly suited for adaptive implementation in time-varying applications. We now extend the AMBER algorithm of chapter 3 to the multiuser problem.

The numerical algorithm (5-9) can be transformed into a stochastic update equation by using an *error indicator* function I_{by} similar to the error indicator introduced in chapter 3, where

$$I_{by} = \frac{1}{2}(1 - \text{sgn}[b_k^{(i)} y_k]), \tag{5-10}$$

where $y_k = \boldsymbol{c}^T \boldsymbol{r}_k$ is the decision statistic for the k^{th} bit. In other words, $I_{by} = 1$ when an error is made ($\hat{b}_k^{(i)} \neq b_k^{(i)}$) and $I_{by} = 0$ when no error is made ($\hat{b}_k^{(i)} = b_k^{(i)}$). Note that because the multiuser system we are considering is binary, we can effectively treat it as a 2-PAM system where there are no "inner" points in the constellation and thus, simplify the error indicator in (3-9). With the error indicator and following the previous derivation for

approximating the EMSER equalizer algorithm, we transform the EMSER multiuser detector algorithm of (5-9) using the following equalities:

$$\begin{aligned}
\boldsymbol{c}_{k+1} &= \mu f(\boldsymbol{c}_k) \\
&\approx \boldsymbol{c}_k + \mu \mathrm{E}\left[Q\left(\frac{\boldsymbol{c}_k^T \boldsymbol{s}}{\|\boldsymbol{c}_k\| \sigma} \right) \boldsymbol{s} \right] \\
&= \boldsymbol{c}_k + \mu \mathrm{E}\left[Q\left(\frac{b_k^{(i)} \boldsymbol{c}_k^T \mathbf{H} \boldsymbol{b}_k}{\|\boldsymbol{c}_k\| \sigma} \right) b_k^{(i)} \mathbf{H} \boldsymbol{x} \boldsymbol{b}_k \right] \\
&= \boldsymbol{c}_k + \mu \mathrm{E}\left[\mathrm{E}[I_{by} \mid b_k^{(i)} \mathbf{H} \boldsymbol{b}_k] \mathrm{E}[b_k^{(i)} \mathbf{H} \boldsymbol{b}_k] \right] \\
&= \boldsymbol{c}_k + \mu \mathrm{E}[I_{by} b_k^{(i)} \mathbf{H} \boldsymbol{b}_k] \\
&\approx \boldsymbol{c}_k + \mu \mathrm{E}[I_{by} b_k^{(i)} \boldsymbol{r}_k]
\end{aligned} \tag{5-11}$$

The approximation of (5-11) is valid assuming the effect of noise is insignificant at high SNR. We can then form a simple stochastic update algorithm by simply removing the expectation in (5-11):

$$\boldsymbol{c}_{k+1} = \boldsymbol{c}_k + \mu I_{by} b_k^{(i)} \boldsymbol{r}_k \,. \tag{5-12}$$

We refer to this stochastic algorithm as the *AMBER algorithm* for linear multiuser detection. The detector is updated only when an error is made. It has an insightful geometric interpretation. Recall that the noiseless output of the detector when a one is transmitted by the desired user is the inner product of $\boldsymbol{c}$ with $\boldsymbol{s}^{(j)}$. Most errors occur when this inner product is small, *i.e.,* when the eye is nearly closed. The AMBER update of (5-12) dictates that each time an error is made, the detector coefficient vector $\boldsymbol{c}$ takes a small step in space towards the $\boldsymbol{s}^{(j)}$ vector that resulted in the error. Therefore, the next time the interfering

users conspire to produce the same $\boldsymbol{s}^{(j)}$ vector, its inner product with $\boldsymbol{c}$ will be larger. At steady state, the detector $\boldsymbol{c}$ will be attracted to each $\boldsymbol{s}^{(j)}$ by an amount proportional to the conditional error probability given that $\boldsymbol{s}^{(j)}$ is the signal vector, which closely approximates the steady state of $\boldsymbol{c}_{EMSER}$ described by (5-8).

Recall that the LMS algorithm for implementing the MMSE detector is:

$$\boldsymbol{c}_{k+1} = \boldsymbol{c}_k - \mu e_k \boldsymbol{r}_k, \tag{5-13}$$

where $e_k = y_k - b_k^{(i)} = \boldsymbol{c}^T \boldsymbol{r}_k - b_k^{(i)}$ is the error signal. We see that the AMBER and LMS algorithms are nearly identical, the only difference being that $I_{by} = 1 - b_k^{(i)} y_k$ for LMS and $I_{by} = \frac{1}{2}(1 - \text{sgn}[b_k^{(i)} y_k])$ for AMBER. In fact, AMBER has more in common with the sign-LMS algorithm:

$$\boldsymbol{c}_{k+1} = \boldsymbol{c}_k - \mu \text{sgn}\{e_k\} \boldsymbol{r}_k, \tag{5-14}$$

because $b_k^{(i)} = -\text{sgn}\{e_k\}$ when an error occurs ($I_{by} \neq 0$). Thus, we can rewrite the stochastic AMBER algorithm in the form of a modified sign-LMS algorithm:

$$\boldsymbol{c}_{k+1} = \boldsymbol{c}_k - \mu I_{by} \text{sgn}\{e_k\} \boldsymbol{r}_k. \tag{5-15}$$

Simply stated, AMBER can be viewed as the sign-LMS algorithm *modified to update only when an error is made*. The sign-LMS was motivated by its low complexity compared to the LMS algorithm, despite its poorer performance. The simple modification for AMBER, on the other hand, provides dramatic performance improvement, without any cost in complexity.

As mentioned in chapter 3, a major drawback of the AMBER algorithm is its slow convergence at high SNR; because the detector is updated only when an error is made, a low BER necessarily implies slow convergence. We modify the error indicator function of (5-10) by introducing a non-negative threshold $\tau \geq 0$ as follows:

$$I_{by} = \frac{1}{2}(1 - \text{sgn}[b_k^{(i)} y_k - \tau]). \tag{5-16}$$

In other words, the modified indicator function $I_{by} = 1$ if $b_k^{(i)} y_k \leq \tau$ and $I_{by} = 0$ otherwise. This indicator function reverts back to the original (5-10) when τ is zero. In addition, instead of a single update threshold τ and a single update step size μ, we can employ multiple μ's and τ's to further increase the convergence speed of AMBER detector.

From chapter 3, another advantage of the threshold τ is to allow the AMBER multiuser detector algorithm to operate in a decision-directed manner.

5.5 NUMERICAL RESULTS

Lupas and Verdú [4] proposed the asymptotic efficiency to evaluate the error probability performance of a multiuser detector at high SNR. The kth user asymptotic efficiency of the optimal linear two-user detector equals [4]

$$\eta_k^l = \begin{cases} 1 - 2|\rho| A_i / A_k + A_i^2 / A_k^2, & \text{if } (A_i / A_k) \leq |\rho| \\ 1 - \rho^2, & \text{otherwise.} \end{cases} \tag{5-17}$$

On the other hand, the MMSE multiuser detector approaches the decorrelator as the Gaussian noise variance approaches zero, and thus the asymptotic efficiency of the MMSE multiuser detector is the same as that of the decorrelator. The asymptotic efficiency of the decorrelator is [4]

$$\eta_k^d = 1 - \rho^2. \tag{5-18}$$

Finally, the asymptotic efficiency of the MF detector is [4]

$$\eta_k^m = \max^2\left\{0, 1 - \rho\frac{A_i}{A_k}\right\}. \tag{5-19}$$

Given ρ in a two-user system, we can plot the asymptotic efficiencies of the optimal linear multiuser detector, the decorrelator, and the MF detector as functions of A_i/A_k. In Fig. 5-2, we plot user 1 asymptotic efficiencies for ρ = 0.6. The asymptotic efficiencies of the optimum linear multiuser detector and the decorrelator are the same when A_2/A_1 is larger than ρ = 0.6. In addition, the asymptotic efficiencies of the optimum linear multiuser detector and the MF detector are very close when A_2/A_1 is small. When the asymptotic efficiencies of the MF detector and the decorrelator are about the same, the optimum linear multiuser detector performs significantly better than both of them.

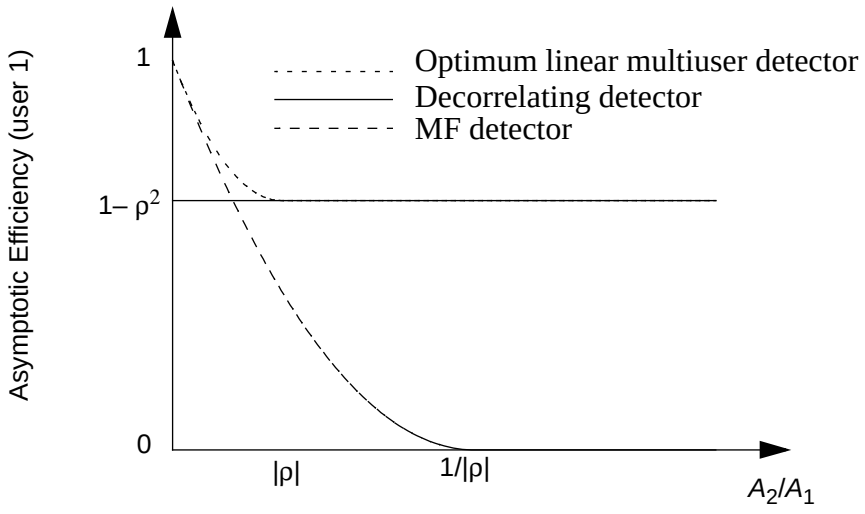

Fig. 5-2. Asymptotic efficiencies in two-user case (ρ = 0.6) [4].

With the asymptotic efficiencies of the optimal linear multiuser detector and decorrelator derived by Lupas and Verdú [4], we can use them as the bounds on gain of the EMBER multiuser detector over the MMSE multiuser detector. We will now compare BER performances of the EMBER, AMBER, MMSE, MAME of Lupas and Verdú [4], decorrelator, and MF detectors on a two-user system with $\boldsymbol{d}_1 = [1, 0]^T$, $\boldsymbol{d}_2 = [\rho, \sqrt{1-\rho^2}]^T$ and $\rho = 0.9$. We choose the interference power of $A_2^2/A_1^2 = -4.15$ dB so that the asymptotic efficiencies of both the decorrelator and the MF detector are significantly less than that of the optimum linear multiuser detector, and thus we expect the EMBER, AMBER, and MAME detectors perform significantly better than the MMSE, decorrelating, and MF detectors at high SNR. In Fig. 5-3 we compare the BER performance of the above six linear multiuser detectors. Observe that the EMBER, AMBER, and MAME detectors are indistinguishable, and that they outperform the MMSE detector by more than 1 dB at high SNR and outperform the matched filter and the decorrelator by an even wider margin.

We also consider a simple three-user system described by (5-3) with $\boldsymbol{d}_1 = [1, 0.1]^T$, $\boldsymbol{d}_2 = [0.9, 1]^T$, $\boldsymbol{d}_3 = [0.1, 1]^T$, and $\text{SNR}_1 = \text{SNR}_2 = \text{SNR}_3 = 20$ dB. In Fig. 5-4 we illustrate the performance of AMBER, with parameters $\tau_1 = 0.2$, $\tau_2 = 0.4$, μ_1 and μ_2 initialized to 0.06 and 0.02, and with μ_1 and μ_2 cut in half every 200 iterations. Although AMBER can not improve the BER performance for user 2, it improves BER of users 1 and 3 over MMSE solutions significantly.

For comparison purposes, we include in Fig. 5-4 the performance of the adaptive detector of Psaromiligkos *et al*. [6]. We used parameters of $a_n = \frac{0.001}{\log(n)}$, $c_n = 0.1n^{-0.25}$ (where n is time), and a threshold $\lambda = 0.08$. The convergence rate of this algorithm is comparable to that of AMBER. Unlike AMBER, however, it requires knowledge of all the signature sequences of users.

5.6 SUMMARY AND CONCLUSIONS

Based on the derived fixed-point equation for the minimum-BER linear multiuser detector, we have proposed a low-complexity stochastic multiuser detector algorithm which approaches the minimum-BER performance. The algorithm has a lower complexity than the LMS algorithm but achieves significantly better BER performance when multiuser interference is severe as demonstrated by the short channels where the number of users is smaller than the dimension of the signal space.

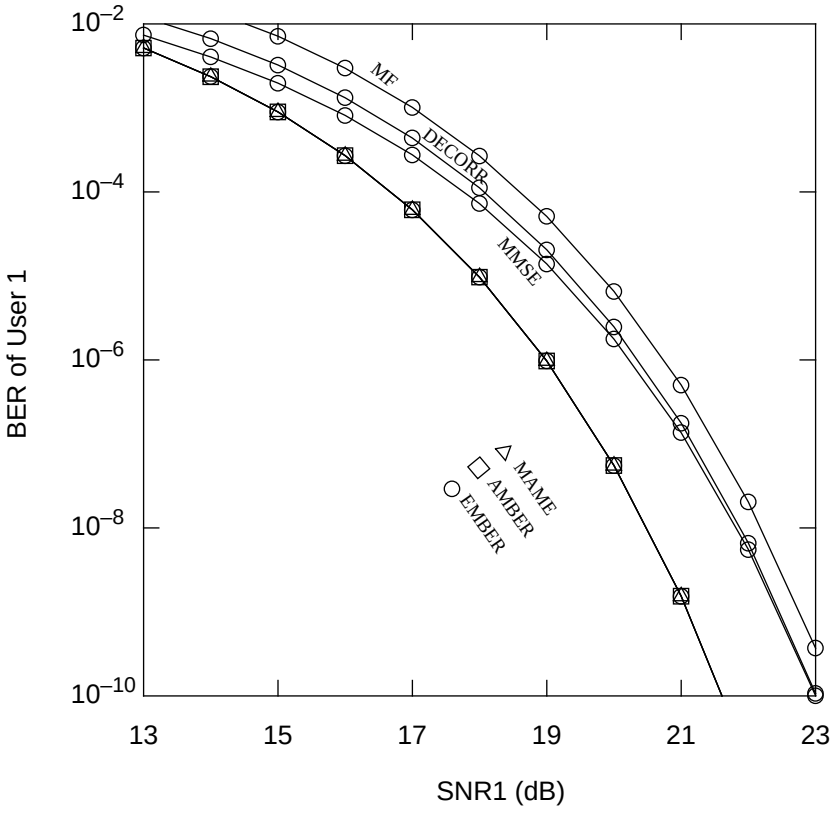

Fig. 5-3. BER comparison of various detectors.

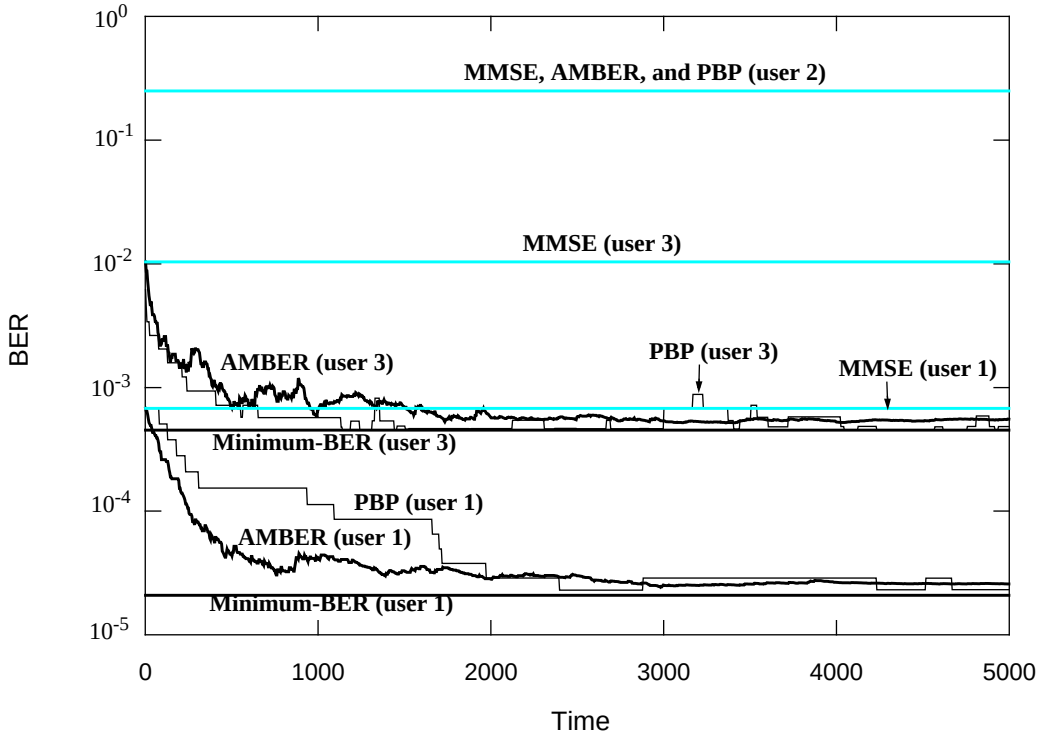

Fig. 5-4. Learning curves of AMBER and the PBP algorithm of [6] for the three-user example.

CHAPTER 6

CONCLUSIONS AND FUTURE WORK

6.1 CONCLUSIONS

This thesis has concentrated on the design and adaptation of finite-tap equalizers and multiuser detectors to minimize error probability. We have proposed low-complexity equalizer and multiuser detector algorithms for combating ISI and multiuser interference in the presence of additive Gaussian noise.

In chapter 2, we have derived and investigated the properties of the minimum-SER equalizer. We have shown that a necessary but not sufficient condition, a fixed-point relationship, has to be satisfied by the minimum-SER equalizer. We then proposed, based on the fixed-point relationship, a numerical algorithm to iteratively recover the minimum-SER equalizer coefficients satisfying the fixed-point relationship. Because satisfaction of the fixed-point relationship does not guarantee the minimum-SER equalizer, we have also

proposed a sufficiency condition for testing the convergence of the numerical algorithm to the global-SER minimum. The sufficiency condition is based on the mild assumption that the noise variance is sufficiently small. In addition, we have conjectured that the MMSE equalizer approaches the minimum-SER equalizer as the number of equalizer taps approaches infinity.

In chapter 3, we have used another exponential-like function, the Gaussian error function or Q function, to approximate the fixed-point relationship derived for the minimum-SER equalizer in chapter 2. Instead of multiple solutions, there is a unique solution to the approximate fixed-point relationship. We have constructed a numerical algorithm to recover the unique solution to the approximate relationship. The numerical algorithm (AMBER) based on the fixed-point relationship yields a low-complexity stochastic equalizer algorithm. We have evaluated its error-probability performance and compared it with the MMSE and the EMSER algorithms. Finally, we have empirically characterized the FIR channels over which the AMBER and the EMSER equalizers significantly outperform the MMSE equalizer.

In chapter 4, we have discussed the convergence properties of the AMBER algorithm. We have first determined the deterministic trajectory of the AMBER algorithm by taking the expectation of the stochastic update equation. The deterministic trajectory turns out to be a complicated nonlinear dynamical system. We have then developed some analytical intuition regarding the dynamical system and have discussed the global convergence property of the AMBER algorithm. Although we have not been able to rigorously prove the global convergence of the algorithm, we have argued that the algorithm is likely to globally converge. We have then proposed some multi-step variants of AMBER to increase

convergence speed. We also have studied the convergence performance of decision-directed mode.

In chapter 5, we have extended results on the minimum-error-probability equalizers and update algorithms to multiuser systems. The concepts of the signal vectors and signal cones in a single-user ISI channel can be extended in a straightforward manner to a multiuser system where multiuser interference is similar to the ISI phenomenon. We have compared the performance of the minimum-BER multiuser detector with the matched filter detector, the MMSE detector, the decorrelator, and the MAME detector proposed by Lupas and Verdú [4].

6.2 FUTURE WORK

6.2.1 MMSE vs. Minimum-SER Equalizers with Infinite Number of Taps

In chapter 2, we made a conjecture that the MMSE equalizer approaches the minimum-BER equalizer when the number of equalizer taps approaches infinity. Other than some simulation results, we currently do not have a rigorous mathematical proof to confirm nor a counter example to contradict the claim. A proof or a counter example to this conjecture would be enlightening in understanding the ultimate connection between the MMSE and the EMSER equalizers.

6.2.2 Global Convergence Proof

In chapter 4 we discussed the global convergence property of the AMBER algorithm. Rather than a formal mathematical proof, we completed the topic with a mixture of observations and analytical reasoning. Proving the global convergence property requires a more thorough understanding of this particular nonlinear dynamical system.

6.2.3 Multiuser Channels with Memory

In this thesis, we developed and evaluated minimum-BER results on single-user ISI channels and memoryless multiuser channels. The theoretical results on single user ISI channels and memoryless multiuser channels can be extended naturally to multiuser channels with memory. However, it will be of practical interest to numerically evaluate the performance of the AMBER algorithm on multiuser channels with memory.

6.2.4 Blind Equalization and Multiuser Detection

The AMBER algorithm in this thesis, similar to the LMS algorithm, requires correct decisions in initializing equalizers and multiuser detectors. Recently there has been a surged interest in blind equalization [42] and multiuser detection research [32]. Blind equalization and multiuser detection are valuable when a training sequence is either costly or impossible to transmit. Similar to the blind multiuser algorithm proposed by Honig, Madhow, and Verdú [43], it will be of practical interest to construct simple and robust equalizer and multiuser detector algorithms to minimize error probability without training data.

REFERENCES

[1] E. Shamash and K. Yao, "On the Structure and Performance of a Linear Decision-Feedback Equalizer Based on the Minimum Error Probability Criterion," *International Conference on Communications*, pp. 25F1-25F5, 1974.

[2] P. Galko and S. Pasupathy, "Optimal Linear Receiver Filters for Binary Digital Signals," *International Conference on Communications*, pp. 1H.6.1-1H.6.5, 1982.

[3] S. Chen, E. Chng, B. Mulgrew, and G. Gibson, "Minimum-BER Linear-Combiner DFE," *International Conference on Communications*, pp. 1173-1177, 1996.

[4] R. Lupas and S. Verdú, "Linear Multiuser Detectors for Synchronous Code-Division Multiple-Access Channels," *IEEE Transactions on Information Theory*, vol. 35, no. 1, pp. 123-136, January 1989.

[5] N. B. Mandayam and B. Aazhang, "Gradient Estimation for Sensitivity Analysis and Adaptive Multiuser Interference Rejection in Code-Division Multiple-Access Systems," *IEEE Transactions on Communications*, vol. 45, no. 7, pp. 848-858, July 1997.

[6] I. N. Psaromiligkos, S. N. Batalama, and D. A. Pados, "Adaptive Minimum Probability of Error Linear-Filter Receivers for DS-CDMA channels," *Proceedings of Conference on Information Sciences and Systems*, pp. 90-94, 1996.

[7] S. U. H. Qureshi, "Adaptive Equalization," *Proceedings of the IEEE*, vol. 73, no. 9, pp. 1349-1387, September 1985.

[8] R. W. Lucky, "Automatic Equalization for Digital Communication," *The Bell System Technical Journal*, vol. 44, pp. 547-588, April 1965.

[9] R. W. Lucky, “Techniques for Adaptive Equalization of Digital Communication Systems,” *The Bell System Technical Journal*, vol. 45, pp. 255-286, February 1966.

[10] R. W. Lucky, J. Salz, and E. J. Weldon, *Principles of Data Communications*, McGraw-Hill, 1968.

[11] A. Gersho, “Adaptive Equalization of Highly Dispersive Channels,” *The Bell System Technical Journal*, vol. 48, pp. 55-70, January 1969.

[12] J. Proakis and J. Miller, “An Adaptive Receiver for Digital Signaling Through Channels with Intersymbol Interference,” *IEEE Transactions on Information Theory*, vol. 15, pp. 484-497, 1969.

[13] J. G. Proakis, *Digital Communications*, Third Edition, McGraw-Hill, 1995.

[14] E. A. Lee and D. G. Messerschmitt, *Digital Communication*, Second Edition, Kluwer Academic Publishers, 1994.

[15] S. Haykin, *Adaptive Filter Theory*, Second Edition, Prentice Hall, 1991.

[16] B. Widrow and M. E. Hoff, “Adaptive Switching Circuits,” *IRE WESCON*, pt. 4, pp. 96-104, August 1960.

[17] B. Widrow and S. D. Stearns, *Adaptive Signal Processing*, Prentice-Hall, 1985.

[18] S. T. Alexander, *Adaptive Signaling Processing*, Springer-Verlag, 1986.

[19] C. P. Kwong, “Dual Sign Algorithm for Adaptive Filtering,” *IEEE Transactions on Communications*, vol. 34, No. 12, December 1986.

[20] R. Sharma, W. Sethares, and J. Bucklew, “Asymptotic Analysis of Stochastic Gradient-Based Adaptive Filtering Algorithms with General Cost Functions,” *IEEE Transactions on Signal Processing*, vol. 44, no. 9, September 1996.

[21] S. C. Bang and S. Ann, “A Robust Algorithm for Adaptive FIR Filtering and Its Performance Analysis with Additive Contaminated-Gaussian Noise,” *IEEE Transactions on Circuits and Systems – 1: Fundamental Theory and Applications*, vol. 43, no. 5, May 1996.

[22] G. D. Forney, Jr., “Maximum-likelihood Sequence Estimation of Digital Sequences in the Presence of Intersymbol Interference,” *IEEE Transactions on Information Theory*, vol. 18, no. 3, pp. 363-377, May 1972.

[23] G. D. Forney, Jr., “The Viterbi Algorithm,” *Proceedings of IEEE*, vol. 61, no. 3, pp. 268-278, March 1973.

[24] D. D. Falconer and F. R. Magee, “Adaptive Channel Memory Truncation for Maximum-Likelihood Sequence Estimation,” *The Bell System Technical Journal*, vol. 52, pp. 1541-1562, November 1973.

[25] A. Duel-Hallen and C Heegard, “Delayed Decision-Feedback Sequence Estimation,” *IEEE Transactions on Communications,* vol. 37, no.5, pp. 428-436, May 1989.

[26] M. V. Eyuboglu and S. U. H. Qureshi, “Reduced-State Sequence Estimation with Set Partitioning and Decision Feedback,” *IEEE Transactions on Communications*, vol. 36, no. 1, January 1988.

[27] M. Austin, “Decision-feedback Equalization for Digital Communication over Dispersive Channels,” Technical Report 437, MIT Lincoln Laboratory, Lexington, Mass, 1967.

[28] P. Monsen, “Feedback Equalization for Fading Dispersive Channels,” *IEEE Transactions on Information Theory,* vol. 17, pp. 56-64, 1971.

[29] C. A. Belfiore and J. H. Park, “Decision Feedback Equalization,” *Proceedings of the IEEE*, vol. 67, no. 8, August 1979.

[30] J. Salz, “Optimum Mean-Square Decision Feedback Equalization,” *The Bell System Technical Journal*, vol. 52, no. 8, pp. 1341-1373, October 1973.

[31] M. S. Mueller and J. Salz, “A Unified Theory of Data-Aided Equalization,” *The Bell System Technical Journal*, vol. 60, no. 11, pp. 2023-2038, November 1981.

[32] J. Barry and A. Batra, “Co-Channel Demodulation Using Multi-Input Multi-Output Equalization,” CRASP Annual Report: Year Two, July 1996.

[33] S. Verdú, “Recent Progress in Multi-User Detection,” in *Advances in Communications and Signal Processing*, W. A. Porter and S. C. Kak, Eds. Springer-Verlag, New York, 1989.

[34] P. A. Voois and J. M. Cioffi, “Multichannel Signal Processing for Multiple-Head Digital Magnetic Recording,” *IEEE Transactions on Magnetics*, 30:6, pp. 5100-5114, November 1994.

[35] J. Salz, “Digital Transmission Over Cross-Coupled Linear Channels,” *AT&T Technical Journal*, 64:6, pp. 1147-1158, July-August 1985.

[36] W. Van Etten, “Maximum Likelihood Receiver for Multiple Channel Transmission Systems,” *IEEE Transactions on Communications*, pp. 276-283, February 1976.

[37] M. K. Varanasi and B. Aazhang, “Near-Optimum Detection in Synchronous Code-Division Multiple-Access Systems,” *IEEE Transactions on Communications*, vol. 39, no. 5, pp. 725-736, May 1991.

[38] C.-C. Yeh and J. R. Barry, “Approximate Minimum Bit-Error Rate Equalization for Binary Signaling,” *International Conference on Communications* (*ICC ‘97*), pp. 1095-1099, 1997.

[39] C.-C. Yeh and J. R. Barry, “Approximate Minimum Bit-Error Rate Equalization for Binary Signaling,” submitted to *IEEE Transactions on Communications*, May 1997.

[40] C.-C. Yeh and J. R. Barry, “Approximate Bit-Error Rate Equalization for Pulse-Amplitude and Quadrature Amplitude Modulation,” to apprear, *International Conference on Communications* (*ICC ‘98*).

[41] C.-C. Yeh, R. P. Lopes, and J. R. Barry, “Approximate Minimum Bit-Error Rate Multiuser Detection,” submitted to *Global Communication Conference* (*Globe-Comm ‘98*).

[42] S. Haykin, *Blind Deconvolution*, Prentice Hall, 1994.

[43] M. Honig, U. Madhow, and S. Verdú, “Blind Adaptive Multiuser Detection,” *IEEE Transactions on Information Theory*, vol. 41, no. 4, pp. 944-960, July 1995.